Check for updates

Geobiology

WILEY

gebiology

ORIGINAL ARTICLE OPEN ACCESS

Red to Green: A Lipid Biomarker Record of Tonian-Ediacaran Algae in Siberia

Adriana I. Rizzo[1] | Andrey Bekker[1,2] | Anton B. Kuznetsov[3] | Victoria B. Ershova[4,5] | Yijun Xiong[6] | Karl E. Karlstrom[7] | Simon W. Poulton[6] | Gordon D. Love[1]

[1]Department of Earth and Planetary Sciences, University of California, Riverside, California, USA | [2]Department of Geology, University of Johannesburg, Johannesburg, South Africa | [3]Institute of Precambrian Geology and Geochronology (IPGG), Russian Academy of Sciences, Saint Petersburg, Russia | [4]Institute of Earth Science, St. Petersburg State University, St. Petersburg, Russia | [5]Geological Institute, Russian Academy of Sciences, Moscow, Russia | [6]School of Earth and Environment, University of Leeds, Leeds, UK | [7]Department of Earth and Planetary Science, University of New Mexico, Albuquerque, New Mexico, USA

Correspondence: Adriana I. Rizzo (adriana.rizzo@email.ucr.edu)

Received: 15 May 2025 | **Revised:** 15 July 2026 | **Accepted:** 14 August 2026

Keywords: eukaryotes | green algae | phosphorus | red algae | seawater redox | steranes | Tonian

ABSTRACT

Multiple lines of evidence point to a major diversification of Eukarya in the late Tonian period, ca. 800–720 Ma ago. Regular steranes, lipid biomarkers primarily sourced from eukaryotes, are first unambiguously reported from multiple sites. Here, we present lipid biomarker stratigraphic records from two drill-cores from the Lena-Anabar Basin in northern Siberia, in addition to new biomarker data from the Walcott Member of the Chuar Group, USA. The Siberian drill-cores span the late Tonian (ca. 800–750 Ma) and late Ediacaran-early Cambrian periods (ca. 565–539 Ma), with Cryogenian strata absent. Compositional differences in sedimentary organic matter were assessed using a suite of biomarker hydrocarbon parameters, with seawater redox and phosphorus availability determined using iron speciation, trace metals, and phosphorus phase partitioning. Steranes were consistently detected in Tonian strata in the Siberian drill-cores, with sterane/hopane (S/H) values being uniformly low (< 0.05), consistent with a low-productivity, marine environment in which bacteria outcompeted eukaryotes for limited nutrients. This was confirmed by phosphorus phase partitioning data that suggest that phosphorus was a key limiter of late Tonian marine eukaryote abundance. Unlike Siberia, late Tonian samples from the Chuar Group showed consistently higher S/H values (up to 0.38) and elevated total organic carbon content (1.3–5.6 wt.%) indicative of higher algal productivity in a eutrophic marine setting. Tonian strata primarily yielded cholestane (C_{27} sterane), indicating red algal dominance with small contributions of cryostane and ergostane (C_{28} steranes), while Ediacaran strata in both Siberian drill-cores were dominated by stigmastane (C_{29} sterane), indicating green algal dominance, capturing this global secular shift in a single location. The distinctive C_{27}-sterane dominance commonly found for the late Tonian is captured here for the first time from an oligotrophic marine environment that sustained oxic to weakly reducing redox conditions, supporting the idea that the Tonian rise of algae occurred widely across the oceans.

1 | Introduction

The Tonian Period (1000–720 millions of years ago, Ma), particularly its final 100 million years, was a dramatic transition in the Earth System, linking the apparent relative stasis of the so-called "Boring Billion" to the upheaval of the late Neoproterozoic (Planavsky et al. 2015). Prior to the ca. 717–635 Ma Snowball Earth glaciations, the supercontinent Rodinia fragmented at ca. 825–720 Ma (Li et al. 2013), atmosphere–ocean oxygen concentrations began to rise

This is an open access article under the terms of the Creative Commons Attribution-NonCommercial License, which permits use, distribution and reproduction in any medium, provided the original work is properly cited and is not used for commercial purposes.

© 2026 The Author(s). *Geobiology* published by John Wiley & Sons Ltd.

in a fluctuating manner (Krause et al. 2022; Turner and Bekker 2016), the first large-magnitude carbon isotope excursions in a billion years occurred (Halverson et al. 2005, 2010), and eukaryotic life flourished and diversified (Cohen and Macdonald 2015; Isson et al. 2018; Riedman and Sadler 2018; Xiao and Tang 2018). Hence, this interval represents a critical period for the evolution of complex life, yet the temporal dynamics, causes, and consequences of the Tonian rise of eukaryotes remain debated.

Evidence for a eukaryotic radiation in the late Tonian derives, in part, from lipid biomarker records. The pre-Sturtian record of regular (4-desmethyl) steranes suggests that eukaryotic life was relatively scarce in the oceans prior to an ecological rise that began in the late Tonian period (Love and Zumberge 2021; Zumberge et al. 2020). Steranes are the diagenetic products of sterols, membrane lipids that are ubiquitous across the Eukaryotic tree of life (Desmond and Gribaldo 2009), although a few species of heterotrophic eukaryotes lack sterols (Takishita et al. 2017). As such, synthesis of regular steroids is often considered a synapomorphy for eukaryotes. The abundance ratio of summed steranes to their bacterial analogue, hopanes (S/H) is a widely used and convenient proxy for the relative contributions of eukaryotes and bacteria to sedimentary organic matter, given the broadly similar recalcitrance of these polycyclic compound classes to degradation during prolonged burial and thermal maturation.

The oldest widely accepted regular steranes are found in the < 820 Ma Bitter Springs Group (Brocks et al. 2017), as well as in the 777–717 Ma Buldya Group (Brocks et al. 2017), the 753 ± 5.9 Ma Visingsö Group (Brocks et al. 2016; Planavsky et al. 2023; Zumberge et al. 2020) and the 735–729 Ma upper Walcott Member of the Chuar Group (Brocks et al. 2016; Dehler et al. 2023; Summons et al. 1988; Summons and Walter 1990; Vogel et al. 2005; Zumberge et al. 2020). Dakhnova et al. (2014) previously identified regular steranes in solvent extracts from only four samples from a one-meter interval of the Burskaya-3410 drill-core in the Tonian Lena-Anabar Basin but did not report sterane distributions or provide S/H values.

The possibility of contamination from exogenous sources is a persistent concern in studies of ancient biomarkers, and meticulous analytical protocols and compound screening are required minimize and identify potential organic contamination (French et al. 2015). Pre-Tonian sedimentary units of suitably low thermal maturity that are not compromised by suspicious exogenous lipids commonly yield complex lipid assemblages dominated by bacterial sources, yet typically lack regular steranes. Biomarker assemblages from the ca. 1.0–1.1 Ga Malgina Formation in eastern Siberia (Suslova et al. 2017), the ca. 1.08 Ga Nonesuch Formation in Laurentia (Gallagher et al. 2017), the ca. 1.1 Ga El Mreiti Group in West Africa (Blumenberg et al. 2012; Gueneli et al. 2018), the ca. 1.1 Ga Lakhanda Group in eastern Siberia (Duda et al. 2021), the ca. 1.38 Ga Roper Group in northern Australia (Flannery and George 2014; Jarrett et al. 2019; Nguyen et al. 2019), the ca. 1.38 Ga Xiamaling (Luo et al. 2015) and ca. 1.46 Ga Hongshuizhuang formations (Luo et al. 2016) in North China, and the ca. 1.64 Ga Barney Creek (Brocks et al. 2005; French et al. 2020) and ca. 1.73 Ga Wollongorong formations (Vinnichenko et al. 2020) in northern Australia have yielded no detectable regular steranes, despite the presence of well-preserved bacterial biomarkers, including hopanes and methylhopanes. Taken together, this body of evidence suggests that the scarcity of modern-type steroid-producing eukaryotes is a pervasive feature of mid-Proterozoic open-marine settings.

Although a molecular taphonomic bias resulting from selective destruction of steroids in microbial mats has been proposed to explain this early absence of steranes (the "mat seal" hypothesis; Pawlowska et al. 2013), studies of modern microbial mats that contain eukaryotes (Lee, Love, Jahnke, et al. 2019; Lee et al. 2021; Shen et al. 2018) demonstrate that substantial amounts of steroids survive degradation within mats and are rapidly incorporated into and preserved by covalent binding within a macromolecular matrix ("proto-kerogen") on timescale of only years to decades. Additionally, extensive mat facies persist into the Cambrian (Buatois et al. 2014; Tarhan et al. 2015), long after the full suite of C_{27}–C_{30} steranes became ubiquitous in the Ediacaran Period. Consequently, a mat seal taphonomic bias cannot adequately account for the lack of regular steranes in Mesoproterozoic and older sedimentary rocks and oils. Overall, the composite Proterozoic lipid biomarker record suggests that eukaryotes, including algae, were not environmentally abundant and contributed minimally to Mesoproterozoic open-marine ecosystems.

Multiple lines of evidence from the microfossil record further support a Tonian radiation of microbial eukaryotes (Butterfield 2015; Cohen and Macdonald 2015; Knoll et al. 2006; Riedman and Sadler 2018; Xiao and Tang 2018). Fossils assigned to several crown eukaryote lineages appeared just prior to or during the Tonian, including red and green algae by ca. 1000 Ma (Butterfield 2000; Gibson et al. 2018; Tang et al. 2020), fungi by ca. 1000 Ma or ca. 890 Ma (Hermann and Podkovyrov 2006, 2010; Loron et al. 2019), and amoebozoans by ca. 750 Ma (Lahr et al. 2019; Riedman et al. 2018; Riedman and Sadler 2018). Some microfossil diversity metrics also indicate an increase in the late Tonian (Cohen and Macdonald 2015; Riedman and Sadler 2018; Xiao and Tang 2018), although this pattern has been recently questioned as a potential sampling artifact (Porter et al. 2025). Regardless, innovations such as predation (Cohen and Riedman 2018; Porter 2016) and protist biomineralization (Cohen et al. 2017; Cohen and Knoll 2012; Morais et al. 2017) first appear in the late Tonian ocean.

While eukaryotes—typically algae—are considered the primary ancient producers of regular steroids, biosynthetic precursors of these compounds also have an extensive geological record and may reflect multiple sources (Brocks et al. 2005, 2023). Several upstream steps of sterol biosynthesis may have originated in bacteria (Hoshino and Gaucher 2021, 2024; Wei et al. 2016), and some extant bacteria inhabiting microaerobic ecosystems are capable of synthesizing steroid precursors (Wei et al. 2016), including the principal compounds lanosterol and cycloartenol, which retain A-ring methylations at the C-4 position. These compounds are not accumulated as terminal sterol products in most modern eukaryotes.

Geological forms of 4-methyl steroids, or "protosteroids," include lanostane (aliphatic) and 4-methyl mono-, di-, and triaromatic steroids. Lanostane occurs repeatedly throughout the

14724669, 2026, 5, Downloaded from https://onlinelibrary.wiley.com/doi/10.1111/gbi.70061 by NICE, National Institute for Health and Care Excellence, Wiley Online Library on [07/10/2026]. See the Terms and Conditions (https://onlinelibrary.wiley.com/terms-and-conditions) on Wiley Online Library for rules of use; OA articles are governed by the applicable Creative Commons License

Phanerozoic (Birgel and Peckmann 2008; Chen et al. 1989; Chen and Summons 2001; Parfenova 2011; Peckmann et al. 2004), often associated with methane seeps or redox-stratified saline lakes. The oldest detected lanostane is from the ca. 1640 Ma Barney Creek Formation (Brocks et al. 2023), although lanostanes are not commonly observed as major biomarker constituents of Precambrian sedimentary rocks. Aromatic protosteroids were first reported from immature Paleoproterozoic rocks from the Barney Creek Formation (Brocks et al. 2005) and have also been found in younger Proterozoic and Phanerozoic rocks (Brocks et al. 2023).

Protosteroids have been interpreted as deriving either from bacteria (Brocks et al. 2005) or stem eukaryotes (Brocks et al. 2023), and their record remains a topic of ongoing debate (Hoshino and Gaucher 2024). Additionally, trace amounts of 4,24-methyl, aromatic "ursteroids" reported from four shales of the mid-Proterozoic Velkerri Formation, Roper Group, have been interpreted as potentially sourced from stem-group eukaryotes (Brocks et al. 2023). Taken together, these data suggest a widespread Tonian rise of modern-type steroids derived from eukaryotes is plausible, although additional environmental facies require further investigation.

Changes in sterane compound distributions are important for recognizing shifts in Neoproterozoic microbial ecology and for tracking the evolution of steroid biosynthesis pathways (Hoshino et al. 2017; Knoll et al. 2007). A predominance of C_{29} (stigmastane, 24-ethyl cholestane) over C_{27} (cholestane) and C_{28} steranes is commonly interpreted as a green algal dominance within the eukaryotic phytoplankton community (Kodner et al. 2008). The oldest occurrence of this pattern is found in Oman rocks deposited around the Cryogenian-Ediacaran boundary (Love et al. 2009), after which a C_{29} sterane preference is commonly observed in Ediacaran (Brocks 2018; Brocks et al. 2017; Duda et al. 2020; Dutta et al. 2013; Grosjean et al. 2009; Kelly et al. 2011; Love et al. 2009; Pehr et al. 2018) and Paleozoic (Grantham and Wakefield 1988; Schwark and Empt 2006) marine sedimentary rocks and oils. As a caveat, few Ediacaran units from Australia contain C_{29} steranes, but not as the dominant component (McKirdy et al. 2006).

By contrast, Tonian sediments younger than ca. 820 Ma show a C_{27} predominance, which is interpreted as reflecting major eukaryotic contributions from unicellular heterotrophs (Brocks et al. 2017) and/or red algae (Summons et al. 1988; Zumberge et al. 2020). Red and green algae are evolutionary sister groups within the Archaeoplastida (Burki et al. 2020), and microfossils of both have been reported in rocks as old as ca. 1000 Ma (Butterfield 2000; Gibson et al. 2018; Tang et al. 2020). The delayed first appearance of steroids from these groups therefore appears puzzling. A sampling gap in the rock record between ca. 1000 and 820 Ma, due to a scarcity of thermally immature rocks (Zumberge et al. 2020), partially explains this discrepancy. Additionally, these temporal offsets between the molecular and microfossil records may reflect ecological differences in the relative abundance of each clade, habitat preferences, or the delayed evolution of stigmasteroid and other steroid biosynthetic pathways until the Cryogenian (Hoshino et al. 2017). To date, the timing of the red-to-green algal transition has been inferred only from biomarker records of sedimentary successions at different locations. Observing a switch from C_{27} to C_{29} sterane dominance at a single location, captured across multiple samples in two cores over a significant stratigraphic interval, would provide strong evidence for this first-order, secular change in the pre- versus post-Snowball Earth marine biosphere. Therefore, much remains to be learned about the precise timing and drivers of this fundamental change in Neoproterozoic sterane distributions.

Lipid biomarkers reflect the major, ancient biogenic sources of sedimentary organic matter, which 80% or more is typically derived from primary producers (Killops and Killops 2005; Meyers 1997). As such, the relative and absolute abundance of steranes should track local algal productivity. In modern aquatic environments, eukaryotic phytoplankton contributions to biomass are geographically variable and correlate with nutrient availability across multiple scales (Biddanda et al. 2001; Chisholm 1992; Huete-Ortega et al. 2010; Marañón 2015). Regional heterogeneity in S/H values has been observed in Ediacaran sedimentary rocks, with S/H values ranging from <0.3 in Siberia and Baltica basins (Duda et al. 2020; Pehr et al. 2018) to values above 1.0 (mainly in the 0.5–2.0 range) in source rocks and oils from Oman (Grosjean et al. 2009; Love et al. 2009; Stolper et al. 2017) and oils from Eastern Siberia (Kelly et al. 2011). This variability has been interpreted as representing regional differences in competition and abundance between algae and bacteria, with low S/H corresponding to low algal productivity in an oligotrophic environment (Pehr et al. 2018). A similar pattern has been observed for the late Tonian, where higher sterane abundances correspond to higher algal productivity (Zumberge et al. 2020). Moderate-high S/H values, indicative of a substantial algal contribution to photoautotrophy, were found in organic-rich shales from the Walcott Member of the Kwagunt Formation, Chuar Group (Arizona, USA), compared to more organic-lean, siliciclastic rocks from the Visingsö Group (Sweden).

However, existing late Tonian biomarker data are limited to a few successions that do not fully capture the diversity of marine environments, with highly oligotrophic settings notably underrepresented. Environmental heterogeneity within the global ocean must therefore be considered when assessing changes in marine ecosystem composition between the Tonian and Ediacaran. Local drivers of ecosystem change, such as regional nutrient controls on primary productivity and eukaryotic abundance, must be distinguished from first-order secular changes.

In this study, we combined both organic and inorganic geochemical approaches to assess both the magnitude of eukaryotic contribution and the influence of local environmental controls on Neoproterozoic marine microbial ecology. Our analyses focused primarily on high-resolution studies of thermally immature sedimentary rocks deposited in the late Tonian and Ediacaran-Cambrian in the Lena-Anabar Basin, Siberia. Given that ocean oxygenation has been frequently linked to the rise of eukaryotes (Lenton et al. 2014; Lyons et al. 2021; Xiao and Tang 2018), we used iron speciation and redox-sensitive element concentrations to assess local aquatic redox conditions. Because increased phosphorus availability in the late Tonian ocean has also been proposed as a potential driver for eukaryotic expansion (Planavsky et al. 2023;

14724669, 2026, 5, Downloaded from https://onlinelibrary.wiley.com/doi/10.1111/gbi.70061 by NICE, National Institute for Health and Care Excellence, Wiley Online Library on [07/10/2026]. See the Terms and Conditions (https://onlinelibrary.wiley.com/terms-and-conditions) on Wiley Online Library for rules of use; OA articles are governed by the applicable Creative Commons License

Reinhard et al. 2020), we conducted phosphorus phase partitioning measurements to assess phosphorus availability in the basin.

The above geochemical proxies were coupled with lipid biomarker stratigraphic records, as well as carbon and strontium isotope chemostratigraphy, to reconstruct a comprehensive picture of coupled biosphere-and-environmental changes from the late Tonian to the Ediacaran-Cambrian transition. The late Tonian biomarker records from northern Siberia provide a valuable comparison with other environments, such as the Visingsö Group (Zumberge et al. 2020), and are augmented here with new lipid biomarker data from thermally immature shales of the upper Walcott Member of the Chuar Group. This integrated approach allows us to investigate the secular rise of Neoproterozoic eukaryotes while accounting for local paleoenvironmental conditions, thereby improving our understanding of the dynamic, late Tonian marine biosphere.

2 | Geologic Setting

We analyzed sedimentary rocks from two drill-cores, Burskaya-3410 and Khastakhskaya-930, located about 50 km apart in the Lena-Anabar monocline of northern Siberia (Figure 1), drilled in the 1980s by Lenaneftegazgeologiya. The Neoproterozoic succession sampled from these drill-cores was deposited on the eastern margin of the Siberia Craton, facing the open ocean (Merdith et al. 2017, 2021; figure 1).

The analyzed rocks span the late Tonian to earliest Cambrian (ca. 800–539 Ma) interval. We utilized the stratigraphic subdivisions of Nagovitsin et al. (2015), and the age model for these drill-cores was based on their biostratigraphy, augmented with chemostratigraphy presented in our paper. The acritarch *Cerebrosphaera globosa* (= *C. buickii*) is present in the Kulady and lowermost Khastakh formations in both drill-cores (Figure 2), which constrains these units to ca. 800–743 Ma (Dehler et al. 2023; Riedman and Sadler 2018). The upper Khastakh Formation contains microfossil taxa that lack tightly constrained biostratigraphic ranges, but are typical for the Tonian, including *Chuaria circularis*, *Proterocladus major* and *Osculosphaera* sp. (Butterfield et al. 1994), suggesting that this stratigraphic interval is between ca. 800 and 720 Ma in age. Cryogenian (720–635 Ma) strata are not preserved in these cores, and there is a recognized hiatus corresponding to that interval throughout northern Siberia (Kontorovich et al. 2013) where our drill-cores are located. The region lacks Tonian chemostratigraphic and geochronological age constraints, although a negative carbonate carbon isotope excursion, possibly corresponding to the ca. 810 Ma Bitter Springs Excursion (Halverson et al. 2005; Thomson et al. 2015), has been observed in the nearby Kharaulakh Range (Khabarov and Izokh 2014). As described by Nagovitsin et al. (2015), the Kulady Formation consists of interbedded gray shales and sandstones, transitioning into interbedded gray shales and laminated or hummocky cross-stratified limestones, while the overlying Khastakh Formation consists of gray shales interbedded with lenticular and wave-rippled sandstones. Gray and black shales and micritic limestones were sampled for biomarker analysis.

The Taimylyr Formation, present only in the Burskaya-3410 drill-core (Figure 2), was inferred to be Tonian in age by Nagovitsin et al. (2015); however, the only microfossils described from the unit are long-ranging, biostratigraphically uninformative leiospherid and bacterial *Bavlinella* microfossils that do not provide a specific age constraint. The formation lies stratigraphically beneath the Khatyspyt Formation, which contains Avalon-type Ediacaran macrofossils (Grazhdankin et al. 2008), providing a minimum age constraint of the late Ediacaran (Yang et al. 2021) for the Taimylyr Formation. In this study, we present new carbon and strontium isotope data that refine the age of the formation. The Taimylyr Formation consists of microbially laminated dolostones inferred by Nagovitsin et al. (2015) to represent a shallow-marine setting.

The Oppokun Formation, present in the Khastakhskaya-930 drill-core, contains the small shelly fossils *Cambrotubulus decurvatus* and *Anabarites korobovi* (Grazhdankin et al. 2020; Nagovitsin et al. 2015; Rogov et al. 2015). Nagovitsin et al. (2015) interpreted the unit as Ediacaran-Cambrian in age. The Oppokun Formation has been correlated to the Syhargalakh Formation of the Olenek Uplift, which contains an ash bed that gives the unit a depositional U–Pb age of 542.8 ± 1.3 Ma (Bowring et al. 1993; Maloof et al. 2010). However, these data may have been subject to Pb loss (Maloof et al. 2010), and future reanalysis with modern techniques may revise the date. Carbon isotope chemostratigraphy suggests that the underlying Turkut Formation extends to the Cambrian boundary (Bowyer et al. 2022, 2024). Taken together, this suggests that the Oppokun Formation is likely earliest Cambrian in age, though future geochronology may refine this assignment. Laminated gray to black, calcareous shales were sampled for this study; overall the unit consists of interbedded, gray laminated shales, calcareous shales and micritic limestones interbedded with thin sandstones in the lower part, and grading into shales and mudstones up section (Nagovitsin et al. 2015; Grazhdankin et al. 2020).

To assess paleogeographical heterogeneity and environmental controls on lipid biomarker distributions between our sites in Siberia and other paleotropical locations, we also analyzed new outcrop samples from Laurentia, specifically from the Sixtymile Canyon locality of the Chuar Group, Grand Canyon, Arizona (Dehler et al. 2023). Existing paleogeographical reconstructions suggest the Siberian and Chuar locations were at similar low-latitudes between 1000 and 750 Ma (Eyster et al. 2019; Merdith et al. 2021; figure 1). The Chuar Group was deposited in an intracratonic basin that transitioned from non-marine during deposition of the underlying Galeros Formation (Rooney et al. 2017) to marine by the time the upper Walcott Member of the Kwagunt Formation was deposited (Dehler et al. 2017; Dehler et al. 2001). A tuff dated to 729.0 ± 0.9 Ma at the top of the Walcott Member provides a minimum age for our samples (Rooney et al. 2017), and a Bayesian age model of the entire Chuar Group suggests the upper Walcott was deposited after ca. 735 Ma (Dehler et al. 2023). Previous work on the Chuar Group has identified lateral variations in thermal maturity (Wiley et al. 2002) between different outcrop sites, and the Sixtymile Canyon section has been shown to be generally less thermally mature compared to the Nankoweap Butte section (Zumberge et al. 2020). Black shales and carbonate nodules were collected across a 38 m stratigraphic interval, immediately above the upper dolostone doublet, in the upper Walcott

14724669, 2026, 5, Downloaded from https://onlinelibrary.wiley.com/doi/10.1111/gbi.70061 by NICE, National Institute for Health and Care Excellence, Wiley Online Library on [07/10/2026]. See the Terms and Conditions (https://onlinelibrary.wiley.com/terms-and-conditions) on Wiley Online Library for rules of use; OA articles are governed by the applicable Creative Commons License

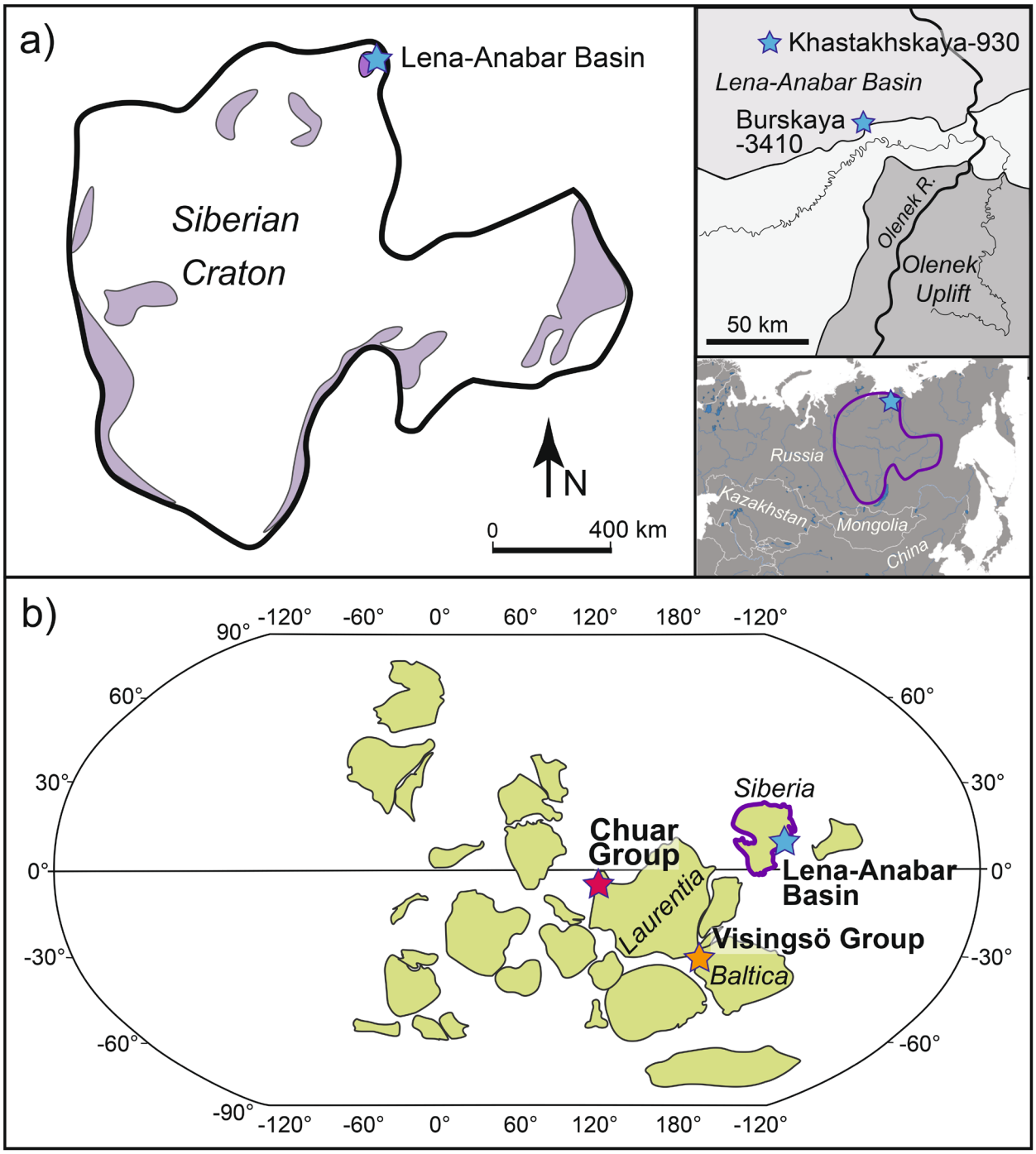


FIGURE 1 | (a) Map of the Siberian Craton showing the location of the Lena-Anabar Basin, with insets showing the location of the Burskaya-3410 and Khastakhskaya-930 drill-cores and the craton's location in modern Asia. Modified from Frolov et al. (2011) and Nagovitsin et al. (2015). Shaded areas in the main map indicate Meso-Neoproterozoic sedimentary deposits. (b) Global continental configuration at 750 Ma (modified from Merdith et al. 2021). Stars show the location of the Lena-Anabar Basin in blue, the Chuar Group in red, and the Visingö Group in orange.

Member of the Kwagunt Formation at the Sixtymile Canyon section. The upper Walcott Member contains vase-shaped microfossils of eukaryotic testate amoebae (Porter and Knoll 2000), and was predominantly deposited under a redox-stratified water column with oxic surface waters overlying anoxic (most commonly ferruginous) bottom waters (Johnston et al. 2010). The upper Walcott Member hosts organic-rich shales with substantial total organic carbon (TOC) content, often lying between 2 and 10 wt% (wt%) (Dehler et al. 2001, 2017), strongly suggesting a highly productive (eutrophic), marine shelf setting.

3 | Materials and Methods

3.1 | Total Organic Carbon Content and HAWK Programmed Pyrolysis Data

To constrain thermal maturity, total organic carbon (TOC) content and HAWK Programmed Pyrolysis parameters were measured at GeoMark Research (Houston, Texas). The TOC content of all samples analyzed for biomarkers was determined using a LECO C230 instrument. Samples were decarbonated with 1 M

14724669, 2026, 5, Downloaded from https://onlinelibrary.wiley.com/doi/10.1111/gbi.70061 by NICE, National Institute for Health and Care Excellence, Wiley Online Library on [07/10/2026]. See the Terms and Conditions (https://onlinelibrary.wiley.com/terms-and-conditions) on Wiley Online Library for rules of use; OA articles are governed by the applicable Creative Commons License

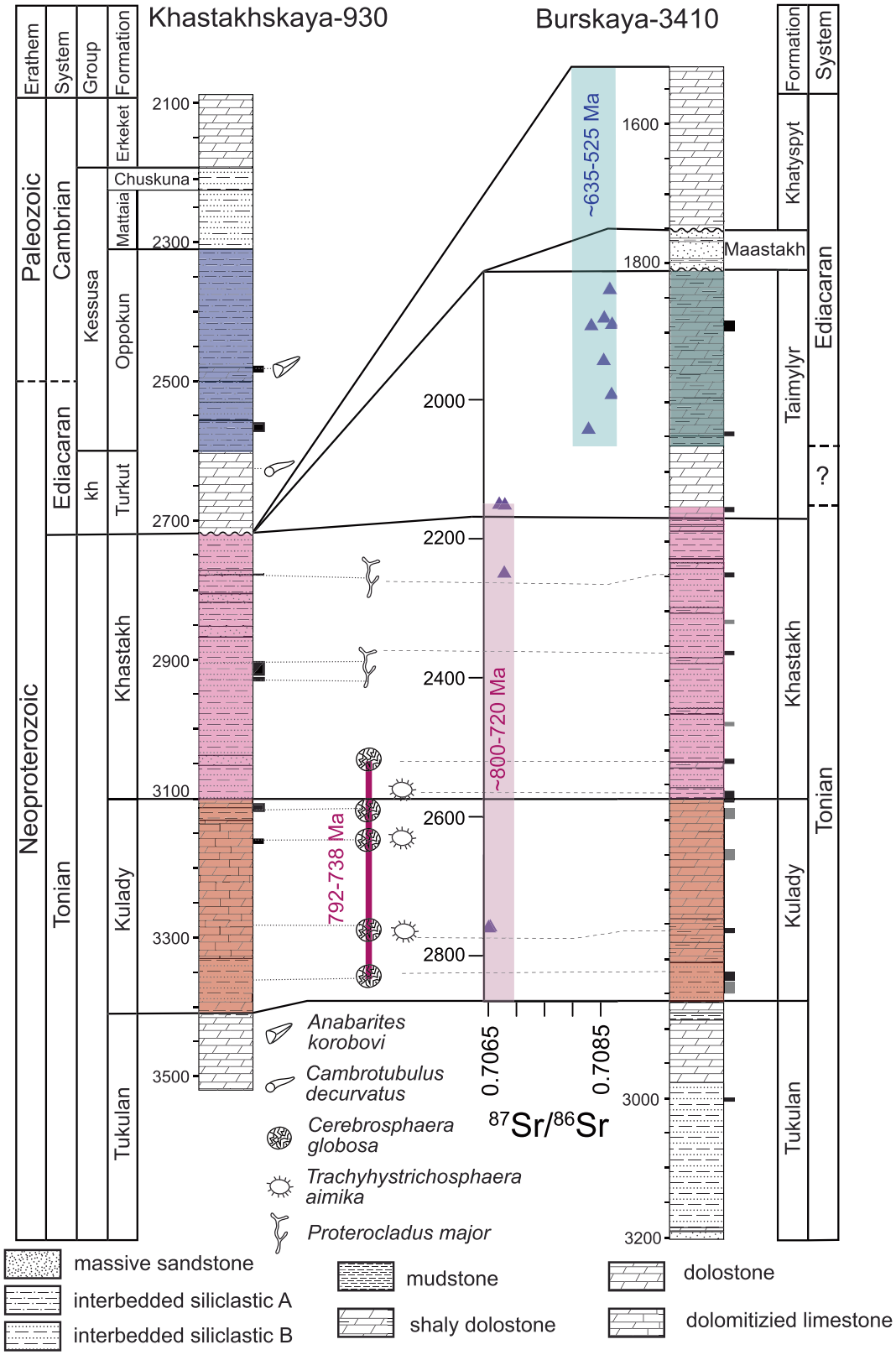


FIGURE 2 | Refined stratigraphy of the Khastakhskaya-930 and Burskaya-3410 drill-cores, modified from Nagovitsin et al. (2015) and Grazhdankin et al. (2020), showing selected, biostratigraphically important microfossil taxa from these references and new Sr. isotope data for the Burskaya-3410 drill-core. All depths in meters (m). Black boxes indicate intervals sampled for biomarkers. Here and in other figures, each formation is shaded a distinct color. Dashed lines in the System for the Burskaya-3410 indicate, based on Sr. isotope composition, the maximum depth of the onset of the Ediacaran at 2150 m and a more conservative boundary estimate at ~2070 m, which corresponds to a lithologic change. The red bar over the *Cerebrosphaera globosa* distribution range indicates its age estimate scaled by the CONOP algorithm (Riedman and Sadler 2018). Age constrains for the Sr. isotope ratios are inferred from Halverson et al. (2010). Kh = Khorbusuonka Group. Interbedded siliclastic A = alternating siltstone and mudstone, interbedded siliciclastic B = interstratified planar-bedded sandstone, siltstone, and mudstone.

14724669, 2026, 5, Downloaded from https://onlinelibrary.wiley.com/doi/10.1111/gbi.70061 by NICE, National Institute for Health and Care Excellence, Wiley Online Library on [07/10/2026]. See the Terms and Conditions (https://onlinelibrary.wiley.com/terms-and-conditions) on Wiley Online Library for rules of use; OA articles are governed by the applicable Creative Commons License

HCl for at least 2 h, with longer extraction times used for samples containing more recalcitrant carbonate minerals, rinsed through a filtration apparatus to remove the acid, dried at low temperature, and weighed to obtain an estimate of the carbonate content based on weight loss. Samples were then combusted on the LECO C230, which was calibrated with standards having known carbon content. Samples and standards were combusted by heating to 1200°C in the presence of oxygen; both carbon monoxide (CO) and carbon dioxide (CO_2) were generated, and the CO was converted to CO_2 with a catalyst. The CO_2 product mass was measured with an infrared cell. Instrument calibration was achieved using a rock standard with values determined from a calibration curve for pure hydrocarbons of varying concentration. An acceptable standard deviation for TOC content is typically ≤3% variation from the established value for rock standards, which cover the TOC range of the rock samples used in our study.

To obtain an independent measure of host-rock maturity, approximately 100 mg of washed, whole-rock powder was analyzed with programmed pyrolysis using a HAWK instrument. Measurements included S1: free bitumen content (mg hydrocarbons/g rock), S2: remaining oil and gas generation potential from labile kerogen (mg hydrocarbons/g rock), T_{max}: temperature at which the maximum signal of the S2 hydrocarbon peak is generated (°C), and S3: organic carbon dioxide yield (mg CO_2/g rock). Hydrogen Index values (HI, in mg/g TOC) were calculated from [(S2 × 100)/TOC] with TOC content expressed in units of wt.%. Production Index (PI) was calculated from [S1/(S1 + S2)]. Instrument calibration was achieved using a rock standard performed after every 10 sample runs.

3.2 | Lipid Biomarker Extraction and Analysis

Lipid biomarker extraction and characterizations followed protocols verified to minimize contamination for Precambrian biomarkers (e.g., Duda et al. 2020; Nguyen et al. 2019; Pehr et al. 2018; Zumberge et al. 2018, 2020). The rock exterior was removed with a water-chilled (solvent-cleaned) diamond saw. Samples were then crushed in a puck mill that was treated with solvents and crushed sand in between samples. Rocks containing veins, obvious external weathering, or that were too small to remove the exterior were excluded from analysis. Procedural blanks of crushed sand, combusted at 800°C for 24 h, were run in parallel to assess the background signal. Solvent extraction of rock bitumen was performed on 5–20 g of rock powder per sample, using a 9:1 (v:v) dichloromethane (DCM):methanol (MeOH) mixture in a CEM Microwave Accelerated Reaction System (MARS) at 100°C for 15 min. Elemental sulfur was removed from the total lipid extract with the addition of activated copper. 0.8–2 mm copper pellets were activated by immersion in 1 M HCl for 1 h, followed by successive washes in deionized water, MeOH, DCM, and *n*-hexanes to remove the acid. The total bitumen extract was separated into aliphatic hydrocarbons, aromatics, and polar fractions on a 1 mL column with 60 mesh silica gel, eluting with *n*-hexane, a 1:1 (v:v) mixture of DCM and *n*-hexane, and a 4:1 (v:v) DCM to MeOH mixture, respectively. Aliphatics were eluted in 1 mL of solvent plus the ~1.5 mL "dead volume", while the other fractions were eluted in 4× the "dead volume" (approximately 6 mL).

Total ion chromatograms of the aliphatic and aromatic hydrocarbon fractions were generated in full-scan mode (monitoring from *m/z* 50–600 amu) on an Agilent 7890A gas chromatography system coupled to an Agilent 5975C inert MSD mass-spectrometer. The GC was equipped with a DB1-MS capillary column (60 m × 0.32 mm internal diameter, 0.25-μm film thickness). Samples were injected as *n*-hexane solutions in splitless injection mode with a programmable temperature vaporizing (PTV) inlet and using He as the carrier gas. The GC temperature program for full-scan analysis was 60°C (held for 2 min), heated to 150°C at 20°C/min, then to 325°C at 2°C/min, and held at 325°C for 20 min.

Aliphatic hydrocarbons were analyzed and biomarker ratios generated by gas chromatography-metastable reaction monitoring- mass spectrometry (GC-MRM-MS) on a Waters Autospec Premier mass-spectrometer equipped with an Agilent 7890A gas-chromatograph and DB-1MS coated capillary column (60 m × 0.25 mm internal diameter, 0.25-μm film thickness), using He as a carrier gas. Analyses were performed via splitless injection and the GC temperature was programmed with an initial hold at 60°C for 2 min, then heating to 150°C at 10°C/min rate, followed by heating to 320°C at 3°C/min rate, and a final hold for 22 min. Mass spectrometry was performed in electron-impact mode, with an ionization energy of 70 eV, a source temperature of 300°C and an accelerating voltage of 8 kV. MRM parent-fragment ion pair transitions were monitored for a suite of biomarker hydrocarbon compounds (comprising C_{27}–C_{35} hopanes, C_{31}–C_{36} methylhopanes, C_{19}–C_{26} tricyclic terpanes, C_{24} tetracyclic terpanes, C_{21}–C_{22} and C_{26}–C_{30} steranes, and C_{30} methylsteranes, including transitions for lanostane and its derivatives), and individual compounds were identified by retention time, published mass spectra (for lanostane, Parfenova 2011), and comparison to in-house standards. Lanostane was additionally identified by co-elution with a pure lanostane (ααα R) standard (from Chiron AS, Norway). Compounds were quantified using relative peak areas in comparison with a deuterated C_{29} sterane standard, d_4-ααα-24-ethylcholestane (20*R*), assuming equal response factors for analytes versus this standard compound. Individual peaks had to have a minimum signal of at least five times the area of equivalent peaks in the corresponding full procedural blank, and compound series at least 10 times the total area of the equivalent series in the blank, to qualify as a positive occurrence. Full procedural blanks typically yielded less than 0.1 ng of individual hopane or sterane compounds per gram of rock/combusted silica.

To verify the identity of C_{27} sterane isomers, selected samples were additionally analyzed under a different temperature program with an initial hold at 60°C for 2 min, then heating to 150°C at 10°C/min rate, followed by heating to 320°C at 2°C/min rate, and a final hold for 14 min.

3.3 | Kerogen-Bound Biomarker Analysis

Complementary to bitumen analysis, kerogen-bound biomarkers were liberated from selected samples which had been exhaustively solvent-extracted and then subjected to continuous-flow catalytic hydropyrolysis (HyPy; Love et al. 1995). Kerogen, or insoluble macromolecular organic matter, makes up the

14724669, 2026, 5, Downloaded from https://onlinelibrary.wiley.com/doi/10.1111/gbi.70061 by NICE, National Institute for Health and Care Excellence, Wiley Online Library on [07/10/2026]. See the Terms and Conditions (https://onlinelibrary.wiley.com/terms-and-conditions) on Wiley Online Library for rules of use; OA articles are governed by the applicable Creative Commons License

vast majority (typically >90 wt% in ancient rocks) of organic matter in sediments (Burdige 2007). Lipid biomarkers are incorporated into kerogen from the earliest stages of early diagenesis (Farrimond et al. 2003; Lee, Love, Jahnke, et al. 2019; Lee et al. 2021), and HyPy is an established temperature-programmed and continuous-flow method that avoids disrupting the main structural and stereochemical features of bound biomarkers (Love et al. 1995, 2005). Kerogen-bound biomarkers provide a useful self-consistency check for verifying biomarker pedigree, as these are bound covalently within a pre-extracted immobile matrix which is unaffected by oil migration and drilling fluids. The HyPy-released bound biomarker pool has been used in a number of Precambrian biomarker studies as a valuable self-consistency check to assess syngeneity of hydrocarbon constituents in the bitumen phase and to assess possible contaminant contributions (Duda et al. 2021; French et al. 2015; Love et al. 2009; Nguyen et al. 2019; Zumberge et al. 2018, 2020).

The HyPy procedure for hydrogen-gas pyrolysis of solvent-extracted rocks and kerogen concentrates in a continuous-flow configuration has been described in detail previously (French et al. 2015; Grotheer et al. 2015; Love et al. 1995, 2009; Zumberge et al. 2020). Pre-extracted rock powders were heated in a stainless-steel reactor tube from ambient temperature to 250°C at 100°C/min then to 520°C at 8°C/min, a hydrogen gas pressure of 15 MPa with a continuous hydrogen sweep gas flow of 6 L/min to recover products quickly from the hot zone. The hydropyrolysate generated from 1.0 g of powdered sample was flushed out and adsorbed onto silica gel (36–70 mesh, activated at 450°C overnight) contained within a dry ice-cooled product trap. The hydropyrolysate was separated into three fractions (aliphatics, aromatics, and polars) using the same silica gel column chromatography and analyzed by the same GC-MRM-MS methods described above. Full procedural HyPy blanks were conducted as separate runs using combusted silica gel as the heated solid substrate.

3.4 | Carbon, Oxygen and Strontium Isotope Analyses of Bulk Rocks

Carbon isotope values were measured on bulk organic carbon ($\delta^{13}C_{org}$) and, where possible, carbonate carbon ($\delta^{13}C_{carb}$). All carbon isotope values are reported relative to the Vienna Pee Dee Belemnite (VPDB) standard. For organic carbon isotope analysis, 30 mL of 6 N HCl was added to approximately 1 g of powdered rock and decarbonated overnight. The mixture was repeatedly centrifuged and rinsed with deionized water until supernatant pH reached 7, then dried in an oven and weighed. The decarbonated powders were analyzed with a Costech ECS4010 Elemental Analyzer (EA) coupled to a Thermo Scientific Delta V Advantage Isotope Ratio Mass Spectrometer (IRMS) through a Thermo Scientific Conflo IV device. In the EA combustion reactor, TOC reacts with O_2 at a set temperature of 1000°C (1800°C with tin sample capsule burning), forming CO_2, which is carried by helium carrier gas to the Conflo IV and further to the IRMS to determine the $\delta^{13}C$ value. Three certified standards (USGS40, USGS41a and SDO-1) and one internal lab standard (EMSOIL) were utilized in the same runs and the $\delta^{13}C_{org}$ precision was ~0.2‰. Samples with $\delta^{13}C$ values above −20‰ were subjected to a second round of acidification of the already decarbonated powders to exclude the possibility of carbonate contribution to $\delta^{13}C_{org}$ values, and only values obtained following the second round are reported for these samples. TOC content was measured by EA as well as by LECO; EA TOC values are on average of 0.06 wt% higher than LECO values, which is negligible for our purposes, but allows a cross-check on the accuracy of LECO values.

For $\delta^{13}C_{carb}$ and oxygen isotope analysis, whole-rock powders were treated with 104% phosphoric acid at 50°C for 24 h in a Thermo Scientific GasBench II device, followed by the analysis of the product CO_2 gas for $\delta^{13}C$ and $\delta^{18}O$ isotope compositions with a Thermo Scientific Delta V Advantage IRMS. Two calibration standards, NBS18 and IAEA603 (NBS19 replacement), were included in the same runs. Generally, the precision for $\delta^{13}C_{carb}$ was ~0.1‰ and for $\delta^{18}O$ was ~0.2‰.

Strontium isotope analyses of carbonates were performed using a stepwise dissolution procedure (Gorokhov et al. 1995). First, the sample powder (~100 mg) was treated twice with 1 N ammonium acetate at room temperature for 30 min. This leachate (called AMA phase) represents the late epigenetic generation of carbonate minerals since it has higher radiogenic Sr. and Rb contents (Gorokhov et al. 1995, 2022; Kuznetsov et al. 2003, 2006, 2013, 2019). Following this step, samples were dissolved in 10% acetic acid (Kuznetsov et al. 2003; Montañez et al. 1996). This leachate (called ACA phase) could still contain a contribution from epigenetic minerals, but mainly targets the primary carbonate fraction and so is more likely to record seawater Sr. isotope composition. Sr. isotope composition of the ACA-phase was measured without a spike using a Triton Ti mass-spectrometer. Average $^{87}Sr/^{86}Sr$ ratios of NIST SRM-987 and USGS EN-1 standards measured during this study and normalized to the $^{86}Sr/^{88}Sr$ ratio of 0.1194 were 0.710272 ± 0.000005 (2σ, $n = 23$) and 0.709197 ± 0.000007 (2σ, $n = 16$), respectively. Reproducibility of $^{87}Sr/^{86}Sr$ based on duplicate analyses of the ACA fraction was better than 0.00004.

3.4.1 | Iron Speciation and Major and Trace Element Analyses

Iron speciation analyses were conducted via the sequential extraction procedure of Poulton and Canfield (2005), where acid-volatile sulphides (Fe_{AVS}; below detection in all cases) and pyrite Fe (Fe_{py}) were quantified gravimetrically via a two-step chromous chloride distillation (Canfield et al. 1986). The sequential extraction protocol extracts different, operationally defined Fe pools, including carbonates such as siderite (Fe_{carb}), ferric oxides such as goethite and hematite (Fe_{ox}), and magnetite (Fe_{mag}). These phases define an Fe pool considered "highly reactive" (Fe_{HR}) to sulfidization during sedimentation and diagenesis (Raiswell and Canfield 1998), determined as the sum of $Fe_{carb} + Fe_{ox} + Fe_{mag} + Fe_{py}$. A boiling HCl extraction was performed to determine an Fe pool (consisting largely of sheet-silicate Fe) that is poorly reactive during diagenesis (Fe_{PRS}; Raiswell and Canfield 1996), but which includes Fe-rich clay minerals that may have been formed from non-sulfidized Fe_{HR} during diagenesis (Doyle et al. 2018; Poulton et al. 2010). Iron solutions were analyzed by atomic adsorption spectrometry (AAS). Accuracy was ensured by comparison to international reference material, WHIT (Alcott et al. 2020), with a RSD of <5% for all analyses (including Fe_{carb}, Fe_{ox}, Fe_{mag}, Fe_{py}, and total Fe; Fe_T). Carbonate rocks with TOC < 0.5 wt% (measured by EA)

14724669, 2026, 5, Downloaded from https://onlinelibrary.wiley.com/doi/10.1111/gbi.70061 by NICE, National Institute for Health and Care Excellence, Wiley Online Library on [07/10/2026]. See the Terms and Conditions (https://onlinelibrary.wiley.com/terms-and-conditions) on Wiley Online Library for rules of use; OA articles are governed by the applicable Creative Commons License

and $Fe_T < 0.5$ wt% were excluded from analysis, as these can lead to spurious results (Clarkson et al. 2014).

To determine major and trace elements, samples were ashed at 550°C for 8 h, followed by quantitative digestion using concentrated HNO_3, HF, and $HClO_4$. H_3BO_3 was added to prevent the formation of Al-hexafluorate complexes. Finally, the residues were re-dissolved with near-boiling HNO_3 and diluted with ultrapure 18MΩ H_2O prior to analysis by inductively coupled plasma–optical emission spectrometry (ICP-OES) for major elements (specifically Al, P, Fe) and inductively coupled plasma–mass spectrometry (ICP-MS) for trace elements (specifically V, Mo, U). Accuracy and precision, estimated from repeat analyses of USGS standard SGR- 1b (Green River Shale), were better than 5% for all reported elements.

3.4.2 | Phosphorus Phase Partitioning

We used a modified SEDEX sequential extraction scheme for ancient rocks (Thompson et al. 2019) to analyze phosphorus partitioning. Briefly, samples were extracted at room temperature in a pH 7.6 citrate-dithionite-bicarbonate (CDB) buffer for 8 h to remove Fe-bound P (P_{Fe}). After each step, residues were washed up to three times with 1 M $MgCl_2$ and then with water until the concentration of P in solution was less than 0.2 ppm to reverse secondary re-adsorption of extracted P. For the next step, residues were extracted in a pH 4.0 Na-acetate solution for 6 h to dissolve authigenic, carbonate-associated and biogenic P (P_{auth}). The residue was then extracted in 1 M HCl for 16 h to release detrital, crystalline apatite (P_{cryst}). This was followed immediately by a 6 h extraction in 0.2 M ammonium oxalate/0.17 M oxalic acid solution (Poulton and Canfield 2005) to release P associated with magnetite (P_{mag}). After additional washes, the residue was ashed at 550°C for 2 h and then extracted in 1 M HCl for 16 h to recover organic P (P_{org}). Total phosphorus (P_{total}) was determined in a separate HNO_3-HF-$HClO_4$-H_3BO_3-HCl extraction on whole-rock samples. For the late Tonian Khastakh Formation, phosphate recovery ($\sum P/P_{total}$) dropped to consistently below 66%, which is unusual given that this sequential extraction scheme typically yields recovery above 75% (Thompson et al. 2019). We thus added an additional HNO_3-HF-$HClO_4$-H_3BO_3-HCl extraction step on the residue from the P_{org} extraction (e.g., Guilbaud et al. 2020) for these samples to extract any remaining recalcitrant P phases associated with silicate minerals and Al oxides, termed P_{det2} to differentiate from the P_{det} of Thompson et al. (2019), which corresponds to our P_{cryst}. When the P_{det2} fraction is included, the average recovery was 95% ± 6%. Reactive P (P_{reac}) was calculated as the sum of P_{Fe}, P_{auth}, P_{mag}, and P_{org}. Phosphorus concentrations were determined spectrophotometrically using the molybdate-blue method on a Spectonic GENESYS 6 at 880 nm, except for the CDB step, which was measured using ICP-OES. Replicate extractions gave a RSD of < 5% for all steps.

4 | Results

4.1 | Chemostratigraphy

In the Tonian strata, a secular increase of *ca.* 15‰ in $\delta^{13}C_{org}$ values is observed in both drill-cores. Values range from as low as −32.8‰ at the base of Burskaya-3410 core in the Tukulan Formation and to as high as −15.5‰ in the upper Khastakh Formation (Figure 3i, Table S1). In the Taimylyr Formation, $\delta^{13}C$ org values range from −29.0‰ to −21.7‰. Carbon isotope values in the earliest Cambrian Oppokun Formation range from −33.1‰ to −25.6‰ and show no clear stratigraphic trend. In the Burskaya-3410 drill-core, an 8.3‰ shift is observed between depths of 2244 and 2150 m, similar in magnitude to the difference between the Tonian Khastakh Formation and the earliest Cambrian Oppokun Formation in the Khastakhskaya-930 drill-core.

To better constrain the age of the Taimylyr Formation and its boundary with the underlying Khastakh Formation, carbonates from the Burskaya-3410 drill-core were analyzed for $\delta^{13}C_{carb}$ and $^{87}Sr/^{86}Sr$ ratios. Because Tonian units are largely siliciclastic, only a limited number of $\delta^{13}C_{carb}$ data points are available. In the Khastakhskaya-930 drill-core, $\delta^{13}C_{carb}$ values for carbonates in the upper Kulady Formation range between 5‰ and 6‰ (Figure 3iii, Table S1). In the Taimylyr Formation, $\delta^{13}C_{carb}$ values vary from 2.7‰ to 5.7‰. The few $\delta^{13}C_{carb}$ values obtained

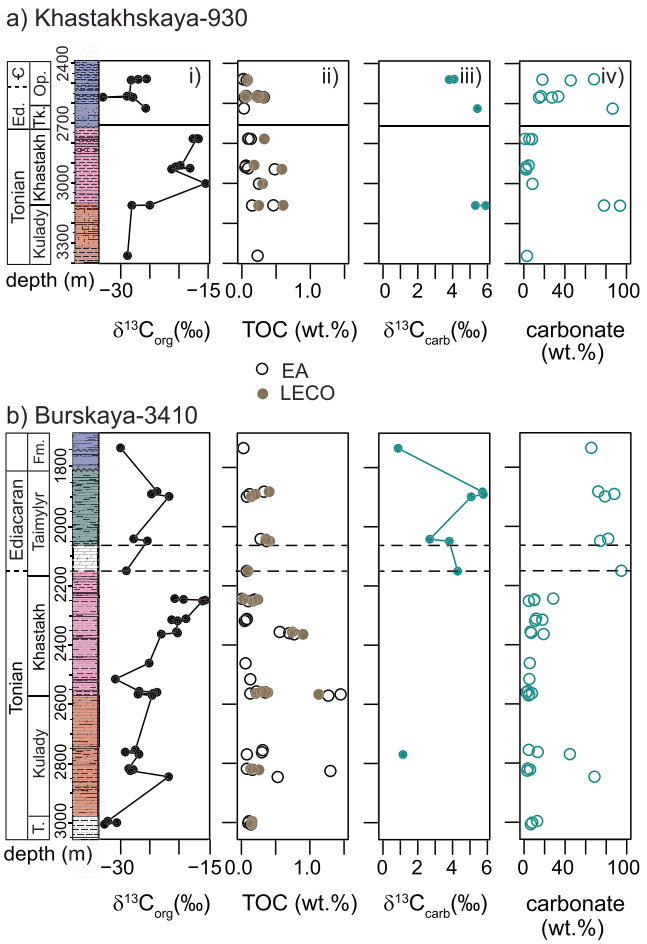


FIGURE 3 | Selected chemostratigraphy for the (a) Khastakhskaya-930 and (b) Burskaya-3410 drill-cores. Ed. = Ediacaran, T. = Tukulan Formation, Tk. = Turkut Formation, Op. = Oppokun Formation. See Figure 2 caption for more detailed explanation of stratigraphy. (i) $\delta^{13}C$ of bulk organic matter (‰ VPDB) (ii) wt.% TOC content of bulk rock, measured by EA-IRMS. (iii) $\delta^{13}C$ of carbonates (‰ VPDB) (iv) wt.% carbonate content of bulk rock.

14724669, 2026, 5, Downloaded from https://onlinelibrary.wiley.com/doi/10.1111/gbi.70061 by NICE, National Institute for Health and Care Excellence, Wiley Online Library on [07/10/2026]. See the Terms and Conditions (https://onlinelibrary.wiley.com/terms-and-conditions) on Wiley Online Library for rules of use; OA articles are governed by the applicable Creative Commons License

from the Oppokun Formation are close to 4‰, with an overall variation of only 0.28‰.

For strontium isotope composition, following Kuznetsov et al. (2017), carbonate samples are considered relatively unaltered with and capable of recording seawater Sr isotope composition if they have Mn/Sr < 5; based on this criteria, samples were selected for Sr isotope analyses (Figure S1). All but one sample also meet the more stringent Mn/Sr < 3 threshold of Kaufman et al. (1993). Although carbon and oxygen isotope values were not measured on the same samples analyzed for strontium isotope ratios, carbonate samples analyzed for C and O isotopes have values above the above −10‰ VPDB cutoff proposed by Kuznetsov et al. (2017) for carbonates likely to preserve a seawater signal (Table S1). Limestones of the Kulady and Khastakh formations are well-preserved, as indicated by Mn/Sr < 0.2 and Fe/Sr < 5 (Kuznetsov et al. 2003).

Dolostones of the Taimylyr Formation exhibit Mn/Sr ratios ranging from 0.8 to 4.1, and Fe/Sr ratios ranging from 21 to 38. Although Fe/Sr and Mn/Sr show no correlation with $^{87}Sr/^{86}Sr$ values within the Taimylyr Formation (Figure S1), there is an overall positive association between Fe/Sr and both Mn/Sr. and $^{87}Sr/^{86}Sr$ across the entire drill-core. The Taimylyr Formation consistently exhibits higher values for all these parameters, suggesting that partial disturbance of the Sr isotope system is possible. Nevertheless, all but one Taimylyr Formation dolostone sample selected for Sr isotope analysis meet the Mn/Sr < 2–3 threshold proposed by Gorokhov et al. (2022) and Kaufman and Knoll (1995), indicating that these samples preserve a primary seawater Sr isotope signal.

Having established that the samples most likely preserve a robust seawater Sr isotope signature. $^{87}Sr/^{86}Sr$ values in the Burskaya-3410 drill-core between 2760 and 2151 m—spanning the Kulady and Khastakh formations—range from 0.70651 to 0.70680 (Figure 2). At 2050 m depth, however, Sr concentrations decrease by approximately an order of magnitude (Table S2), indicating a change in primary carbonate mineralogy and potentially in environmental conditions. Above 2043 m, $^{87}Sr/^{86}Sr$ values increase markedly from 0.70829 to 0.70870.

4.2 | Organic Geochemistry

Both drill-cores contain thermally well-preserved strata within the early- to middle-oil window maturity. T_{max} values (Table 1) derived from HAWK pyrolysis for the Burskaya-3410 drill-core range from early-mid oil window maturity (T_{max} = 436°C–441°C, Espitalie et al. 1977; Peters 1986; Peters and Cassa 1994) at the base of the sampled interval to early oil window in the Taimylyr Formation (T_{max} = 434°C–435°C). The Khastakhskaya-930 drill-core succession, which experienced slightly greater burial, yields consistently higher Tmax values of 445°C–448°C, although these values may be influenced by thermal maturity and source composition effects. It should be noted that T_{max} does not represent the actual burial temperatures experienced during subsurface maturation; rather, it is a parameter obtained using an industry-standard pyrolysis technique but applied elevated temperature and a helium sweep gas to simulate oil generation on a rapid timescale. The S2 peak exceeds 0.2 mg HC/g rock for all samples except Bur-29 (S2 = 0.17 mg/g), suggesting that T_{max} values are generally reliable for this sample set (Peters 1986).

HI, a measure of labile kerogen content, ranges from 44 to 376 mg/g TOC, with the highest values observed in the Ediacaran Taimylyr Formation. These elevated HI values correspond to the highest biomarker yields within this dataset (Table S5). HI values do not show a simple or systematic decrease with depth, which is expected given the strong influence of organic matter type, extent of microbial reworking, and thermal maturity on HI. PI values are < 0.15 for all samples, indicating an absence of migrated bitumen and a low-moderate thermal maturity of the host rocks (Espitalie et al. 1977; Peters 1986), even in samples with low HI values (< 100 mg/g TOC).

Biomarker maturity indicators (Table 1, Figure 4) are broadly consistent with T_{max} values indicating overall maturities ranging from early to middle oil window. The C_{31} αβ S/S + *R* hopane isomer ratio is close to its equilibrium value (Peters et al. 2005) of ~0.6 throughout both drill-cores. In the Burskaya-3410 drill-core, C_{27} ααα S/(S + *R*) sterane isomer ratios (5α(H), 14α(H),17α(H)-20S/5α(H), 14α(H),17α(H)-20S + 5α(H), 14α(H),17α(H)-20R) for the bitumen phase range from 0.40 to 0.49, whereas in the Khastakhskaya-930 drill-core approach the thermal equilibrium value of 0.54 (Peters et al. 2005), indicating a maturity near peak (middle) oil window conditions. Calculated vitrinite reflectance equivalents (%R_c) derived from the methylphenanthrine index (MPI-1) range from 0.59% to 0.87%, with a mean of 0.75% in the Burskaya-3410 drill-core and 0.73% (*n* = 2) in the Khastakhskaya-970 drill-core. The Chuar Group shales used here for comparative biomarker analysis exhibit very similar thermal maturity with vitrinite reflectance equivalent of ~0.8% (Table S4). Overall, the level of thermal maturity is well matched across the rock sample set used for geochemical investigation in this study.

Steranes are detectable in all but one of 13 samples from the Lena-Anabar Basin, highlighting the near-ubiquity of steranes in the late Tonian in northern Siberia (Table 1). The sole exception, sample Khast-17, also exhibits a very low hopane yield (0.62 ppm of TOC, Table S5), suggesting generally poor lipid preservation rather than a true absence of steranes. All samples yielded a typical suite of *n*-alkanes in addition to the other biomarkers discussed here (Figure S2).

C_{27} steranes are the primary sterane in all the Tonian units, and their presence as a primary constituent is confirmed by HyPy fragmentation of the corresponding (insoluble) kerogen phase (Figure 4). Low abundance of ergostane (C_{28}, 24-methylcholestane, reaching up to 46% of total steranes but at a low absolute concentration of 0.02 ppm of TOC) occurs in a subset of Khastakh Formation samples from both drill-cores. Cryostane (C_{28}, 26-methylcholestane), an unusual C_{28} sterane that may be a diagenetic alteration product from C_{27} steranes or a primary sterane structure (Adam et al. 2018; Brocks et al. 2016; Zumberge et al. 2018, 2020), is present in some, but not all, samples at 11% or less of the total sterane pool. C_{29} steranes are absent from all Tonian rock samples in both drill-cores, and peaks observed in the mass 400 > 217 ion chromatograms instead reflect background hopane signals (Figure 4). In contrast,

14724669, 2026, 5, Downloaded from https://onlinelibrary.wiley.com/doi/10.1111/gbi.70061 by NICE, National Institute for Health and Care Excellence, Wiley Online Library on [07/10/2026]. See the Terms and Conditions (https://onlinelibrary.wiley.com/terms-and-conditions) on Wiley Online Library for rules of use; OA articles are governed by the applicable Creative Commons License

TABLE 1 | Selected organic source, environmental and thermal maturity parameters. wt.% TOC (total organic carbon content from LECO). HI = hydrogen index (mg S_2 hydrocarbons ×100/g TOC). T_{MAX} (°C) = temperature at which labile kerogen pyrolysis signal (S_2) records its highest value using standard HAWK pyrolysis. Production index (PI) = ($S_1/S_1 + S_2$). $\%R_c$ = calculated vitrinite reflectance (%), ($\%R_c = 0.6*MPI\text{-}1 + 0.40$), where MPI-1 = 1.5*(3-methylphenanthrene +2-methylphenanthrene)/(phenanthrene+9-methylphenanthrene+1-methylphenanthrene). S = sterane, H = hopane. C_{27} Ts = 18α(H)-trisnorneohopane; C_{27} Tm: 17α(H)-trisnorhopane; C_{30} αβ H = 17α(H),21β(H)-hopane; C_{31} H = 17α(H),21β(H)-homohopane; G.R. = 3-MeHI (%) = 100 × $\sum C_{32}$ 3β-methyl hopanes/($\sum C_{31}$ αβ hopanes + $\sum C_{32}$ 3β-methyl hopanes). C_{26}/C_{25} TT = C_{26}/C_{25} tricyclic terpane. S/H (B) = $\sum C_{27}$-C_{29} regular steranes and diasteranes, including cryostane/$\sum$(C_{27}-C_{35} αβ hopanes, including C_{27} Ts), shown in Figure 6. S/H (C), shown in Figure 8, includes all C_{26}-C_{29} regular steranes and diasteranes including cryostane in the numerator and is equivalent to S/H (1) in Zumberge et al. (2020). % C_{27} sterane = C_{27} sterane/$\sum C_{27}$-C_{29} steranes, %, and similarly for other steranes. Asterisks indicate values below detection limits.

Core	Age	Formation	Sample	Depth (m)	Carbonate (wt.%)	TOC (wt.%)	HI (mg/g TOC)	Production Index	T_{MAX} (°C)	% Rc	C_{31} H 22S/(S+*R*)	C_{27} S ααα S/(S+*R*)	Dia/reg C_{27} S	C_{27} S αββ/ααα	C_{27} H Ts/(Ts+Tm)	Gam./C_{30} αβ H	3-MeHI (%)	C_{26}/C_{25} TT	S/H (B)	S/H (C)	$\%C_{27}$	$\%C_{28}$ ergostane	$\%C_{28}$ cryostane	$\%C_{28}$ total	$\%C_{29}$
Burskaya-3410	Ediacaran	Taimylyr	Bur-76	1882.0	70.9	0.41	—	—	—	0.73	0.59	0.45	1.35	0.60	0.33	0.28	4.3	0.57	0.92	0.97	18%	16%	0%	16%	66%
			Bur-75	1890.4	83.3	0.21	—	—	—	0.65	0.59	0.47	1.03	0.66	0.25	0.23	1.2	0.60	0.51	0.52	12%	11%	0%	11%	78%
			Bur-74	1898.7	77.5	0.14	—	—	—	0.84	0.60	0.46	1.94	0.51	0.19	0.46	2.2	0.42	0.47	0.48	21%	17%	0%	17%	62%
			Bur-68	2042.0	76.0	0.36	376	0.09	434	0.76	0.59	0.47	0.31	0.43	0.22	0.94	1.8	0.58	0.63	0.64	8%	12%	0%	12%	81%
			Bur-67	2049.0	70.9	0.41	286	0.06	435	0.76	0.59	0.43	0.49	0.49	0.29	0.24	1.3	0.64	0.55	0.55	8%	13%	0%	13%	79%
	Late Tonian	Khastakh	Bur-63	2246.7	9.3	0.24	—	—	—		0.60	0.49	0.20	0.14	0.01	0.02	2.7	1.23	0.01	0.01	100%*	0%*	0%	0%*	0%
			Bur-61	2249.3	9.8	0.17	—	—	—	—	0.61	0.46	0.15	0.07	0.02	0.01	2.2	0.96	0.01	0.01	95%	0%*	5%	5%	0%
			Bur-56	2356.0	5.7	0.75	44	0.06	441	0.87	0.58	0.43	0.14	0.04	0.02	0.03	5.2	1.28	0.02	0.02	90%	9%	2%	10%	0%
			Bur-54	2364.0	5.6	0.90	—	—	—	0.79	0.58	0.41	0.19	0.06	0.02	0.02	3.9	1.07	0.01	0.01	97%	0%*	3%	3%	0%
			Bur-44	2557.0	4.5	0.30	116	0.03	434	—	0.58	0.40	0.63	0.05	0.08	0.03	9.4	0.78	0.01	0.01	100%*	0%*	0%	0%*	0%
			Bur-43	2560.5	3.8	0.39	—	—	—	—	0.59	0.48	0.52	0.24	0.02	0.00	3.8	0.56	0.01	0.01	64%	32%	3%	36%	0%
			Bur-40 kerogen	2567.0	1.1	1.13	281	0.02	436	—	0.44	0.38	0.00	0.02	0.00	0.00	9.2	0.98	0.02	0.02	93%	0%*	7%	7%	0%
			Bur-40							0.59	0.59	0.45	0.73	0.07	0.03	0.01	8.5	0.69	0.01	0.01	100%*	0%*	0%	0%*	0%
		Kulady	Bur-29	2822.0	4.4	0.26	66	0.15	431	—	0.59	—	—	—	0.03	0.00	6.1	0.45	0.02	0.02	100%*	0%*	0%	0%*	0%
Khastakhskaya-930	Earliest Cambrian	Oppokun	Khast-41	2565.1	41.2	0.21	—	—	—	—	0.59	0.51	0.12	0.40	0.04	0.10	1.0	0.91	0.06	0.06	27%	6%	0%	6%	67%
			Khast-40	2569.7	25.1	0.31	118	0.07	445	—	0.60	—	—	0.66	0.08	0.12	0.6	0.96	0.03	0.03	15%	12%	0%	12%	73%
	Late Tonian	Khastakh	Khast-33	2778.0	8.0	0.33	—	—	—	—	0.59	0.49	0.61	0.45	0.15	0.06	3.9	0.74	0.05	0.05	54%	46%	0%	46%	0%
			Khast-30	2909.0	7.5	0.18	—	—	—	0.74	0.60	0.54	0.55	0.46	0.09	0.03	3.4	0.94	0.03	0.03	59%	41%	0%	41%	0%
			Khast-17	2929.6	6.6	0.58	—	—	—	—	0.59	—	—	0.76	0.16	0.00	5.2	0.69	0.00	0.00	0%*	0%*	0%	0%*	0%
		Kulady	Khast-10	3109.7	76.3	0.60	204	0.11	446	0.69	0.60	0.47	1.59	1.85	0.60	0.19	7.0	0.83	0.03	0.03	89%	0%*	11%	11%	0%
			Khast-9	3110.7	82.2	0.25	118	0.12	448	—	0.60	0.46	1.68	1.25	0.68	0.00	8.8	0.91	0.04	0.04	92%	3%	5%	8%	0%

14724669, 2026, 5, Downloaded from https://onlinelibrary.wiley.com/doi/10.1111/gbi.70061 by NICE, National Institute for Health and Care Excellence, Wiley Online Library on [07/10/2026]. See the Terms and Conditions (https://onlinelibrary.wiley.com/terms-and-conditions) on Wiley Online Library for rules of use; OA articles are governed by the applicable Creative Commons License

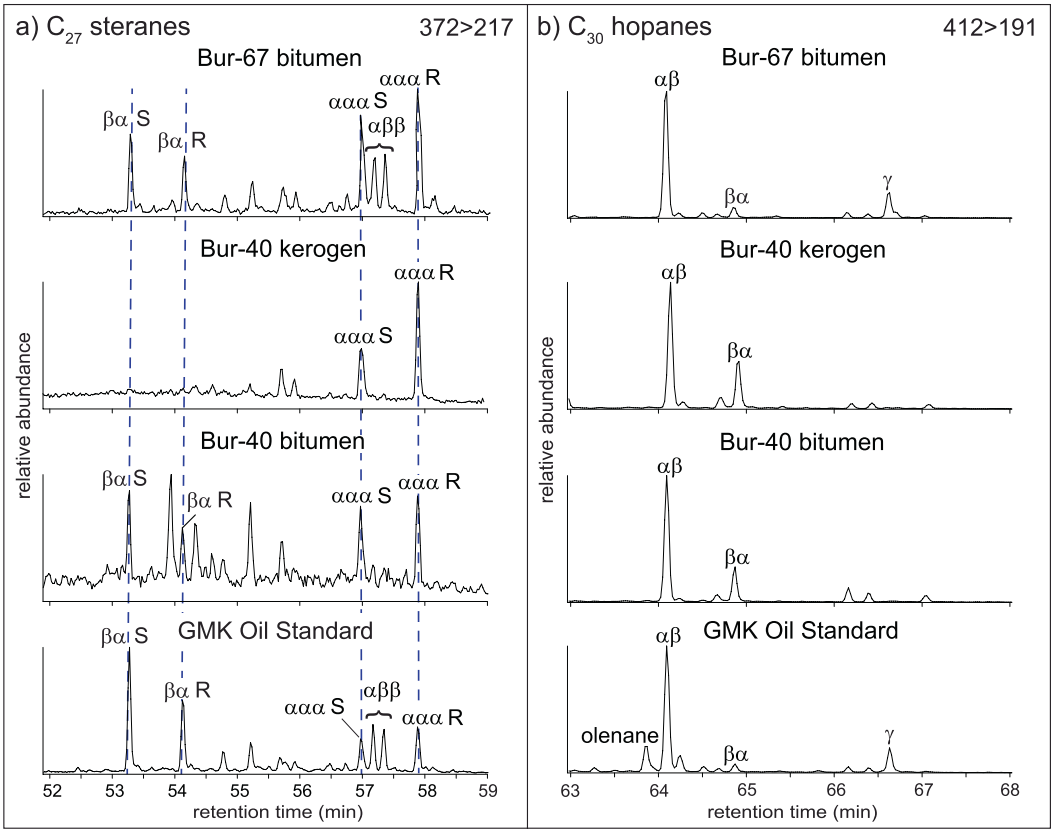


FIGURE 4 | GC-MRM-MS chromatograms comparing compound distributions for: (a) C_{27} steranes, using m/z 372 > 217 transition, and (b) C_{30} hopanes, using m/z 412 > 191 transition, for an Ediacaran sample (Bur-67, for extractable bitumen), and a late Tonian sample (Bur-40, for both bitumen and kerogen). The in-house mixed oil standard (GMK Oil Standard) is shown for compound identification verification. γ = gammacerane. Note, the absence of diasteranes (βα S and βα R) in the kerogen product, since diasteranes (and diahopanes) predominantly occur only as free hydrocarbons in the extractable bitumen, but not as kerogen-bound constituents (Duda et al. 2016; Love et al. 1995, 2009; Wang et al. 2025; Zumberge et al. 2020). The ααα S peak identification for cholestane in Bur-40 was confirmed using an authentic standard and analyzed using different GC conditions (Figure S3).

all seven Ediacaran-Cambrian samples from the Taimylyr and Oppokun formations contain a diverse series of C_{27}–C_{29} steranes, with C_{29} commonly the most abundant steranes (Figures 4 and 5). C_{30} steranes are generally absent or present only at trace levels, consistent with the previous observations from late Ediacaran rocks of the Khatyspyt Formation from Siberia (Duda et al. 2020). Notably, all three series of C_{30} steranes—24-n-propylcholestane (24-npc), 24-isopropylcholestane (24-ipc), and 26-methylstigmastanes (26-mes)—are absent from all the Tonian rock samples analyzed in this study.

Lanostanes (C_{30} methylsteranes), derived from lanosterol and/or cycloartenol sterol precursors, may be sourced from bacteria and/or eukaryotes (Wei et al. 2016, and references therein) are not present as significant hydrocarbon constituents in any of the samples analyzed in this study (Figure S4). Lanostane is detected only at trace levels (< 0.2% of total C_{27}–C_{30} steranes) in biomarker-rich samples from the Ediacaran Taimylyr Formation. Lanostane is not detectable above trace levels (< 0.5% of steranes) in any of the Tonian samples, including those with elevated 3-MeHI values, and is below the detection limits in most of the rock extracts.

Gammacerane ratio (G.R. = Gammacerane/C_{30} αβ hopane) are commonly used to identify hypersaline and highly restricted basinal settings (Sinninghe Damsté et al. 1995; Tulipani et al. 2015). In the Tonian strata, G.R. values are generally very low- (< 0.05), with the exception of sample Khast-10, which yields a low-to-moderate value of 0.2 (Table 1, Figure 6). In contrast, the Taimylyr Formation exhibits substantially elevated and variable gammacerane contents, with G.R. values ranging from 0.23 to 0.94 (Figure 6; Table 1). GRs for the Oppokun Formation are higher than those for the Tonian strata (mean = 0.11), but remain markedly lower than those observed in the Taimylyr Formation.

Most samples display low to moderate 3β-methylhopane index (3-MeHI) values within the typical ancient marine range of 1%–3% (Farrimond et al. 2004; Rohrssen et al. 2013). However, several samples from the upper Kulady to lower Khastakh formations in both drill-cores show substantially higher values, reaching up to 9%. For consistency, C_{32} 3β-methylhopanes are used in all the 3-MeHI calculations (3-MeHI = 100 × $\sum C_{32}$ 3β-methyl hopanes/($\sum C_{31}$ αβ hopanes + $\sum C_{32}$ 3β-methyl hopanes)), as the main C_{31} 3β-methylhopane compound coelutes with a methygammacerane peak (Duda et al. 2020) in gammacerane-rich samples from the Taimylyr Formation.

The C_{26}/C_{25} tricyclic terpane ratio provides an additional proxy for depositional salinity, with values < 1.0 typically associated with normal marine conditions and values > 1.2

14724669, 2026, 5, Downloaded from https://onlinelibrary.wiley.com/doi/10.1111/gbi.70061 by NICE, National Institute for Health and Care Excellence, Wiley Online Library on [07/10/2026]. See the Terms and Conditions (https://onlinelibrary.wiley.com/terms-and-conditions) on Wiley Online Library for rules of use; OA articles are governed by the applicable Creative Commons License

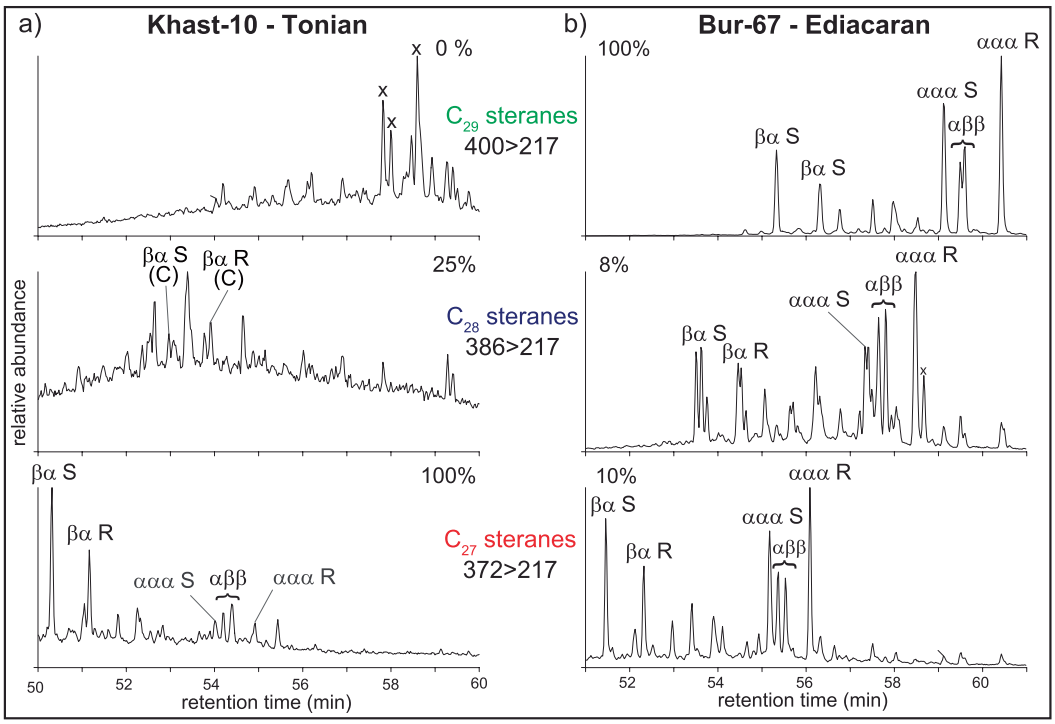


FIGURE 5 | GC-MRM-MS chromatograms showing the distributions of C_{27}–C_{29} steranes in the extractable bitumen for (a) Khast-10, a Tonian rock sample, and (b) Bur-67, an Ediacaran sample. x's mark hopane ghost peaks. Compound *C* in the 386 > 217 ion chromatograms refers to cryostane (26-methylcholestane, an unconventional C_{28} sterane), which is commonly found in late Tonian rocks (Brocks et al. 2016; Zumberge et al. 2020). Relative abundances (as % highest signal intensity) are listed as a guide for each MRM transition.

indicative of freshwater/brackish settings across a range of geologic ages (Zumberge 1987). In this dataset, the C_{26}/C_{25} ratio value is < 1.0 for most late Tonian samples from both drill-cores. Stratigraphically higher in the late Tonian succession, values between 1.1 and 1.3 occur only in the upper Khastakh Formation of the Burskaya-3410 drill-core. In the Taimylyr Formation, C_{26}/C_{25} tricyclic triterpenoid ratios are consistently (> 0.7), while in the Oppokun Formation, the C_{26}/C_{25} tricyclic terpane ratios are < 1.0, with a mean value of 0.93.

Although steranes are ubiquitous in the late Tonian strata of the Lena-Anabar Basin, S/H ratios are substantially lower than those reported for other Tonian localities (Figure 8). In both drill-cores, S/H ratios range only from 0.01 to 0.05 (Figures 6 and 8, Table 1), while absolute sterane yields range from 0.01 to 2.55 ppm of TOC (mean: 1.2 ppm of TOC; Table S5). These S/H values are approximately an order of magnitude lower than those observed for the Chuar Group (Figure 8, Table S4), which range from 0.13 to 0.3 in this study and up to 0.38 in previous work Zumberge et al. (2020). Sterane yields in the Lena-Anabar Basin are also orders of magnitude lower than those for the Chuar Group, which range from 6.0 to 123 ppm of TOC (mean: 52.0 ppm of TOC; Table S5). TOC contents in Tonian Lena-Anabar Basin samples are correspondingly low, ranging from 0.17 to 1.13 wt.% (LECO) in biomarker-analyzed samples (Figure 6, Table 1), compared to 1.33–3.9 wt.% in new Chuar Group data and up to 5.61 wt.% reported previously Zumberge et al. (2020).

Sedimentary rocks from the Ediacaran Taimylyr Formation display much higher S/H values (0.50–0.90; mean = 0.63), within the lower end for the Phanerozoic average (0.5 to 2.0; Peters et al. 2005), and yield much higher sterane concentrations (174–1236 ppm of TOC), despite low TOC contents (0.14–0.41 wt.%). However, the younger, early Cambrian Oppokun Formation samples exhibit low S/H ratios (0.03–0.06, mean = 0.05), within the Tonian range, with their total sterane yields only slightly higher than the Tonian samples (2.26–9.24 ppm of TOC) and contain very low TOC (0.21–0.31 wt%, mean = 0.31 wt%).

4.3 | Iron and Phosphorus Phase Partitioning

The environmental redox conditions during deposition of the successions sampled from the drill-cores of the Lena-Anabar Basin were determined through two independent measures: iron speciation and redox-sensitive trace-element concentrations (Figure 7; Table S3). For iron speciation, most samples plot in the equivocal Fe_{HR}/Fe_T range of 0.22–0.38 (Poulton and Canfield 2011). While a handful of samples record anoxic Fe_{HR}/Fe_T values (> 0.38), only one Tonian sample (Khast-24) has an elevated U content (U/Al = 1.84 ppm/wt% Al), while the remainder, ranging between 0.01 and 0.43 ppm/wt%, fall close to the upper continental crust average of 0.34 ppm/wt% (McLennan 2001). This U/Al range also falls below the threshold for low-oxygen environments such as oxygen-minimum zones (OMZs; Bennett and Canfield 2020). Uranium enrichment factors ($U/Al_{sample}/U/Al_{crustal\ av}$) are also below the threshold of 1.37 inferred by Li et al. (2023) to reflect anoxic depositional settings (Figures S5 and S6) for all Tonian samples barring the outlier.

14724669, 2026, 5, Downloaded from https://onlinelibrary.wiley.com/doi/10.1111/gbi.70061 by NICE, National Institute for Health and Care Excellence, Wiley Online Library on [07/10/2026]. See the Terms and Conditions (https://onlinelibrary.wiley.com/terms-and-conditions) on Wiley Online Library for rules of use; OA articles are governed by the applicable Creative Commons License

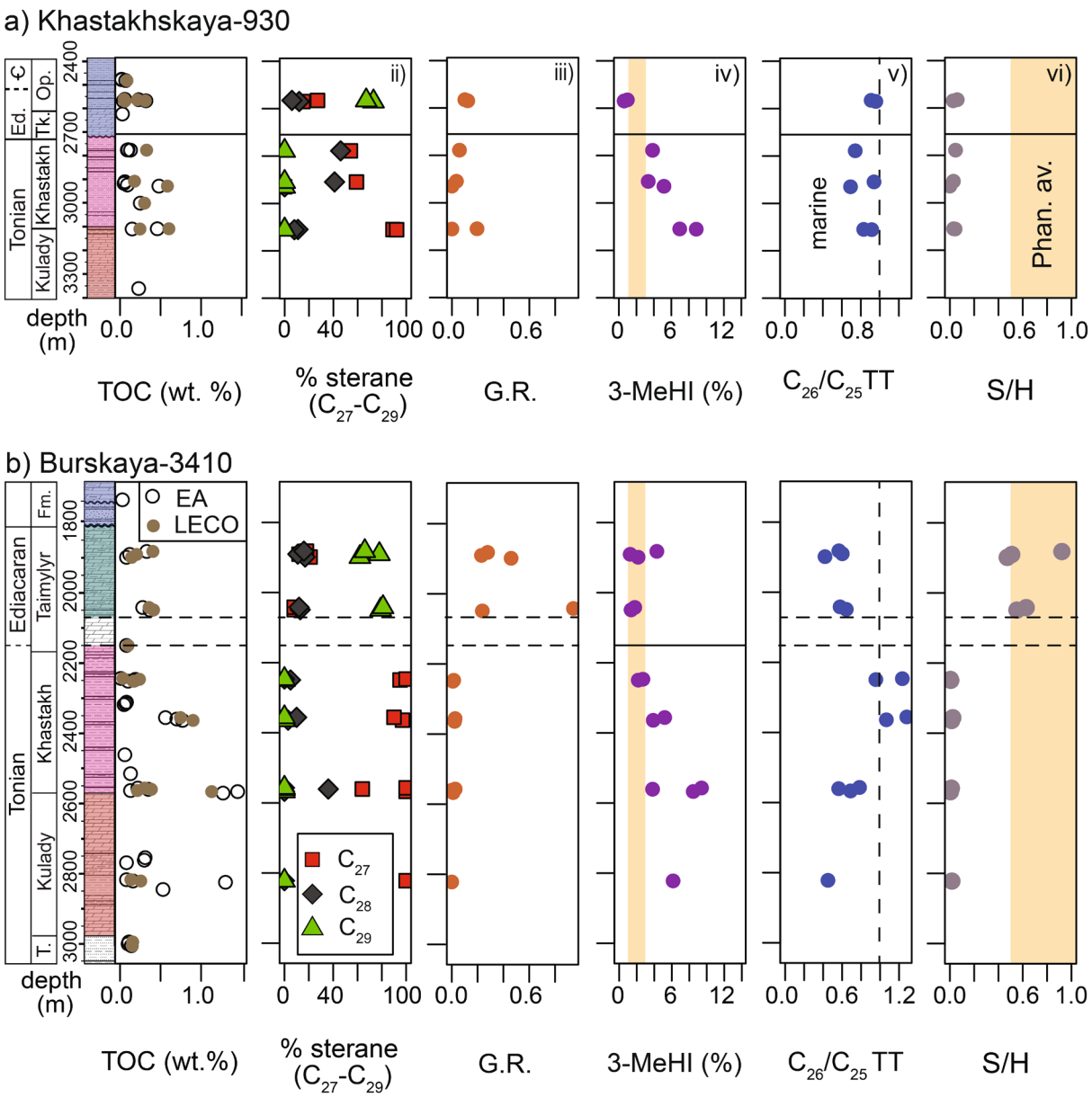


FIGURE 6 | Selected organic source and environmental biomarker parameters for (a) Khastakhskaya-930 and (b) Burskaya-3410 drill-cores. See Figures 2 and 3 captions for stratigraphic abbreviations and explanations. All biomarker parameters plotted are from bitumen. (i) wt.% TOC, with LECO values in filled circles and EA values in open circles (ii) $\%C_{27\text{-}29}$ steranes. C_{28} includes both ergostane and cryostane, the latter of which does not exceed 10% of total steranes. (iii) Gammacerane ratio (G.R) = Gammacerane/C_{30} αβ hopane. (iv) 3-MeHI = 100 × $\sum C_{32}$ 3β-methyl hopanes/($\sum C_{31}$ αβ hopanes + $\sum C_{32}$ 3β-methyl hopanes). The Phanerozoic average of 1%–3% (Rohrssen et al. 2013) is shaded in yellow. (v) C_{26}/C_{25} tricyclic terpane ratio (TT). Values <1.0 (shown by vertical line) indicate normal marine salinity, 1.0–1.2 indicate marginal marine salinity, >1.2 indicates fresh/brackish salinity. (vi) Sterane/hopane: S/H = $\sum C_{27}$-C_{29} regular steranes and diasteranes, including cryostane/$\sum$(C_{27}-C_{35} αβ hopanes, including C_{27} Ts). S/H (B) in Table 1. Phanerozoic average range for S/H of 0.5–2 (upper end cut off) is shaded in yellow.

Data are limited for the Taimylyr Formation (Burskaya-3410 drill-core; figure 7), as most samples do not pass the iron-mineral speciation screening criteria due to low Fe_T (< 0.5 wt%) concentrations (cf. Clarkson et al. 2014). However, the single sample that does contain sufficient Fe_T (Bur-67) yields strongly anoxic ($Fe_{HR}/Fe_T = 1.0$) and marginally euxinic ($Fe_{py}/Fe_{HR} = 0.71$) values (note that redox-sensitive trace-metal concentrations are not presented for this interval, due to interpretational complications when applied to carbonates). In the Oppokun Formation, one sample, Khast-41, with an elevated Fe_{HR}/Fe_T and an Fe_{py}/Fe_{HR} in the possibly euxinic range (Poulton 2021), has a U/Al ratio of 5.50 ppm/wt% and a Mo/Al ratio of 3.41 ppm/wt%, consistent with deposition under a stable OMZ (Bennett and Canfield 2020). However, the remaining Oppokun Formation samples have iron speciation and redox-sensitive trace element values below thresholds for anoxia, with Fe_{HR}/Fe_T, U/Al, and Mo/Al ranging between 0.13 and 0.35, 0.14 and 0.26 ppm/wt%, and 0.6 and 0.7 ppm/wt%, respectively.

Phosphorus phase partitioning was used to constrain paleoenvironmental phosphorus availability in the water column

14724669, 2026, 5, Downloaded from https://onlinelibrary.wiley.com/doi/10.1111/gbi.70061 by NICE, National Institute for Health and Care Excellence, Wiley Online Library on [07/10/2026]. See the Terms and Conditions (https://onlinelibrary.wiley.com/terms-and-conditions) on Wiley Online Library for rules of use; OA articles are governed by the applicable Creative Commons License

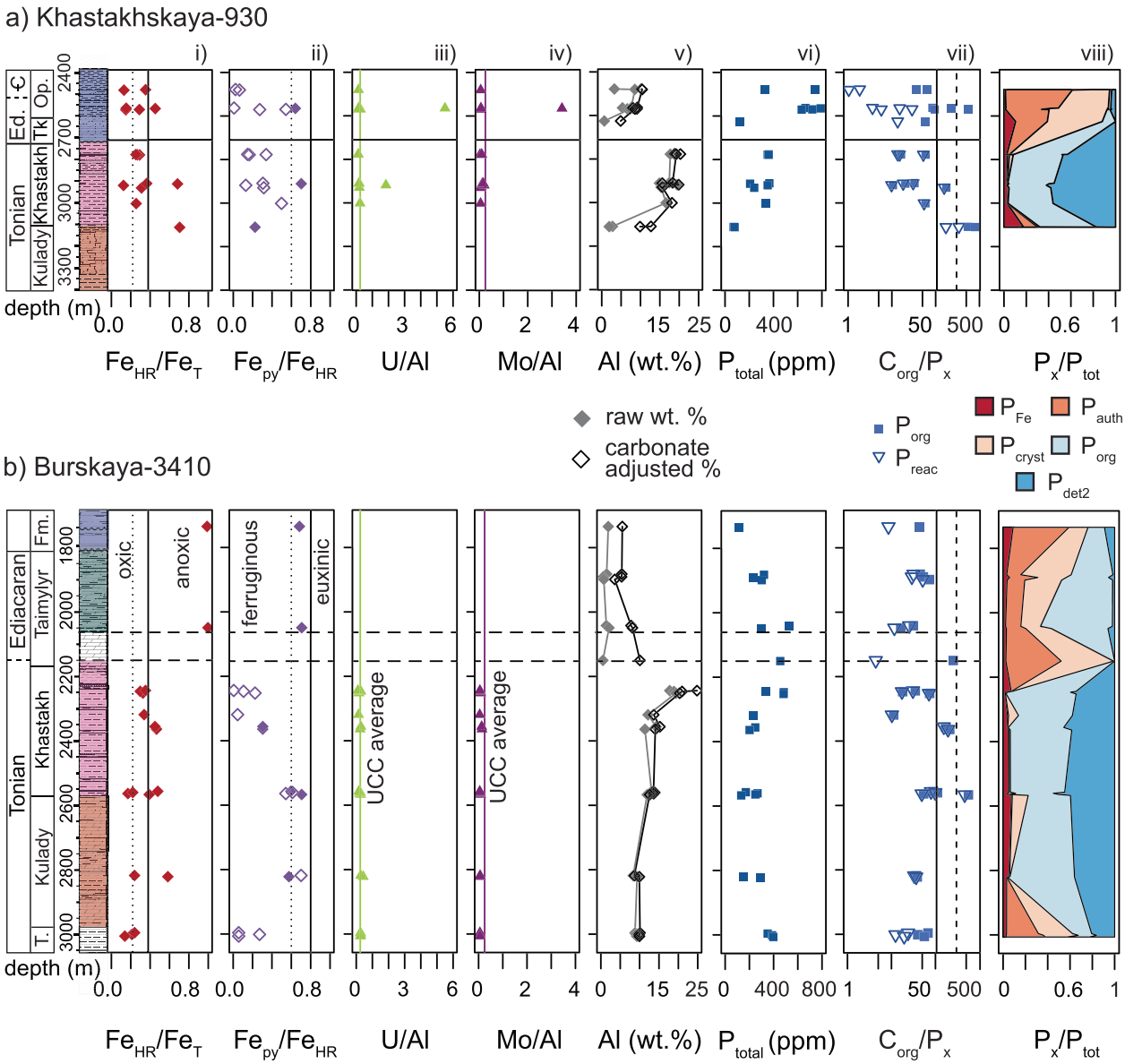


FIGURE 7 | Inorganic environmental redox and phosphorus speciation parameters for (a) Khastakhskaya-930 and (b) Burskaya-3410 drill-cores. Stratigraphic abbreviations as for Figure 3. (i) Fe_{HR}/Fe_T. Dotted line indicates the 0.22 cutoff for oxic conditions; solid line indicates the 0.38 threshold cutoff for anoxic samples. (ii) Fe_{py}/Fe_{HR}. Dotted line indicates the equivocal euxinic cutoff of 0.6; solid line indicates the common euxinic lower threshold value of 0.8 (Poulton 2021). Filled boxes indicate samples with $Fe_{HR}/Fe_T > 0.38$. (iii) U/Al (ppm/wt %). Solid line indicates the upper continental crust average ratio of 0.34 ppm/wt.% (McLennan 2001). (iv) Mo/Al (ppm/wt.%). Solid line indicates the upper continental crust average ratio of 0.22 ppm/wt.% (McLennan 2001). (v) Aluminum (wt.%). Filled boxes = Al wt.% of total rock; open boxes = Al wt.%/% non-carbonate. (vi) Total phosphorus (ppm). (vii) Molar ratio of organic carbon to organic phosphorus (solid squares) and reactive phosphorous (open triangles). Solid line is the conventional Redfield ratio (C:P of 106:1); dashed line is 300:1, a proposed value for P-limited Precambrian biomass (Reinhard et al. 2017). (viii) Phosphorus speciation parameters showing P_{Fe}, P_{auth}, P_{cryst}, P_{org}, and P_{det2} (residual recalcitrant phosphorus following the P_{org} extraction step, prominent in Tonian samples only). P_{mag} was < 2.5% of total P in all samples and is not plotted here.

during sediment deposition in the Lena-Anabar Basin. Total phosphorus contents are consistently low in the Kulady and Khastakh formations (Figure 7), with a mean of 284 ± 112 ppm (in comparison with 700 ppm for average upper continental crust; McLennan 2001). The average P content of stratigraphically shallower sedimentary rocks in the drill-cores is also below the upper continental crust average (700 ppm; McLennan 2001; figure 7), with a mean of 355 ± 100 and 571 ± 271 ppm for the Taimylyr and Oppokun formations, respectively.

Molar C_{org}/P_{org} and C_{org}/P_{reac} ratios (Figure 7, Figure S7) are also low in the Tonian samples, with most values falling below the conventional Redfield Ratio values for atomic ratios of C:N:P = 106:16:1 found in marine organic matter. However, a limited number of Tonian samples have C_{org}/P_{org} ratios above the usual Redfield Ratio value (up to 792; Figure 7), and these samples also have elevated C_{org}/P_{reac} ratios (up to 450; Figure 7). In the Taimylyr Formation, all C_{org}/P_{org} and C_{org}/P_{reac} ratios lie below the Redfield Ratio. The Oppokun Formation also has C_{org}/P_{org} and C_{org}/P_{reac} ratios values below

14724669, 2026, 5, Downloaded from https://onlinelibrary.wiley.com/doi/10.1111/gbi.70061 by NICE, National Institute for Health and Care Excellence, Wiley Online Library on [07/10/2026]. See the Terms and Conditions (https://onlinelibrary.wiley.com/terms-and-conditions) on Wiley Online Library for rules of use; OA articles are governed by the applicable Creative Commons License

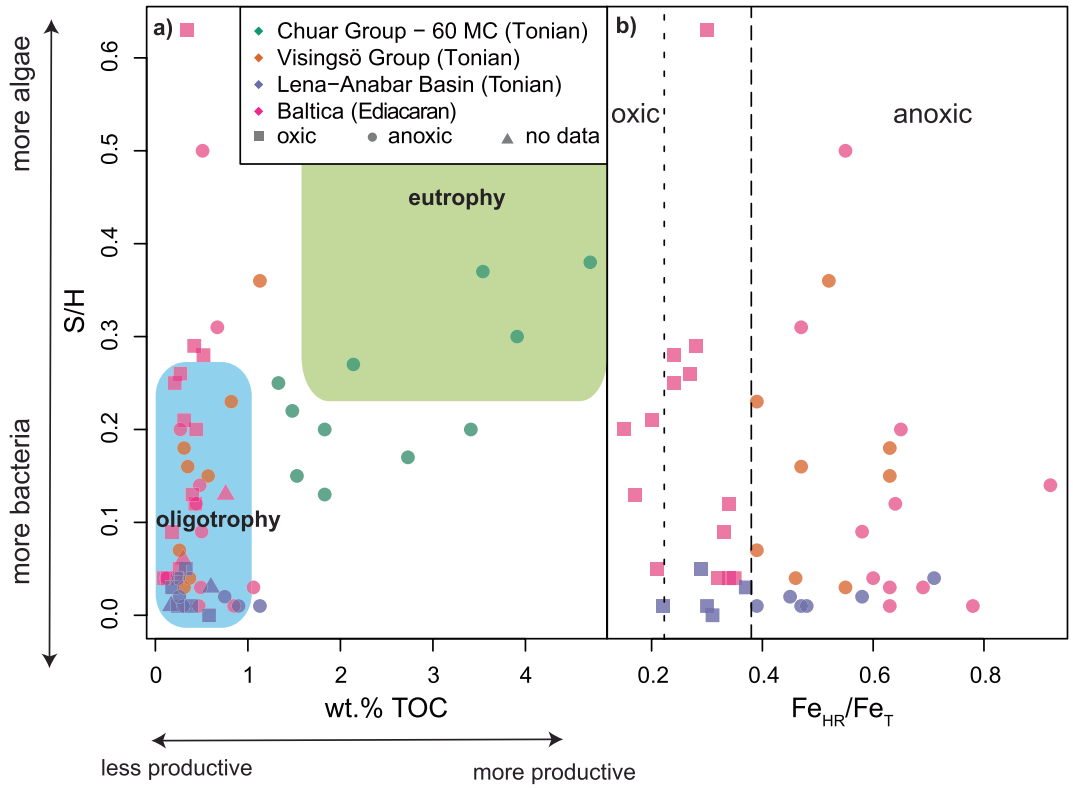


FIGURE 8 | (a) Comparison of Total Organic Carbon (TOC) content, sterane/hopane (S/H) ratio, and water-column redox (Fe_{HR}/Fe_T) from available Neoproterozoic studies with available data. S/H measured from GC-MRM-MS using the free saturated hydrocarbon fractions from this study, in Zumberge et al. (2020), and Pehr et al. (2023). S/H values use summed C_{26}-$_{28}$ steranes/$\sum$(C_{27}-C_{35} αβ hopanes, including C_{27} and C_{29} Ts). Data for Lena-Anabar Basin samples are listed in Table 1 with S/H (formula C) plotted here. For Chuar Group, TOC and S/H values are listed in Table S4, with S/H (formula C) plotted here. See Zumberge et al. (2020) for Visingsö Group data (their S/H (2) values were plotted here). For Walcott Member rocks (Chuar Group), samples from Sixtymile Canyon (60 MC) outcrop location were used since these were of a low thermal maturity similar to the other rocks plotted (from early to middle oil window maturity, with none exceeding 0.9% for equivalent vitrinite reflectance level). Chuar Group data are assumed to be anoxic based on Johnston et al. (2010), who inferred persistent anoxia in the upper Walcott Member based on iron speciation data. (b) S/H vs. Fe_{HR}/Fe_T using the same data as in (a). Dotted lines indicate the 0.22 cutoff for oxic conditions and the 0.38 threshold cutoff for anoxic samples. Chuar Group rocks are excluded because same-sample iron speciation data were not available.

the Redfield Ratio, except for two stratigraphically adjacent samples with C_{org}/P_{org} up to 564, one of which also has elevated Fe_{py}/Fe_{HR} and Mo/Al, but with C_{org}/P_{reac} below the Redfield value.

Through the upper Tonian Khastakh Formation there is a distinct increase in Al content in both drill-cores, reaching levels as high as 19.5 wt% (Figure 7), which is well above the upper continental crust average of 8.04 wt% (McLennan 2001). Across the same stratigraphic interval, the proportion of P present in the P_{det2} fraction increases considerably, largely at the expense of the P_{auth} and P_{cryst} fractions, which are almost completely absent (Figure 7, Table S3). This very unusual depletion in P_{auth} and enrichments in P_{det2} and Al are not observed in either the Taimylyr or Oppokun formations.

5 | Discussion

5.1 | Age of the Studied Units

A combined evaluation of Sr. and carbonate carbon isotope ratios suggests that the Taimylyr Formation, starting above 2150 m depth in the Burskaya-3410 drill-core, is of Ediacaran age (Figure 2). Between 2760 and 2151 m depth, $^{87}Sr/^{86}Sr$ ratios fall within the range previously reported for the interval 800–720 Ma (Cox et al. 2016; Halverson et al. 2010; Kuznetsov et al. 2017, 2019), consistent with microfossil indicators of a late Tonian age for these units. However, above 2043 m, $^{87}Sr/^{86}Sr$ ratios are significantly higher than Tonian seawater values, but remain well within the range typical for Ediacaran seawater range. Comparable values were observed in the overlying late Ediacaran Khatyspyt Formation (Cui et al. 2016). $\delta^{13}C_{carb}$ values of the Taimylyr Formation likely place the unit in the late Ediacaran after the Shuram Excursion (ca. 656–539 Ma, Bowyer et al. 2022, 2024; Halverson et al. 2018; Yang et al. 2021). These observations imply that the Tonian-Ediacaran boundary occurs between 2150 and 2050 m depth, perhaps at a lithologic boundary at approximately 2070 m shown by Nagovitsin et al. (2015). Further work is needed to determine whether carbonates in the lowermost Taimylyr Formation should be stratigraphically reassigned and the stratigraphic boundary moved.

$\delta^{13}C_{org}$ isotope values (Figure 3) also support a post-Bitter Springs Anomaly (ca. 802 Ma), Tonian age for the Kulady and Khastakh formations, which our biomarker data suggest were

14724669, 2026, 5, Downloaded from https://onlinelibrary.wiley.com/doi/10.1111/gbi.70061 by NICE, National Institute for Health and Care Excellence, Wiley Online Library on [07/10/2026]. See the Terms and Conditions (https://onlinelibrary.wiley.com/terms-and-conditions) on Wiley Online Library for rules of use; OA articles are governed by the applicable Creative Commons License

deposited in an open-marine setting (see next section). Similarly high $\delta^{13}C_{org}$ values to those reported here have been observed in the 751 ± 7 Ma Awatubi Member of the Chuar Group (Dehler et al. 2017; Rooney et al. 2017). Global compilations of late Tonian $\delta^{13}C_{carb}$ values, which range from approximately −5‰ during the ca. 810–802 Ma Bitter Springs Excursion to 10‰ at ca. 750 Ma (Halverson et al. 2010, 2018; Thomson et al. 2015; Turner and Bekker 2016), see a similar magnitude increase to that observed in $\delta^{13}C_{org}$ values in our study. If we assume that $\delta^{13}C_{org}$ values track the global dissolved inorganic carbon pool with the typical pre-Mesozoic offset ($\Delta^{13}C$) of 25‰–32‰ (Hayes et al. 1999), our $\delta^{13}C_{org}$ values are consistent with previously published late Tonian $\delta^{13}C_{carb}$ values. Together with biostratigraphic and Sr. isotope constraints, the whole-rock $\delta^{13}C_{org}$ signatures suggest that the upper Khastakh Formation was most likely deposited at ca. 750 Ma during the late Tonian. The carbon isotope discontinuity in the Burskaya-3410 drill-core further supports a significant difference in age and deposition in this depth interval.

5.2 | Biomarker Data Integrity

Throughout both drill-cores in the Lena-Anabar Basin, biomarker maturity indicators based on hopanes, steranes, and aromatics align with independent HAWK pyrolysis-based maturity indicators. C_{31} hopane 22S/(S + *R*) ratios, C_{27} sterane ααα S/(S + *R*) ratios, MPI-1 based % R_c (not exceeding 0.9%), and HAWK T_{MAX} all indicate early to peak oil window maturity, with a maximum burial temperature not exceeding 100°C (Mackenzie and McKenzie 1983) and variation consistent with increasing maturity at depth. This maturity is appropriately low to preserve a diverse range of lipid biomarkers, including steranes, with good retention of primary structural features. Given that the thermal maturity of extracted bitumen is like that indicated by HAWK pyrolysis, biomarker patterns most likely represent endogenous organic matter rather than contamination.

A few molecular maturity ratios, namely the C_{27} hopane Ts/(Ts + Tm), C_{27} αββ/ααα sterane, and C_{27} diasterane/regular sterane ratios vary in a manner that deviates from a simple relationship with burial depth (Table 1). However, these parameters are all affected by organic matter source and early diagenesis as well as maturity and observed discrepancies correspond to significant changes in lithology and inferred depositional environment. Elevated Ts/(Ts + Tm) and αββ/ααα have been associated with high salinity (Rullkötter and Marzi 1988), plausible for the Taimylyr Formation, which was inferred to represent a shallow-marine depositional environment (Nagovitsin et al. 2015). Ts/(Ts + Tm) has been found to be elevated in carbonates and suppressed by high clay content (French et al. 2012), consistent with our data, where Ts/(Ts + Tm) is highest in carbonates and consistently lower in the Khastakh and Oppokun Formation shales. All samples in the Khastakh Formation have Al content that exceeds the upper crustal average (8.04 wt.%, McLennan 2001) by at least 3% (Table S3), further supporting this mineralogical control. Low ααβ steranes in some of the late Tonian samples may indicate a source from 5α(H)-stanols as primary inputs, generating mainly ααα steranes during diagenesis and catagenesis. 5α(H)-stanols are found in various algae (Volkman et al. 1990, 1998), and the ααα stereochemistry in a fully saturated tetracyclic core is already found in 5α(H)-stanols, while stenol precursors are more prone to yielding αββ stereoisomers through diagenesis (Peakman and Maxwell 1988). Elevated diasteranes, like those found the Taimylyr Formation, are not uncommon in carbonates and may be enhanced in rocks with high clay/TOC (van Kaam-Peters et al. 1998) particularly for low-TOC rocks. Despite these complications, the HAWK pyrolysis and molecular maturity parameters less sensitive to lithology and organic matter source are consistent and confirm an overall mild thermal history for the studied drill-cores.

HyPy data from fragmentation of exhaustively extracted rock powders further confirms the syngeneity of extracted bitumens. The kerogen-bound biomarkers from the Tonian sample Bur-40 closely replicate key features of the bitumen (Figure 4, Table 1), with the exception of an absence of diasteranes, which is a characteristic feature of a genuine covalently linked sterane pool (Love et al. 1995, 2009; Zumberge et al. 2020, and references therein). Rearranged steranes, particularly diasteranes, are not typically generated from the kerogen-bound pool from chemolysis or pyrolysis since diasteranes are exclusively formed as free hydrocarbons in the bitumen phase (Love et al. 1995). Major biomarker features of the Tonian samples from both drill-cores, particularly the C_{27} dominance and absence of C_{29} and C_{30} steranes, replicate and validate the Bur-40 kerogen sterane profiles.

5.3 | The Ediacaran Rise of Green Algae: Changing Sterane Sources

This study confirms the ubiquity of C_{27} steranes in the Tonian Period. The observed absence of C_{29} steranes in the Tonian samples of this study is also consistent with previous studies of Tonian biomarker distributions (Brocks et al. 2016, 2017; Zumberge et al. 2020). These sterane distributions support molecular clock data that places the acquisition of the second sterol methyltransferase (SMT2) gene necessary for stigmasteroid biosynthesis in algae (Hoshino et al. 2017) as well as in other lineages of eukaryotes (Brunoir et al. 2023) in the late Cryogenian. The dominance of C_{27} steroids and the absence of C_{29} steroids for the late Tonian as a primary biomarker signal was further confirmed here by analysis of the distribution of triaromatic steroids (Figure S8; Table S6), which show compatible carbon number patterns with the steranes in the same samples.

Likewise, the strong C_{29} sterane dominance observed in all Ediacaran samples in this study is consistent with other Ediacaran biomarker investigations of well-preserved rocks and oils (Duda et al. 2016, 2020; Dutta et al. 2013; Goryl et al. 2018; Grosjean et al. 2009; Kelly et al. 2011; Love et al. 2009; Melnik et al. 2024; Pehr et al. 2018). While a fundamental shift from C_{27} to C_{29} sterol producers from the Tonian to the Ediacaran has been proposed before from composite records (Brocks et al. 2017; Hoshino et al. 2017; Isson et al. 2018; Summons et al. 1988; Zumberge et al. 2020), this study is the first to capture both endpoints of this secular and stratigraphic change in one location, with consistent sterane pattern trends obtained for both cores investigated.

14724669, 2026, 5, Downloaded from https://onlinelibrary.wiley.com/doi/10.1111/gbi.70061 by NICE, National Institute for Health and Care Excellence, Wiley Online Library on [07/10/2026]. See the Terms and Conditions (https://onlinelibrary.wiley.com/terms-and-conditions) on Wiley Online Library for rules of use; OA articles are governed by the applicable Creative Commons License

A C_{29} sterane dominance characterizes both the Taimylyr and Oppokun formations, despite their contrasting depositional environments. The Taimylyr Formation was deposited on a shallow-marine, carbonate platform that periodically experienced elevated salinity and basin restriction (Nagovitsin et al. 2015; this study), while the Oppokun Formation was deposited under more distal conditions (see discussion below); yet, the sterane carbon number patterns are very similar. This lends further support to the idea that the C_{27}-C_{29} sterane shift represents a global secular trend rather than just environmental difference within the ocean (see later discussion).

The transition from a C_{27} dominance to a C_{29} sterane preference seems to occur broadly around the Cryogenian-Ediacaran boundary (Love et al. 2009), although a sparsity of samples and poor radiometric age constraints means that the timing of the switch in patterns needs to be verified with more biomarker data. C_{27} sterols are produced by a wide range of eukaryotes including animals, but they are the major sterol of red algae (Kodner et al. 2008; Patterson 1971) and are often attributed to phytoplankton sources in modern oceans (Volkman 2005), leading Zumberge et al. (2020) and Brocks et al. (2023) to interpret that these late Tonian C_{27} steranes were mainly sourced from populations of red algae, especially in eutrophic marine settings. The 27-to-29 sterane switch likely records an ecological shift from a eukaryotic population consisting mainly of red algae to one dominated by green algae, though both algal clades were present before and after the Cryogenian glaciations. Brocks et al. (2016, 2017) argued that Tonian C_{27} steranes were primarily sourced from heterotrophic protists, and indeed *de novo* cholesterol biosynthesis has been identified in a few heterotrophic bacteria (Lee et al. 2023). Given the low abundance of steranes in the Tonian strata from Siberia (mean 0.37 ppm of TOC; Table S5), we cannot rule out contributions to C_{27} steranes from biogenic sources other than red algae for the Lena-Anabar Basin samples. However, for the upper Walcott Member of the Chuar Group, the higher S/H values approach those found for Phanerozoic source rocks (0.5–2.0, mean value = 1.0, Love and Zumberge 2021), which together with high absolute abundance of total steranes strongly suggests a eukaryotic primary producer (algal) origin rather than from a primary consumer. The secular trend in C_{27} sterane ubiquity appears to be consistent with fossil evidence for a radiation of (possibly crown-group) eukaryotes in the late Tonian (Xiao and Tang 2018), supporting an eukaryotic primary producer source for most of the late Tonian C_{27} sterane signals.

Our detection of ergostane (a C_{28} regular sterane, Figure 6) alongside higher amounts of C_{27} steranes confirms previous reports from the late Tonian Visingsö Group, confirmed by the detection in pyrolysis products from the parallel analysis of the kerogen-bound biomarker pool (Zumberge et al. 2020). Additionally, the presence of low amounts of ergostane might speculatively point to a more cryptic record of pre-Sturtian green algae prior to the predicted Cryogenian evolution of stigmasteroid biosynthesis (Hoshino et al. 2017). Prasinophyte algae produce C_{28} sterols as their major sterol, and many other green algae also produce them in addition to C_{29} sterols (Kodner et al. 2008), so Tonian ergostane could have a green algal source, though red algae and other organisms can also produce C_{28} sterols. In the Lena-Anabar Basin, the green algal fossil *Proterocladus major* has been detected in the upper Khastakh Formation of both drill-cores (figure 2; Nagovitsin et al. 2015), supporting the possibility of a minor contribution from green algae during deposition of this stratigraphic interval. Given that ergostane is nevertheless a relatively rare component of Tonian sterane assemblages, green algae were relatively minor contributors to photosynthetic primary production in the late Tonian marine realm in the Lena-Anabar Basin and elsewhere until after the Sturtian glaciation. No traces of either C_{29} or C_{30} (24-npc, 24-ipc or 26-mes) steranes are found in any of the pre-Sturtian rocks from northern Siberia or from our Chuar Group rocks, consistent with the sterane patterns reported previously from late Tonian rocks from the Visingsö and Chuar groups (Zumberge et al. 2020).

5.4 | Marine Paleoenvironment Evolution in Northern Siberia

Lipid biomarker proxies help further constrain the depositional environments of the Tonian successions in the Lena-Anabar Basin of northern Siberia (Figure 6). Gammacerane, derived from tetrahymanol, sourced by ciliates inhabiting redox gradients and certain groups of bacteria (see Duda et al. 2020, and references therein), has been used as a proxy for stratification in salinity and/or redox (Moldowan et al. 1985; Peters et al. 2005; Sinninghe Damsté et al. 1995; ten Haven et al. 1988, 1989; Tulipani et al. 2015). Low GRs in our Tonian samples are more consistent with normal marine salinity than sustained redox stratification or hypersalinity in the water column.

While most samples record low to moderate 3β-methylhopane index (3-MeH) values, within the typical, Phanerozoic marine range of 1%–3% (Farrimond et al. 2004; Rohrssen et al. 2013), several samples in the upper Kulady to lower Khastakh formations have values up to 14%, an indicator of bacterial methanotrophy and a strong methane cycle in the depositional environment. The samples in the Burskaya-3410 drill-core with the highest 3-MeH also have Fe_{HR}/Fe_T values that plot as anoxic, and as such this interval may represent an incursion of anoxic deep waters. While 3-MeH is often elevated in lacustrine settings (Farrimond et al. 2004), our samples with high 3-MeH lack other distinguishing biomarker characteristics typically associated with ancient saline, alkaline lakes (Xia et al. 2021), such as high GRs and β-carotane, arguing for a marine rather than lacustrine depositional environment.

The C_{26}/C_{25} tricyclic terpane ratio has less commonly been applied to Tonian (Zumberge et al. 2020) and Ediacaran (Pehr et al. 2023) rocks, but there is no a priori reason why this proxy will not work for thermally well preserved Neoproterozoic rocks. Indeed, a biomarker study by Pehr et al. (2023) showed that unusual ^{13}C-enriched bulk carbon isotope signatures found for late Ediacaran rocks were consistently associated with C_{26}/C_{25} tricyclic values of > 1.2, consistent with a coastal brackish water environment for this stratigraphic interval in Baltica. Most Tonian samples in the Lena-Anabar Basin have C_{26}/C_{25} tricyclic terpane ratios < 1.0, typical for a normal marine salinity setting (Peters et al. 2005; Zumberge 1987). Additionally, an increase in the C_{26}/C_{25} tricyclic terpane value in the upper Khastakh Formation of the Burskaya-3410 drill-core corresponds with an increase in $\delta^{13}C_{org}$ value (Figure 3), wt% Al (Figure 7) and upward-coarsening lithological trend (Figure 2; Nagovitsin et al. 2015) for the same stratigraphic interval. Together, this suggests an upward-shallowing

14724669, 2026, 5, Downloaded from https://onlinelibrary.wiley.com/doi/10.1111/gbi.70061 by NICE, National Institute for Health and Care Excellence, Wiley Online Library on [07/10/2026]. See the Terms and Conditions (https://onlinelibrary.wiley.com/terms-and-conditions) on Wiley Online Library for rules of use; OA articles are governed by the applicable Creative Commons License

trend below the major, protracted hiatus in deposition in northern Siberia that encompasses the entire Cryogenian, before subsidence resumed in the late Ediacaran. Overall, these lipid biomarker proxies support a marine depositional environment for most of the late Tonian succession in the studied drill-cores.

Several lipid biomarker proxies in the Ediacaran Taimylyr Formation differ considerably from the Tonian strata of the Lena-Anabar Basin, suggesting a change in depositional environment. GR values are uniformly higher but variable, reaching up to 0.94, indicating variably stratified conditions with input from marine ciliates or certain groups of bacteria (Sinninghe Damsté et al. 1995; ten Haven et al. 1988). Variable G.R. values (0.06–0.58) have also been reported for carbonate-rich strata of the late Ediacaran Khatyspyt Formation in the Olenek Uplift, Siberia (Duda et al. 2020), a stratigraphic unit that sits above the Taimylyr Formation in the Burskaya-3410 drill-core. Gammacerane-based evidence for stratification as well as the microbially laminated dolostone lithology of the Taimylyr Formation (Nagovitsin et al. 2015) are consistent with episodically high salinity and basin restriction in the Lena-Anabar Basin in the late Ediacaran. Higher salinity could also account for previously discussed discrepancies in Ts/(Ts + Tm) and C_{27} sterane αββ/ααα ratios in the Taimylyr Formation (cf. Rullkötter and Marzi 1988). Widespread deposition of halite and sulfate evaporites during the Ediacaran-Cambrian have been documented across Siberia during the so-called Yudomski Event (Claypool et al. 1980; Crockford et al. 2019; Mel'nikov 2009). Combined sedimentologic and organic geochemistry evidence indicate deposition in a semi-restricted, shallow-marine setting that experienced environmental variability.

Environment-related lipid biomarker proxies in the earliest Cambrian Oppokun Formation are more like those from the late Tonian strata of northern Siberia analyzed in our study than those from the Taimylyr Formation. GRs are lower than those for the Taimylyr Formation and do not point to significant stratification. The 3-MeHI value is also low (< 1%), indicating limited bacterial methanotrophy in the water column and in sediment pore-waters during deposition of the unit. C_{26}/C_{25} tricyclic terpane ratios are also within the typical Phanerozoic marine range of < 1 (Peters et al. 2005; Zumberge 1987) and similar to Tonian values in the Khastakhskaya-930 drill-core. Overall, these lipid biomarker proxies suggest that the Oppokun Formation was deposited under open marine, rather than restricted conditions.

5.5 | Environmental Redox Reconstruction From Inorganic Geochemistry

While most Tonian samples in the Lena-Anabar Basin have Fe_{HR}/Fe_T ratios in the equivocal zone with some anoxic values, the lack of U enrichment suggests that the water column in the Tonian Lena-Anabar Basin was oxic for most of the time. Possible rare incursions of upwelled, deep anoxic waters could account for moderately elevated Fe_{HR}/Fe_T in some samples. Upwelling would have resulted in precipitation of Fe_{HR} phases in oxic, shallow-marine waters, which would have led to elevated Fe_{HR}/Fe_T but with an absence of U enrichment (e.g., Song et al. 2023). Alternatively, high Fe_{HR}/Fe_T values may reflect intense chemical weathering recorded in a fluvially-influenced, tropical depositional environment (Wei et al. 2021; but see below). Tropical, fluvial sediments commonly have elevated Fe_{HR}/Fe_T ratios relative to oxic, marine sediments and locally, where the fluvial sediments bypass the inner shore that normally traps Fe_{HR} phases (Poulton and Raiswell 2002), elevated Fe_{HR}/Fe_T ratios may develop in nearshore, marine environments (Wei et al. 2021).

Nevertheless, despite the potential for occasional upwelling of anoxic, ferruginous waters into shallower settings, there is no compelling evidence for sustained euxinia in the Tonian Lena-Anabar Basin. A number of samples have Fe_{HR}/Fe_T ratios higher than 0.38, potentially indicating anoxic conditions, and Fe_{py}/Fe_{HR} values of 0.6–0.8 within the *possible* euxinic range (Poulton 2021). However, Mo/Al (0.03–0.20 ppm/wt%, Figure 7), as an independent indicator of possible euxinia (Bennett and Canfield 2020), consistently falls below the upper continental crust average (0.22 ppm/wt%; McLennan 2001) in the range for sediments deposited under oxic conditions (Mo/Al < 0.4; Bennett and Canfield 2020). The potentially anoxic samples are distinct from the definitively oxic samples by commonly having elevated Fe_{py}/Fe_{HR}, and the few oxic samples that have elevated Fe_{py}/Fe_{HR} occur stratigraphically close to these samples (Figure 7). The elevated Fe_{py}/Fe_{HR} suggests enhanced pyrite formation during periods with more rapid development of anoxic pore-waters in shallow sediments, which is more consistent with short-lived episodes of more reducing water-column conditions (likely during upwelling of deep, anoxic waters) than a chemical weathering control on iron-mineral speciation.

Limited data for the Taimylyr Formation make redox interpretation difficult, but the one sample with reliable iron speciation data plots as possibly euxinic. For this sample, moderate G.R. of 0.23 (Figure 7) supports water-column redox stratification. Elevated G.R. is shared to some degree across all the Taimylyr Formation samples, leaving open the possibility of redox stratification in the basin during deposition of these samples as well. The lower interval of the overlying Khatyspyt Formation, exposed at the nearby Olenek Uplift, has been inferred to been deposited in euxinic conditions on the basis of $\delta^{34}S$ values and high total sulfur content (Cui et al. 2016), although this does not rule out that sulfidization processes occurred within shallow sediments rather than in the water column.

The earliest Cambrian Oppokun Formation (Khastakhskaya-930 drill-core) was likely deposited under fluctuating redox conditions, based on trends in iron speciation and redox-sensitive, trace element data (Figure 7). Elevated Fe_{HR}/Fe_T, Fe_{Py}/Fe_{HR}, U/Al and Mo/Al values in one sample point to deposition under a stable OMZ (Bennett and Canfield 2020), but other samples appear to have been deposited under oxic conditions. Like the late Tonian Kulady and Khastakh formations, the Oppokun Formation thus appears to have been deposited in a predominantly oxic and open-marine setting, with only episodically developed redox stratification.

5.6 | Phosphorus Partitioning and Nutrient Cycling

Total phosphorus concentrations (Figure 7) in the Tonian strata of the Lena-Anabar Basin are very low, falling below the

14724669, 2026, 5, Downloaded from https://onlinelibrary.wiley.com/doi/10.1111/gbi.70061 by NICE, National Institute for Health and Care Excellence, Wiley Online Library on [07/10/2026]. See the Terms and Conditions (https://onlinelibrary.wiley.com/terms-and-conditions) on Wiley Online Library for rules of use; OA articles are governed by the applicable Creative Commons License

pre-Cryogenian mean (Reinhard et al. 2017) and similar to values for the oligotrophic early Tonian Huainan basin (Guilbaud et al. 2020). Accurate interpretation of phosphorus abundance data requires careful consideration of the redox characteristics gleaned from iron speciation and trace metal geochemistry. This integrated interpretation is necessary since, in theory, low sedimentary phosphorus contents could be caused by either low phosphorus delivery to the basin, indicating nutrient-depleted conditions, or from extensive regeneration of sedimentary phosphorus back to the water column (Ingall et al. 1993; Ingall and Jahnke 1994, 1997).

However, extensive P recycling from sediments results in elevated C_{org}/P_{org} ratios, well above the conventional Redfield ratio (Ingall and Jahnke 1997; Slomp et al. 2004; Van Cappellen and Ingall 1994), as anaerobic remineralization preferentially releases P relative to aerobic organic matter oxidation. The low molar C_{org}/P_{org} ratios observed in most Tonian samples (Figure 7) rule out extensive phosphorus release from sediments to the water column. Additionally, low C_{org}/P_{reac} ratios indicate additional P drawdown and sequestration from the water column in sedimentary Fe-oxides (Guilbaud et al. 2020). Taken together, low P_{total}, C_{org}/P_{org}, and C_{org}/P_{reac} values point to a water column with little available P due to limited P delivery to the basin and limited recycling from sediments.

However, a few Tonian samples with C_{org}/P_{org} and C_{org}/P_{reac} ratios above the Redfield Ratio indicate some degree of regeneration of phosphorus from the sediments back to the water column, which commonly occurs under anoxic conditions, particularly when sulfide is generated in the water column or during early sedimentary diagenesis (e.g., Alcott et al. 2022; Ingall and Jahnke 1994, 1997). Indeed, most of these outlier samples have elevated Fe_{HR}/Fe_T and/or relatively high Fe_{PY}/Fe_{HR}, suggesting that episodic development of anoxic conditions (as discussed above), with enhanced sulfide generation during early sedimentary diagenesis, promoted some P recycling. This may have led to limited interval infrequent episodes of increased productivity, since these samples commonly have somewhat higher TOC content (Figure 7) and higher lipid yields (Table S5). The extent of P recycling was likely moderate, however, since the C_{org}/P_{reac} ratios are typically lower than C_{org}/P_{org}, consistent with those found in low-sulfate, modern euxinic settings that are considered analogous to Precambrian oceans (Xiong et al. 2019).

Taken together, the P phase partitioning data thus provide strong support for our redox interpretation, whereby dominantly oxic conditions led to retention of phosphorus in the sediments, and the occasional development of more reducing conditions led to a limited degree of phosphate recycling. Since the total P contents of the Tonian samples are below the pre-Cryogenian mean of 510 ppm (Reinhard et al. 2017), these observations suggest that the late Tonian Lena-Anabar Basin was persistently phosphorus-limited, with low overall marine primary productivity (see the following section). This relationship between P availability, marine productivity and the prevailing redox conditions supports the idea of marine chemical and biological heterogeneity from region to region, due to non-uniform biogeochemical cycling affecting nutrient delivery to the late Tonian ocean system.

The phosphorus phase partitioning dataset allows additional insights into controls on P delivery to the Lena-Anabar Basin. For most of the Tonian strata, sedimentary P is primarily present as the recalcitrant P_{det2}, which is strongly correlated with Al ($R^2 = 0.87$; Figure S9), suggesting that this refractory phosphorus fraction is associated with aluminum phases, either in the form of silicate minerals or discrete Al-oxides. Al concentrations more than two times crustal values in the same stratigraphic interval strongly suggest that terrestrial weathering was enhanced in the late Tonian in northern Siberia, which was located at tropical latitudes (figure 1; Merdith et al. 2021). Together, these results suggest that rather than becoming bioavailable, the P released upon weathering from detrital apatite (i.e., P_{cryst}) and other phases was incorporated into secondary Al-minerals on land. Phosphorus retention within aluminum oxides and hydroxides (Bortoluzzi et al. 2015; Fonseca et al. 2011) and/or clay minerals (Xiong et al. 2022) has been demonstrated in modern, deeply weathered tropical soils and sediments, and we propose that the same mechanism may have operated locally in the late Tonian in northern Siberia. This would have offset the increase in P influx that otherwise would have been expected due to increased chemical weathering. In this proposed scenario, rather than being exported to the Lena-Anabar Basin, some fraction of solid P was retained in terrestrial catchments, contributing to the low P_{total} observed in this study. A substantial remainder would have been delivered to the marine realm in non-bioavailable, particulate form as P_{det2}, rather than in dissolved or reactive particulate form, leading to high P_{det2} contribution to sedimentary P in the late Tonian Lena-Anabar Basin. Neoformed clay minerals, produced via reverse weathering (Isson and Planavsky 2018; Poulton et al. 2010) during early diagenesis, may also have contributed to P retention in a recalcitrant form as P_{det2} in the marine sediments. Together, these mechanisms would have maintained low water-column P availability and sustained chronic oligotrophic conditions in the late Tonian Lena-Anabar Basin.

While ocean upwelling is generally regarded as a major source of P to coastal marine settings (Van Cappellen and Ingall 1994), upwelling was likely limited in the Lena-Anabar Basin due to ocean circulation at its paleogeographic position on a tropical western ocean margin (figure 1; Merdith et al. 2021), contributing to low P availability. Upwelled waters may have also been nutrient-depleted in the late Tonian (Guilbaud et al. 2020; Laakso and Schrag 2019). However, the late Tonian Lena-Anabar Basin provides a counterexample to the Laakso and Schrag (2019) proposal that terrestrially influenced environments were more productive. Despite evidence for a high terrestrial weathering influence on the Khastakh Formation depositional site, such as high Al content, increased incidence of sandstone units, and an upward-shallowing trend (Nagovitsin et al. 2015), this stratigraphic interval remained P-limited as indicated by low C/P values and total P content. Phosphorus sequestration via Al-rich mineral phases, as proposed herein, explains this apparent conundrum.

Given that a secular rise in bioavailable P has been proposed more broadly for the late Tonian oceans (Planavsky et al. 2023), the strong suppression of bioavailable P delivery to the marine settings in the Lena-Anabar Basin may have been a regional

14724669, 2026, 5, Downloaded from https://onlinelibrary.wiley.com/doi/10.1111/gbi.70061 by NICE, National Institute for Health and Care Excellence, Wiley Online Library on [07/10/2026]. See the Terms and Conditions (https://onlinelibrary.wiley.com/terms-and-conditions) on Wiley Online Library for rules of use; OA articles are governed by the applicable Creative Commons License

phenomenon that further exacerbated oligotrophic conditions in comparison with other late Tonian marine settings. Further investigation is needed to verify whether enhanced Al contents and associated P dynamics were a common feature of late Tonian sedimentary rocks or whether this mode of chronic P limitation was restricted to the northern Siberian region.

Ediacaran-Cambrian sedimentary rocks of the Lena-Anabar Basin are also characterized by P contents below the upper continental crustal average and predominantly low C/P ratios. In the Taimylyr Formation, C_{org}/P_{org} and C_{org}/P_{reac} ratios are mostly below the conventional Redfield Ratio, including for the single rock sample tentatively identified as possibly euxinic. This suggests that preferential regeneration of phosphorus from organic matter was not substantial (indicated by low C_{org}/P_{org} ratios), and that phosphorus was not substantially recycled back to the water column (indicated by low C_{org}/P_{reac} ratios). Instead, phosphorus was either retained in preserved organic matter (P_{org} is the most abundant phase) or converted to authigenic forms via sink switching (Ingall et al. 1993; Ingall and Jahnke 1994, 1997; Ruttenberg and Berner 1993). Most samples in the Oppokun Formation have C_{org}/P_{org} and C_{org}/P_{reac} below the Redfield Ratio, but a few have elevated C_{org}/P_{org} paired with low C_{org}/P_{reac}. These latter samples suggest that while phosphorus regeneration back to the water column may have been slightly more efficient during deposition of the Oppokun Formation, P was largely retained in the sediments by sorption onto Fe-(oxyhydr)oxides. The Oppokun Formation also has a very low TOC content (0.02–0.31 wt%, mean < 0.1 wt%), which may have been maintained by low productivity and nutrient-limited conditions as indicated by phosphorus phase partitioning. In contrast to the Tonian part of the succession, P_{det2} was not a major constituent of any of the Ediacaran-Cambrian sedimentary rocks in this study (< 10% of summed phosphorus; Figure 7), suggesting that sequestration with Al-rich mineral phases described above was not a major contributor to P cycling during the Ediacaran-Cambrian interval at this location.

5.7 | S/H Ratios and Environmental Heterogeneity in the Neoproterozoic Oceans

The chronic phosphate limitation in the late Tonian Lena-Anabar Basin has important implications for understanding the local environmental controls modulating the rise of eukaryotes to ecological prominence in Neoproterozoic oceans. In modern aquatic environments, the nutrient budget, the amount of primary productivity that can be sustained and the eukaryotic contribution to biomass are all tightly correlated, with eukaryotic plankton generally thriving in more eutrophic and nutrient-replete environments (Biddanda et al. 2001; Chisholm 1992; Huete-Ortega et al. 2010; Marañón 2015). The S/H ratio broadly reflects the ratio of algal to bacterial productivity. Accordingly, organic-lean sedimentary successions with low S/H values in the Ediacaran (S/H < 0.1, and as low as 0.01, Pehr et al. 2018) and Paleozoic (S/H < 0.1, Lee, Love, Hopkins, et al. 2019; Marshall et al. 2023; Rohrssen et al. 2013) have been interpreted as oligotrophy-prone environments with low algal productivity. Low S/H ratios in Cryogenian rocks are also associated with P limitation in marine settings as indicated by phosphorus phase partitioning (Bowyer et al. 2023). Further, absolute sterane yields normalized to TOC content help assess the relative contribution of eukaryotes to sedimentary organic matter across sample sets of similar thermal maturity, providing a broad comparative measure of algal contribution to productivity.

With this in mind, we interpret the low S/H and corresponding low sterane yields for the late Tonian Lena-Anabar Basin rocks in our drill-cores as representing low algal productivity. S/H values from the late Tonian Lena-Anabar Basin (< 0.05) are an order of magnitude lower than the minimum end of the Phanerozoic marine average range for oils and source rocks (S/H = 0.5–2.0), while sterane yields normalized to TOC are 3–4 orders of magnitude lower than those of the Ediacaran Taimylyr Formation (Table S5). These differences in sterane yields constitute large magnitude differences with eutrophic paleoenvironments. The persistent phosphorus limitation inferred in this study for the Lena-Anabar Basin during the late Tonian would have maintained low primary productivity and favored bacterial dominance, given the limited nutrient resources for growth (Reinhard et al. 2020). The unusual partitioning of P into a recalcitrant Al-rich mineral phase in northern Siberia effectively suppressed the delivery supply of bioavailable phosphorus into this marine basin and sustained chronic local P-limitation.

The higher S/H values (> 0.2) found for our late Tonian rocks are associated with moderate-high TOC rocks (Figure 8) across these basins, suggesting that heterogeneity in algal productivity reflects regional differences in total productivity (Zumberge et al. 2020), linked strongly to nutrient availability. While TOC content of ancient rocks is also controlled by sedimentation rate and water-column redox conditions, in addition to productivity (Felix 2014), differences in spatial variations in sedimentary TOC in modern oceans often broadly track productivity in overlying waters (Berger and Herguera 1992). The large range of TOC values within our sample set encompassing over an order of magnitude difference between the organic-lean and organic-replete rocks helps identify the high and low productivity end-members. The Lena-Anabar samples consistently plot near the origin (Figure 8), all having consistently low TOC and low S/H values, which is where samples from a low productivity setting in which bacteria outcompete algae are predicted to fall.

S/H values from the Lena-Anabar Basin are typically an order of magnitude lower than S/H for the Chuar Group (Figure 8, Table S4) and near the lower end of those for the Visingsö Group (Zumberge et al. 2020), but are similar to the range of ratios reported for the ca. 800 Ma Bitter Springs Group (Brocks et al. 2017). Sterane yields for the upper Walcott Member of the Chuar Group are also three orders of magnitude higher than those for the Lena-Anabar Basin (Table S5). This evidence for low algal productivity in the Lena-Anabar Basin, as indicated by very low S/H and total sterane abundance yields, supported by our phosphorus phase partitioning data, is consistent with deposition in an oligotrophic, marine environment. Additionally, mean total phosphorus content for shales in the Visingsö Group is an order of magnitude higher (2350 ppm, $n = 124$, Planavsky et al. 2023) than in the Lena-Anabar Basin, suggesting that greater P availability may have been a factor in higher S/H and algal productivity found for the Visingsö Group.

14724669, 2026, 5, Downloaded from https://onlinelibrary.wiley.com/doi/10.1111/gbi.70061 by NICE, National Institute for Health and Care Excellence, Wiley Online Library on [07/10/2026]. See the Terms and Conditions (https://onlinelibrary.wiley.com/terms-and-conditions) on Wiley Online Library for rules of use; OA articles are governed by the applicable Creative Commons License

Low sterane abundances persisted in northern Siberia under predominantly oxic conditions (Figure 8a), while they are significantly more abundant in the strongly redox-stratified marine environments in which the Chuar Group was deposited, counter to hypotheses suggesting oxygen availability was the dominant local control on eukaryotic environmental abundance. In our data and in other Neoproterozoic biomarker data with same-sample redox controls, there is no relationship between redox as indicated by Fe_{HR}/Fe_T and S/H (Figure 8b). Bobrovskiy et al. (2024) have argued that oxic decomposition can lower the S/H ratio from the original biological material, but the results of this study are not consistent with their materials or methods. Their ancient samples consist of thin organic films removed with tweezers, rather than multiple grams of powdered rock analyzed here, and their ancient samples lack maturity and oxidation controls from programmed pyrolysis and contain TOC of $<0.1\%$. Moreover, their experimental results predict that C_{28} and C_{29} steranes are preferentially lost under oxidizing conditions. Amongst Ediacaran samples from this study and the literature, there is no relationship between C_{29}/C_{27} and Fe_{HR}/Fe_T (Figure S10), while C_{29} steranes are absent even from the most anoxic and high TOC Tonian samples. This suggests that within the carefully screened samples examined here, sterane ratios are driven by age, not redox, and that careful sample screening for biomarker preservation using established protocols (French et al. 2015) avoids taphonomic biases created by intense oxidative degradation.

Anoxia and productivity are not unconnected. Indeed, sustained primary productivity from phytoplankton in the photic zone can drive prolonged euxinia in the lower part of the water column (Liu et al. 2018; Meyer and Kump 2008; Zimmerman and Canuel 2000), as organic matter exported from the oxic surface layer to deeper waters consumes oxidants (including dissolved O_2), such that P availability and the biological pump are major controls on marine redox on long timescales (Meyer et al. 2016; Van Cappellen and Ingall 1996). Highly productive and alga-rich ancient marine settings are often associated with redox-stratification and anoxic-euxinic bottom waters (Martinez et al. 2019), and similar mechanisms may explain the association between algal productivity and redox in the Chuar Group. However, sulfide-limited, ferruginous anoxic conditions and oligotrophy often coexist for Proterozoic rocks (e.g., Song et al. 2023), where iron minerals retain P in sediments and prevent its release into the water column, limiting its availability to marine organisms. These nuances may explain the lack of any obvious relationship between S/H and redox state observed in our data.

The S/H values also vary considerably in Ediacaran samples (Figure 6), consistent with spatial and temporal heterogeneity in eukaryote abundance driven by variations in local environmental conditions through time. Samples from the Taimylyr Formation yielded moderate S/H values within the lower end of the Phanerozoic average. These S/H values are similar to those for the Ediacaran Ara Group carbonates of Oman (0.43–1.30, mean = 0.85; Grosjean et al. 2009; Love et al. 2009), from a similar, shallow-marine, carbonate environment, and overlap with the lower end of S/H values for oils from eastern Siberia (0.47–4.63, mean = 1.18; Kelly et al. 2011). High sterane yields (mean = 616 ppm of TOC; Table S5), along with some evidence for intermittent euxinia, suggest that the Taimylyr Formation was deposited in a generally more productive setting than that of the late Tonian interval given the relationship between euxinia and productivity (Meyer and Kump 2008). However, the moderately low TOC contents (mean = 0.31 wt%), together with temporal variations in salinity and basin restriction, further complicate the overall interpretation for this interval.

Unlike the Taimylyr Formation, the early Cambrian Oppokun Formation exhibits similar S/H (<0.06) to Tonian samples and only slightly higher sterane yields, suggesting similarly low levels of algal productivity. Comparably low S/H ratios and TOC contents have been observed in late Ediacaran rocks deposited in shallow-marine, epicontinental basins of Baltica (Pehr et al. 2018). In northern Siberia, S/H ratios for the Khatyspyt Formation (Duda et al. 2020; Melnik et al. 2024), stratigraphically positioned between the Taimylyr and Oppokun formations, are intermediate between those for these units (0.1–0.3). The phosphorus phase partitioning results from this study also suggest phosphorus limitation during deposition of the Oppokun Formation. Our results for Ediacaran-Cambrian sedimentary rocks support previous work highlighting regional heterogeneity in eukaryote abundance in the Ediacaran ocean, with low S/H typically associated with low productivity environments and deposition of organic-lean sediments (Duda et al. 2020; Goryl et al. 2018; Pehr et al. 2018).

A strong nutrient control on ocean ecology and carbon cycling may also explain a broader, secular trend proposed for Neoproterozoic oxygenation and the evolution of complex life. Specifically, increased phosphate input to the late Tonian ocean system may have facilitated the rise of eukaryotes and more complex food webs leading to a stronger biological carbon pump and increased atmosphere–ocean oxygenation (Reinhard et al. 2020). While our results are consistent with this hypothesis, our data underscore the importance of local environmental phenomena in potentially interacting with this global secular trend. Closer examination of Tonian biomarker datasets might also point speculatively to a secular shift in ecology in the latest Tonian, as the Walcott Member of the Chuar Group, with the highest S/H values found in this study, was deposited between 735 and 729 Ma (Rooney et al. 2017; Dehler et al. 2023). The highest known Tonian S/H value, 0.42, is from the Steptoe Formation of Western Australia, with an estimated age of 725–717 Ma (Brocks et al. 2017). In comparison, the carbonaceous shales of the upper Visingsö Group, which contain appreciable regular steranes and low to moderate TOC contents (Zumberge et al. 2020), were dated at 753.3 ± 5.9 Ma with Re-Os geochronology (Planavsky et al. 2023), while the Tonian strata from northern Siberia with lower S/H are unlikely to be much younger than 750 Ma, based on our chemostratigraphic data. Enhanced continental weathering associated with the Tonian breakup of Rodinia may be a common cause behind both the proposed increase in marine phosphorus inputs and eukaryote abundance as well as the onset of the Sturtian glaciation (Cox et al. 2016; Horton 2015) that commenced at ca. 717 Ma (Macdonald and Swanson-Hysell 2023) and persisted till ca. 661 Ma. However, as our phosphorus data indicate, sequestration of weathered phosphorus into a recalcitrant mineral phase that was not readily bioavailable and was not efficiently delivered from continents to the adjacent marine basins may have created competing and net counterintuitive local effects that need to be recognized.

14724669, 2026, 5, Downloaded from https://onlinelibrary.wiley.com/doi/10.1111/gbi.70061 by NICE, National Institute for Health and Care Excellence, Wiley Online Library on [07/10/2026]. See the Terms and Conditions (https://onlinelibrary.wiley.com/terms-and-conditions) on Wiley Online Library for rules of use; OA articles are governed by the applicable Creative Commons License

This possible secular trend in S/H highlights the need for better radiometric age constraints for late Tonian sedimentary records, together with strategic sampling to obtain organic geochemical data, especially to fill the conspicuous ca. 1000–800 Ma gap in the lipid biomarker record. Better temporal control should be accompanied by examination of different basins and environmental settings to constrain the onset and trajectory of the Neoproterozoic rise of eukaryotes. Assessments of first-order changes in eukaryote abundance through time need to factor in paleogeographic mapping to gauge the degree of regional heterogeneity in community structure between nutrient-replete and oligotrophic settings through a particular geologic interval.

A late Tonian radiation of oxygenic algal phytoplankton in the oxic surface waters of the open ocean may have enhanced organic carbon export and burial of organic matter in the underlying deep ocean and boosted the net production of oxygen (Lenton et al. 2014; Tziperman et al. 2011). While these first-order secular changes in microbial ecology happened in concert with contemporaneous shifts in paleogeography and plate tectonics, a planktonic algal conquest of the Neoproterozoic surface ocean distal from the shoreline may have ushered in a transition to an Earth System with a modified ocean carbon cycle and major glaciations (Hülse and Ridgwell 2025) and presaged the evolution of complex multicellular life.

6 | Conclusions

Lipid biomarker distributions from the Lena-Anabar Basin of northern Siberia confirm the ubiquity of regular steranes in late Tonian sedimentary rocks, with a strong C_{27} sterane preference and an absence of C_{29} sterane in the geological record prior to the Sturtian glaciation contrasting with the full C_{27}-C_{29} series and C_{29} preference found for Ediacaran intervals. Our detailed geochemical investigation of multiple samples from two adjacent drill-cores from Siberia adds to a growing body of biomarker evidence suggesting that the shift from red algal (C_{27}) to green algal (C_{29}) preference likely reflects a first order secular trend related to widespread ecological and environmental change in the Neoproterozoic ocean, perhaps in response to the Snowball Earth glaciations and/or other natural selection drivers.

The Lena-Anabar Basin represents an oligotrophic endmember within late Tonian marine settings, with very low S/H ratios (<0.05) and substantially lower absolute sterane abundances compared to the Chuar Group for equivalent thermal maturity samples, reflecting a low, but non-zero environmental abundance of marine eukaryotes, including algae. Oligotrophy was sustained locally by chronic phosphorus limitation in these dominantly oxic to weakly reducing marine environments. The Taimylyr Formation, determined here to be of late Ediacaran age and deposited in a shallow-marine, redox-stratified setting, sustained higher levels of algal (eukaryotic) productivity in surface waters. The younger (earliest Cambrian) Oppokun Formation was deposited under open-marine conditions that were strongly nutrient-limited, consistent with very low TOC content and uniformly low S/H values. No discernible environmental redox controls on S/H values and sterane carbon number distribution patterns were observed for the suite of Tonian and Ediacaran rocks. These results emphasize the strong influence of nutrient limitation, particularly of bioavailable phosphorus, in regulating primary productivity and sustaining biological and chemical regional heterogeneity within the Neoproterozoic ocean. Our study also underscores the importance of sampling a variety of depositional environments and locations when assessing the evolution of the ancient marine biosphere.

Unlike Mesoproterozoic records, regular steranes are ubiquitous lipid biomarker constituents in late Tonian and younger sedimentary rocks, even for highly oligotrophic ancient paleoenvironments in which bacteria outcompete eukaryotes for scarce nutrient resources. C_{27} steranes are the dominant steranes, and no significant amounts of C_{29} or C_{30} (24-ipc, 24-npc, or 26-mes) steranes are found in the pre-Sturtian sedimentary rocks from northern Siberia, consistent with the biomarker distributions previously reported for late Tonian sedimentary rocks from the Visingsö and Chuar groups. The emergence and ecological rise of oxygenic algal phytoplankton in the surface layer of the deep ocean during the late Tonian may have irreversibly changed the carbon cycle, allowing for higher organic carbon burial in the deep ocean and an oxygenation of the biosphere.

Acknowledgements

The authors acknowledge Ying Lin for contributions to analytical work, as well as funding from NASA Exobiology, NSF Biodiversity on a Changing Planet (BoCP) and the Petroleum Foundation of the American Chemical Society grant 624840ND2. Sr isotope analyses were funded by the research projects of IPGG RAS (no. FMUW-2021-0003). A. K. Khudoley and A.V. Prokopiev are gratefully acknowledged for access to samples used in this study. We thank Grand Canyon National Park for research and collecting permits for Chuar Group samples.

Funding

This work received funds from NASA Exobiology grant 80NSSC25K7812, NSF Biodiversity on a Changing Planet (BoCP) grant 2449386, and the Petroleum Foundation of the American Chemical Society grant 624840ND2. Sr isotope analyses were funded by the research projects of IPGG RAS (no. FMUW-2021-0003).

Conflicts of Interest

The authors declare no conflicts of interest.

Data Availability Statement

All data are available in the Supporting Information.

References

Adam, P., P. Schaeffer, and J. J. Brocks. 2018. "Synthesis of 26-Methyl Cholestane and Identification of Cryostanes in Mid-Neoproterozoic Sediments." *Organic Geochemistry* 115: 246–249. https://doi.org/10.1016/j.orggeochem.2017.11.006.

Alcott, L. J., A. J. Krause, E. U. Hammarlund, et al. 2020. "Development of Iron Speciation Reference Materials for Palaeoredox Analysis." *Geostandards and Geoanalytical Research* 44, no. 3: 581–591. https://doi.org/10.1111/ggr.12342.

Alcott, L. J., B. J. W. Mills, A. Bekker, and S. W. Poulton. 2022. "Earth's Great Oxidation Event Facilitated by the Rise of Sedimentary

14724669, 2026, 5, Downloaded from https://onlinelibrary.wiley.com/doi/10.1111/gbi.70061 by NICE, National Institute for Health and Care Excellence, Wiley Online Library on [07/10/2026]. See the Terms and Conditions (https://onlinelibrary.wiley.com/terms-and-conditions) on Wiley Online Library for rules of use; OA articles are governed by the applicable Creative Commons License

Phosphorus Recycling." *Nature Geoscience* 15, no. 3: 3. https://doi.org/10.1038/s41561-022-00906-5.

Bennett, W. W., and D. E. Canfield. 2020. "Redox-Sensitive Trace Metals as Paleoredox Proxies: A Review and Analysis of Data From Modern Sediments." *Earth-Science Reviews* 204: 103175. https://doi.org/10.1016/j.earscirev.2020.103175.

Berger, W. H., and J. C. Herguera. 1992. "Reading the Sedimentary Record of the Ocean's Productivity." In *Primary Productivity and Biogeochemical Cycles in the Sea*, edited by P. G. Falkowski and A. D. Woodhead, 455–486. Plenum Press.

Biddanda, B., M. Ogdahl, and J. Cotner. 2001. "Dominance of Bacterial Metabolism in Oligotrophic Relative to Eutrophic Waters." *Limnology and Oceanography* 46, no. 3: 730–739. https://doi.org/10.4319/lo.2001.46.3.0730.

Birgel, D., and J. Peckmann. 2008. "Aerobic Methanotrophy at Ancient Marine Methane Seeps: A Synthesis." *Organic Geochemistry, Stable Isotopes in Biogeosciences (II)* 39, no. 12: 1659–1667. https://doi.org/10.1016/j.orggeochem.2008.01.023.

Blumenberg, M., V. Thiel, W. Riegel, L. C. Kah, and J. Reitner. 2012. "Biomarkers of Black Shales Formed by Microbial Mats, Late Mesoproterozoic (1.1Ga) Taoudeni Basin, Mauritania." *Precambrian Research* 196–197: 113–127. https://doi.org/10.1016/j.precamres.2011.11.010.

Bobrovskiy, I., S. W. Poulton, J. M. Hope, and J. J. Brocks. 2024. "Impact of Aerobic Reworking of Biomass on Steroid and Hopanoid Biomarker Parameters Recording Ecological Conditions and Thermal Maturity." *Geochimica et Cosmochimica Acta* 364: 114–128. https://doi.org/10.1016/j.gca.2023.11.024.

Bortoluzzi, E. C., C. A. S. Pérez, J. D. Ardisson, T. Tiecher, and L. Caner. 2015. "Occurrence of Iron and Aluminum Sesquioxides and Their Implications for the P Sorption in Subtropical Soils." *Applied Clay Science* 104: 196–204. https://doi.org/10.1016/j.clay.2014.11.032.

Bowring, S. A., J. P. Grotzinger, C. E. Isachsen, A. H. Knoll, S. M. Pelechaty, and P. Kolosov. 1993. "Calibrating Rates of Early Cambrian Evolution." *Science* 261, no. 5126: 1293–1298. https://doi.org/10.1126/science.11539488.

Bowyer, F. T., A. J. Krause, Y. Song, et al. 2023. "Biological Diversification Linked to Environmental Stabilization Following the Sturtian Snowball Glaciation." *Science Advances* 9, no. 34: eadf9999. https://doi.org/10.1126/sciadv.adf9999.

Bowyer, F. T., R. A. Wood, and M. Yilales. 2024. "Sea Level Controls on Ediacaran-Cambrian Animal Radiations." *Science Advances* 10, no. 31: eado6462. https://doi.org/10.1126/sciadv.ado6462.

Bowyer, F. T., A. Y. Zhuravlev, R. Wood, et al. 2022. "Calibrating the Temporal and Spatial Dynamics of the Ediacaran—Cambrian Radiation of Animals." *Earth-Science Reviews* 225: 103913. https://doi.org/10.1016/j.earscirev.2021.103913.

Brocks, J. J. 2018. "The Transition From a Cyanobacterial to Algal World and the Emergence of Animals." *Emerging Topics in Life Sciences* 2, no. 2: 181–190. https://doi.org/10.1042/ETLS20180039.

Brocks, J. J., A. J. M. Jarrett, E. Sirantoine, et al. 2016. "Early Sponges and Toxic Protists: Possible Sources of Cryostane, an Age Diagnostic Biomarker Antedating Sturtian Snowball Earth." *Geobiology* 14, no. 2: 129–149. https://doi.org/10.1111/gbi.12165.

Brocks, J. J., A. J. M. Jarrett, E. Sirantoine, C. Hallmann, Y. Hoshino, and T. Liyanage. 2017. "The Rise of Algae in Cryogenian Oceans and the Emergence of Animals." *Nature* 548: 578–581. https://doi.org/10.1038/nature23457.

Brocks, J. J., G. D. Love, R. E. Summons, A. H. Knoll, G. A. Logan, and S. A. Bowden. 2005. "Biomarker Evidence for Green and Purple Sulphur Bacteria in a Stratified Palaeoproterozoic Sea." *Nature* 437: 7060. https://doi.org/10.1038/nature04068.

Brocks, J. J., B. J. Nettersheim, P. Adam, et al. 2023. "Lost World of Complex Life and the Late Rise of the Eukaryotic Crown." *Nature* 618, no. 7966: 767–773. https://doi.org/10.1038/s41586-023-06170-w.

Brunoir, T., C. Mulligan, A. Sistiaga, et al. 2023. "Common Origin of Sterol Biosynthesis Points to a Feeding Strategy Shift in Neoproterozoic Animals." *Nature Communications* 14, no. 1: 7941. https://doi.org/10.1038/s41467-023-43545-z.

Buatois, L. A., G. M. Narbonne, M. G. Mángano, N. B. Carmona, and P. Myrow. 2014. "Ediacaran Matground Ecology Persisted Into the Earliest Cambrian." *Nature Communications* 5, no. 1: 3544. https://doi.org/10.1038/ncomms4544.

Burdige, D. J. 2007. "Preservation of Organic Matter in Marine Sediments: Controls, Mechanisms, and an Imbalance in Sediment Organic Carbon Budgets?" *Chemical Reviews* 107, no. 2: 467–485. https://doi.org/10.1021/cr050347q.

Burki, F., A. J. Roger, M. W. Brown, and A. G. B. Simpson. 2020. "The New Tree of Eukaryotes." *Trends in Ecology & Evolution* 35, no. 1: 43–55. https://doi.org/10.1016/j.tree.2019.08.008.

Butterfield, N. J. 2000. "Bangiomorpha Pubescens n. Gen., n. sp.: Implications for the Evolution of Sex, Multicellularity, and the Mesoproterozoic/Neoproterozoic Radiation of Eukaryotes." *Paleobiology* 26, no. 3: 386–404. https://doi.org/10.1666/0094-8373(2000)026%3C0386:BPNGNS%3E2.0.CO;2.

Butterfield, N. J. 2015. "Early Evolution of the Eukaryota." *Palaeontology* 58, no. 1: 5–17. https://doi.org/10.1111/pala.12139.

Butterfield, N. J., A. H. Knoll, and K. Swett. 1994. "Paleobiology of the Neoproterozoic Svanbergfjellet Formation, Spitsbergen." *Lethaia* 27, no. 1: 76. https://doi.org/10.1111/j.1502-3931.1994.tb01558.x.

Canfield, D. E., R. Raiswell, J. T. Westrich, C. M. Reaves, and R. A. Berner. 1986. "The Use of Chromium Reduction in the Analysis of Reduced Inorganic Sulfur in Sediments and Shales." *Chemical Geology* 54, no. 1: 149–155. https://doi.org/10.1016/0009-2541(86)90078-1.

Chen, J., and R. E. Summons. 2001. "Complex Patterns of Steroidal Biomarkers in Tertiary Lacustrine Sediments of the Biyang Basin, China." *Organic Geochemistry* 32: 115–126.

Chen, J. H., R. P. Philip, J. M. Fu, and G. Y. Sheng. 1989. "The Occurrence and Identification of C30-C32 Lanostanes: A Novel Series of Tetracyclic Triterpenoid Hydrocarbons." *Geochimica et Cosmochimica Acta* 53: 2775–2779.

Chisholm, S. W. 1992. "Phytoplankton Size." In *Primary Productivity and Biogeochemical Cycles in the Sea*, edited by P. G. Falkowski and A. D. Woodhead, 213–237. Plenum Press.

Clarkson, M. O., S. W. Poulton, R. Guilbaud, and R. A. Wood. 2014. "Assessing the Utility of Fe/Al and Fe-Speciation to Record Water Column Redox Conditions in Carbonate-Rich Sediments." *Chemical Geology* 382: 111–122. https://doi.org/10.1016/j.chemgeo.2014.05.031.

Claypool, G. E., W. T. Holser, I. R. Kaplan, H. Sakai, and I. Zak. 1980. "The Age Curves of Sulfur and Oxygen Isotopes in Marine Sulfate and Their Mutual Interpretation." *Chemical Geology* 28: 199–260. https://doi.org/10.1016/0009-2541(80)90047-9.

Cohen, P. A., and A. H. Knoll. 2012. "Scale Microfossils From the Mid-Neoproterozoic Fifteenmile Group, Yukon Territory." *Journal of Paleontology* 86, no. 5: 775–800. https://doi.org/10.1666/11-138.1.

Cohen, P. A., and F. A. Macdonald. 2015. "The Proterozoic Record of Eukaryotes." *Paleobiology* 41, no. 4: 610–632. https://doi.org/10.1017/pab.2015.25.

Cohen, P. A., and L. A. Riedman. 2018. "It's a Protist-Eat-Protist World: Recalcitrance, Predation, and Evolution in the Tonian–Cryogenian Ocean." *Emerging Topics in Life Sciences* 2, no. 2: 173–180. https://doi.org/10.1042/ETLS20170145.

14724669, 2026, 5, Downloaded from https://onlinelibrary.wiley.com/doi/10.1111/gbi.70061 by NICE, National Institute for Health and Care Excellence, Wiley Online Library on [07/10/2026]. See the Terms and Conditions (https://onlinelibrary.wiley.com/terms-and-conditions) on Wiley Online Library for rules of use; OA articles are governed by the applicable Creative Commons License

Cohen, P. A., J. V. Strauss, A. D. Rooney, M. Sharma, and N. Tosca. 2017. "Controlled Hydroxyapatite Biomineralization in an ~810 Million-Year-Old Unicellular Eukaryote." *Science Advances* 3, no. 6: e1700095. https://doi.org/10.1126/sciadv.1700095.

Cox, G. M., G. P. Halverson, R. K. Stevenson, et al. 2016. "Continental Flood Basalt Weathering as a Trigger for Neoproterozoic Snowball Earth." *Earth and Planetary Science Letters* 446: 89–99. https://doi.org/10.1016/j.epsl.2016.04.016.

Crockford, P. W., M. Kunzmann, A. Bekker, et al. 2019. "Claypool Continued: Extending the Isotopic Record of Sedimentary Sulfate." *Chemical Geology* 513: 200–225. https://doi.org/10.1016/j.chemgeo.2019.02.030.

Cui, H., D. V. Grazhdankin, S. Xiao, et al. 2016. "Redox-Dependent Distribution of Early Macro-Organisms: Evidence From the Terminal Ediacaran Khatyspyt Formation in Arctic Siberia." *Palaeogeography, Palaeoclimatology, Palaeoecology* 461: 122–139. https://doi.org/10.1016/j.palaeo.2016.08.015.

Dakhnova, M. V., T. P. Zheglova, and S. V. Mozhegova. 2014. "Generation Characteristics of Organic Matter and Distribution of Biomarkers in Bitumens of the Riphean, Vendian, and Cambrian Source Rocks of the Siberian Platform." *Russian Geology and Geophysics* 55: 755–762. https://doi.org/10.1016/j.rgg.2014.05.018.

Dehler, C., G. Gehrels, S. Porter, et al. 2017. "Synthesis of the 780–740 ma Chuar, Uinta Mountain, and Pahrump (ChUMP) Groups, Western USA: Implications for Laurentia-Wide Cratonic Marine Basins." *GSA Bulletin* 129, no. 5–6: 607–624. https://doi.org/10.1130/B31532.1.

Dehler, C., M. Schmitz, A. Bullard, et al. 2023. "Precise U-Pb Age Models Refine Neoproterozoic Western Laurentian Rift Initiation, Correlation, and Earth System Changes." *Precambrian Research* 396: 107156. https://doi.org/10.1016/j.precamres.2023.107156.

Dehler, C. M., M. Elrick, K. E. Karlstrom, G. A. Smith, L. J. Crossey, and J. M. Timmons. 2001. "Neoproterozoic Chuar Group (~800–742Ma), Grand Canyon: A Record of Cyclic Marine Deposition During Global Cooling and Supercontinent Rifting." *Sedimentary Geology* 141–142: 465–499. https://doi.org/10.1016/S0037-0738(01)00087-2.

Desmond, E., and S. Gribaldo. 2009. "Phylogenomics of Sterol Synthesis: Insights Into the Origin, Evolution, and Diversity of a Key Eukaryotic Feature." *Genome Biology and Evolution* 1: 364–381. https://doi.org/10.1093/gbe/evp036.

Doyle, K. A., S. W. Poulton, R. J. Newton, V. N. Podkovyrov, and A. Bekker. 2018. "Shallow Water Anoxia in the Mesoproterozoic Ocean: Evidence From the Bashkir Meganticlinorium, Southern Urals." *Precambrian Research* 317: 196–210. https://doi.org/10.1016/j.precamres.2018.09.001.

Duda, J.-P., H. König, M. Reinhardt, J. Shuvalova, and P. Parkhaev. 2021. "Molecular Fossils Within Bitumens and Kerogens From the ~1 ga Lakhanda Lagerstätte (Siberia, Russia) and Their Significance for Understanding Early Eukaryote Evolution." *PalZ* 95, no. 4: 577–592. https://doi.org/10.1007/s12542-021-00593-4.

Duda, J.-P., G. D. Love, V. I. Rogov, D. S. Melnik, M. Blumenberg, and D. V. Grazhdankin. 2020. "Understanding the Geobiology of the Terminal Ediacaran Khatyspyt Lagerstätte (Arctic Siberia, Russia)." *Geobiology* 18, no. 6: 643–662. https://doi.org/10.1111/gbi.12412.

Duda, J.-P., V. Thiel, J. Reitner, and D. Grazhdankin. 2016. "Opening Up a Window Into Ecosystems With Ediacara-Type Organisms: Preservation of Molecular Fossils in the Khatyspyt Lagerstätte (Arctic Siberia)." *PalZ* 90, no. 4: 659–671. https://doi.org/10.1007/s12542-016-0317-5.

Dutta, S., S. Bhattacharya, and S. V. Raju. 2013. "Biomarker Signatures From Neoproterozoic–Early Cambrian Oil, Western India." *Organic Geochemistry* 56: 68–80. https://doi.org/10.1016/j.orggeochem.2012.12.007.

Espitalie, J., M. Madec, B. Tissot, J. J. Mennig, and P. Leplat. 1977. "Source Rock Characterization Method for Petroleum Exploration. Offshore Technology Conference. Offshore Technology Conference." https://doi.org/10.4043/2935-ms.

Eyster, A., B. P. Weiss, K. Karlstrom, and F. A. Macdonald. 2019. "Paleomagnetism of the Chuar Group and Evaluation of the Late Tonian Laurentian Apparent Polar Wander Path With Implications for the Makeup and Breakup of Rodinia." *GSA Bulletin* 132, no. 3–4: 710–738. https://doi.org/10.1130/B32012.1.

Farrimond, P., G. D. Love, A. N. Bishop, H. E. Innes, D. F. Watson, and C. E. Snape. 2003. "Evidence for the Rapid Incorporation of Hopanoids Into Kerogen." *Geochimica et Cosmochimica Acta* 67, no. 7: 1383–1394. https://doi.org/10.1016/S0016-7037(02)01287-5.

Farrimond, P., H. M. Talbot, D. F. Watson, L. K. Schulz, and A. Wilhelms. 2004. "Methylhopanoids: Molecular Indicators of Ancient Bacteria and a Petroleum Correlation Tool." *Geochimica et Cosmochimica Acta* 68, no. 19: 3873–3882. https://doi.org/10.1016/j.gca.2004.04.011.

Felix, M. 2014. "A Comparison of Equations Commonly Used to Calculate Organic Carbon Content and Marine Palaeoproductivity From Sediment Data." *Marine Geology* 347: 1–11. https://doi.org/10.1016/j.margeo.2013.10.006.

Flannery, E. N., and S. C. George. 2014. "Assessing the Syngeneity and Indigeneity of Hydrocarbons in the ~1.4Ga Velkerri Formation, McArthur Basin, Using Slice Experiments." *Organic Geochemistry* 77: 115–125. https://doi.org/10.1016/j.orggeochem.2014.10.008.

Fonseca, R., T. Canário, M. Morais, and F. J. A. S. Barriga. 2011. "Phosphorus Sequestration in Fe-Rich Sediments From Two Brazilian Tropical Reservoirs." *Applied Geochemistry* 26, no. 9: 1607–1622. https://doi.org/10.1016/j.apgeochem.2011.04.017.

French, K. L., J. E. Birdwell, and M. D. Vanden Berg. 2020. "Biomarker Similarities Between the Saline Lacustrine Eocene Green River and the Paleoproterozoic Barney Creek Formations." *Geochimica et Cosmochimica Acta* 274: 228–245. https://doi.org/10.1016/j.gca.2020.01.053.

French, K. L., C. Hallmann, J. M. Hope, et al. 2015. "Reappraisal of Hydrocarbon Biomarkers in Archean Rocks." *Proceedings of the National Academy of Sciences* 112, no. 19: 5915–5920. https://doi.org/10.1073/pnas.1419563112.

French, K. L., N. J. Tosca, C. Cao, and R. E. Summons. 2012. "Diagenetic and Detrital Origin of Moretane Anomalies Through the Permian–Triassic Boundary." *Geochimica et Cosmochimica Acta* 84: 104–125. https://doi.org/10.1016/j.gca.2012.01.004.

Frolov, S. V., G. G. Akhmanov, E. V. Kozlova, O. V. Krylov, K. A. Sitar, and Y. I. Galushkin. 2011. "Riphean Basins of the Central and Western Siberian Platform." *Marine and Petroleum Geology* 28: 906–920. https://doi.org/10.1016/j.marpetgeo.2010.01.023.

Gallagher, T. M., N. D. Sheldon, J. L. Mauk, S. V. Petersen, N. Gueneli, and J. J. Brocks. 2017. "Constraining the Thermal History of the North American Midcontinent Rift System Using Carbonate Clumped Isotopes and Organic Thermal Maturity Indices." *Precambrian Research* 294: 53–66. https://doi.org/10.1016/j.precamres.2017.03.022.

Gibson, T. M., P. M. Shih, V. M. Cumming, et al. 2018. "Precise Age of Bangiomorpha Pubescens Dates the Origin of Eukaryotic Photosynthesis." *Geology* 46, no. 2: 135–138. https://doi.org/10.1130/G39829.1.

Gorokhov, I. M., A. B. Kuznetsov, I. M. Vasil'eva, et al. 2022. "Sr and pb Isotopic Compositions in Dolostones of the Lower Riphean Billyakh Group, Anabar Uplift: Step-Leaching Technique in Chemostratigraphy and Geochronology." *Stratigraphy and Geological Correlation* 30, no. 4: 201–227. https://doi.org/10.1134/S0869593822040049.

Gorokhov, I. M., M. A. Semikhatov, A. V. Baskakov, et al. 1995. "Sr Isotopic Composition in Riphean, Vendian, and Lower Cambrian Carbonates From Siberia." *Geological Correlation* 3: 1–28.

14724669, 2026, 5, Downloaded from https://onlinelibrary.wiley.com/doi/10.1111/gbi.70061 by NICE, National Institute for Health and Care Excellence, Wiley Online Library on [07/10/2026]. See the Terms and Conditions (https://onlinelibrary.wiley.com/terms-and-conditions) on Wiley Online Library for rules of use; OA articles are governed by the applicable Creative Commons License

Goryl, M., L. Marynowski, J. J. Brocks, I. Bobrovskiy, and A. Derkowski. 2018. "Exceptional Preservation of Hopanoid and Steroid Biomarkers in Ediacaran Sedimentary Rocks of the East European Craton." *Precambrian Research* 316: 38–47. https://doi.org/10.1016/j.precamres.2018.07.026.

Grantham, P. J., and L. L. Wakefield. 1988. "Variations in the Sterane Carbon Number Distributions of Marine Source Rock Derived Crude Oils Through Geological Time." *Organic Geochemistry* 12, no. 1: 61–73. https://doi.org/10.1016/0146-6380(88)90115-5.

Grazhdankin, D., K. Nagovitsin, E. Golubkova, et al. 2020. "Doushantuo-Pertatataka-Type Acanthomorphs and Ediacaran Ecosystem Stability." *Geology* 48, no. 7: 708–712. https://doi.org/10.1130/G47467.1.

Grazhdankin, D. V., U. Balthasar, K. E. Nagovitsin, and B. B. Kochnev. 2008. "Carbonate-Hosted Avalon-Type Fossils in Arctic Siberia." *Geology* 36, no. 10: 803–806. https://doi.org/10.1130/G24946A.1.

Grosjean, E., G. D. Love, C. Stalvies, D. A. Fike, and R. E. Summons. 2009. "Origin of Petroleum in the Neoproterozoic–Cambrian South Oman Salt Basin." *Organic Geochemistry* 40, no. 1: 87–110. https://doi.org/10.1016/j.orggeochem.2008.09.011.

Grotheer, H., A. M. Robert, P. F. Greenwood, and K. Grice. 2015. "Stability and Hydrogenation of Polycyclic Aromatic Hydrocarbons During Hydropyrolysis (HyPy) – Relevance for High Maturity Organic Matter." *Organic Geochemistry* 86: 45–54. https://doi.org/10.1016/j.orggeochem.2015.06.007.

Gueneli, N., A. M. McKenna, N. Ohkouchi, et al. 2018. "1.1-Billion-Year-Old Porphyrins Establish a Marine Ecosystem Dominated by Bacterial Primary Producers." *Proceedings of the National Academy of Sciences* 115, no. 30: E6978–E6986. https://doi.org/10.1073/pnas.1803866115.

Guilbaud, R., S. W. Poulton, J. Thompson, et al. 2020. "Phosphorus-Limited Conditions in the Early Neoproterozoic Ocean Maintained Low Levels of Atmospheric Oxygen." *Nature Geoscience* 13, no. 4: 4. https://doi.org/10.1038/s41561-020-0548-7.

Halverson, G. P., P. F. Hoffman, D. P. Schrag, A. C. Maloof, and A. H. N. Rice. 2005. "Toward a Neoproterozoic Composite Carbon-Isotope Record." *GSA Bulletin* 117, no. 9–10: 1181–1207. https://doi.org/10.1130/B25630.1.

Halverson, G. P., S. M. Porter, and T. M. Gibson. 2018. "Dating the Late Proterozoic Stratigraphic Record." *Emerging Topics in Life Sciences* 2, no. 2: 137–147. https://doi.org/10.1042/ETLS20170167.

Halverson, G. P., B. P. Wade, M. T. Hurtgen, and K. M. Barovich. 2010. "Neoproterozoic Chemostratigraphy." *Precambrian Research* 182, no. 4: 337–350. https://doi.org/10.1016/j.precamres.2010.04.007.

Hayes, J. M., H. Strauss, and A. J. Kaufman. 1999. "The Abundance of 13C in Marine Organic Matter and Isotopic Fractionation in the Global Biogeochemical Cycle of Carbon During the Past 800 ma." *Chemical Geology* 161, no. 1: 103–125. https://doi.org/10.1016/S0009-2541(99)00083-2.

Hermann, T. N., and V. N. Podkovyrov. 2006. "Fungal Remains From the Late Riphean." *Paleontological Journal* 40, no. 2: 207–214.

Hermann, T. N., and V. N. Podkovyrov. 2010. "A Discovery of Riphean Heterotrophs in the Lakhanda Group of Siberia." *Paleontological Journal* 44, no. 4: 374–383. https://doi.org/10.1134/S0031030110040027.

Holba, A. G., E. Tegelaar, L. Ellis, and M. S. Singletary. 2000. "Tetracyclic Polyprenoids: Indicators of Freshwater (Lacustrine) Algal Input." *Geology* 28, no. 3: 251–254.

Horton, F. 2015. "Did Phosphorus Derived From the Weathering of Large Igneous Provinces Fertilize the Neoproterozoic Ocean?" *Geochemistry, Geophysics, Geosystems* 16, no. 6: 1723–1738. https://doi.org/10.1002/2015GC005792.

Hoshino, Y., and E. A. Gaucher. 2021. "Evolution of Bacterial Steroid Biosynthesis and Its Impact on Eukaryogenesis." *Proceedings of the National Academy of Sciences* 118, no. 25: e2101276118. https://doi.org/10.1073/pnas.2101276118.

Hoshino, Y., and E. A. Gaucher. 2024. "Impact of Steroid Biosynthesis on the Aerobic Adaptation of Eukaryotes." *Geobiology* 22, no. 4: e12612. https://doi.org/10.1111/gbi.12612.

Hoshino, Y., A. Poshibaeva, W. Meredith, et al. 2017. "Cryogenian Evolution of Stigmasteroid Biosynthesis." *Science Advances* 3, no. 9: e1700887. https://doi.org/10.1126/sciadv.1700887.

Huete-Ortega, M., E. Marañón, M. Varela, and A. Bode. 2010. "General Patterns in the Size Scaling of Phytoplankton Abundance in Coastal Waters During a 10-Year Time Series." *Journal of Plankton Research* 32, no. 1: 1–14. https://doi.org/10.1093/plankt/fbp104.

Hülse, D., and A. Ridgwell. 2025. "Instability in the Geological Regulation of Earth's Climate." *Science* 389: eadh7730. https://doi.org/10.1126/science.adh7730.

Ingall, E., and R. Jahnke. 1994. "Evidence for Enhanced Phosphorus Regeneration From Marine Sediments Overlain by Oxygen Depleted Waters." *Geochimica et Cosmochimica Acta* 58, no. 11: 2571–2575. https://doi.org/10.1016/0016-7037(94)90033-7.

Ingall, E., and R. Jahnke. 1997. "Influence of Water-Column Anoxia on the Elemental Fractionation of Carbon and Phosphorus During Sediment Diagenesis." *Marine Geology, Phosphorus Cycling and Sedimentation in Marine and Freshwater Systems* 139, no. 1: 219–229. https://doi.org/10.1016/S0025-3227(96)00112-0.

Ingall, E. D., R. M. Bustin, and P. Van Cappellen. 1993. "Influence of Water Column Anoxia on the Burial and Preservation of Carbon and Phosphorus in Marine Shales." *Geochimica et Cosmochimica Acta* 57, no. 2: 303–316. https://doi.org/10.1016/0016-7037(93)90433-W.

Isson, T. T., G. D. Love, C. L. Dupont, et al. 2018. "Tracking the Rise of Eukaryotes to Ecological Dominance With Zinc Isotopes." *Geobiology* 16, no. 4: 341–352. https://doi.org/10.1111/gbi.12289.

Isson, T. T., and N. J. Planavsky. 2018. "Reverse Weathering as a Long-Term Stabilizer of Marine pH and Planetary Climate." *Nature* 560: 7719. https://doi.org/10.1038/s41586-018-0408-4.

Jarrett, A. J. M., G. M. Cox, J. J. Brocks, E. Grosjean, C. J. Boreham, and D. S. Edwards. 2019. "Microbial Assemblage and Palaeoenvironmental Reconstruction of the 1.38 ga Velkerri Formation, McArthur Basin, Northern Australia." *Geobiology* 17, no. 4: 360–380. https://doi.org/10.1111/gbi.12331.

Johnston, D. T., S. W. Poulton, C. Dehler, et al. 2010. "An Emerging Picture of Neoproterozoic Ocean Chemistry: Insights From the Chuar Group, Grand Canyon, USA." *Earth and Planetary Science Letters* 290, no. 1: 64–73. https://doi.org/10.1016/j.epsl.2009.11.059.

Kaufman, A. J., S. B. Jacobsen, and A. H. Knoll. 1993. "The Vendian Record of Sr and C Isotopic Variations in Seawater: Implications for Tectonics and Paleoclimate." *Earth and Planetary Science Letters* 120, no. 3: 409–430. https://doi.org/10.1016/0012-821X(93)90254-7.

Kaufman, A. J., and A. H. Knoll. 1995. "Neoproterozoic Variations in the C-Isotopic Composition of Seawater: Stratigraphic and Biogeochemical Implications." *Precambrian Research, Neoproterozoic Stratigraphy and Earth History* 73, no. 1: 27–49. https://doi.org/10.1016/0301-9268(94)00070-8.

Kelly, A. E., G. D. Love, J. E. Zumberge, and R. E. Summons. 2011. "Hydrocarbon Biomarkers of Neoproterozoic to Lower Cambrian Oils From Eastern Siberia." *Organic Geochemistry* 42, no. 6: 640–654. https://doi.org/10.1016/j.orggeochem.2011.03.028.

Khabarov, E. M., and O. P. Izokh. 2014. "Sedimentology and Isotope Geochemistry of Riphean Carbonates in the Kharaulakh Range of Northern East Siberia." *Russian Geology and Geophysics, Urgent Problems of Petroleum Geology (Dedicated to the 80th Birthday of Academician Aleksei E. Kontorovich)* 55, no. 5: 629–648. https://doi.org/10.1016/j.rgg.2014.05.008.

14724669, 2026, 5, Downloaded from https://onlinelibrary.wiley.com/doi/10.1111/gbi.70061 by NICE, National Institute for Health and Care Excellence, Wiley Online Library on [07/10/2026]. See the Terms and Conditions (https://onlinelibrary.wiley.com/terms-and-conditions) on Wiley Online Library for rules of use; OA articles are governed by the applicable Creative Commons License

Killops, S., and V. Killops. 2005. *Introduction to Organic Geochemistry*. 2nd ed. Blackwell.

Knoll, A. H., E. J. Javaux, D. Hewitt, and P. Cohen. 2006. "Eukaryotic Organisms in Proterozoic Oceans." *Philosophical Transactions of the Royal Society, B: Biological Sciences* 361, no. 1470: 1023–1038. https://doi.org/10.1098/rstb.2006.1843.

Knoll, A. H., R. E. Summons, J. R. Waldbauer, and J. E. Zumberge. 2007. "The Geological Succession of Primary Producers in the Oceans." In *Evolution of Primary Producers in the Sea*, 133–163. Elsevier.

Kodner, R. B., A. Pearson, R. E. Summons, and A. H. Knoll. 2008. "Sterols in Red and Green Algae: Quantification, Phylogeny, and Relevance for the Interpretation of Geologic Steranes." *Geobiology* 6, no. 4: 411–420. https://doi.org/10.1111/j.1472-4669.2008.00167.x.

Kontorovich, V. A., A. E. Kontorovich, I. A. Gubin, et al. 2013. "The Neoproterozoic–Phanerozoic Section of the Anabar–Lena Province: Structural Framework, Geological Model, and Petroleum Potential." *Russian Geology and Geophysics, Problems of the Geology and Petroleum Potential of the Arctic* 54, no. 8: 980–996. https://doi.org/10.1016/j.rgg.2013.07.014.

Krause, A. J., B. J. W. Mills, A. S. Merdith, T. M. Lenton, and S. W. Poulton. 2022. "Extreme Variability in Atmospheric Oxygen Levels in the Late Precambrian." *Science Advances* 8, no. 41: eabm8191. https://doi.org/10.1126/sciadv.abm8191.

Kuznetsov, A. B., A. Bekker, G. V. Ovchinnikova, I. M. Gorokhov, and I. M. Vasilyeva. 2017. "Unradiogenic Strontium and Moderate-Amplitude Carbon Isotope Variations in Early Tonian Seawater After the Assembly of Rodinia and Before the Bitter Springs Excursion." *Precambrian Research* 298: 157–173.

Kuznetsov, A. B., I. M. Gorokhov, N. N. Mel'nikov, G. V. Konstantinova, E. P. Kutyavin, and M. A. Semikhatov. 2003. "Sr Isotope Composition in Carbonates of the Karatau Group, Southern Urals, and Standard Curve of 87Sr/86Sr Variations in the Late Riphean Ocean." *Stratigraphy and Geological Correlation* 11, no. 5: 415–449.

Kuznetsov, A. B., B. B. Kochnev, I. M. Vasilyeva, and G. V. Ovchinnikova. 2019. "The Upper Riphean of the Yenisei Range: Sr Chemostratigraphy and pb–pb Age of Limestones of the Tungusik and Shirokaya Groups." *Stratigraphy and Geological Correlation* 27, no. 5: 538–554. https://doi.org/10.1134/S0869593819050058.

Kuznetsov, A. B., G. V. Ovchinnikova, I. M. Gorokhov, E. F. Letnikova, O. K. Kaurova, and G. V. Konstantinova. 2013. "Age Constraints on the Neoproterozoic Baikal Group From Combined Sr Isotopes and pb–pb Dating of Carbonates From the Baikal Type Section, Southeastern Siberia." *Journal of Asian Earth Sciences, Geology of Baikal Region* 62: 51–66. https://doi.org/10.1016/j.jseaes.2011.06.003.

Kuznetsov, A. B., M. A. Semikhatov, A. V. Maslov, et al. 2006. "New Data on Sr-and C-Isotopic Chemostratigraphy of the Upper Riphean Type Section (Southern Urals)." *Stratigraphy and Geological Correlation* 14, no. 6: 602–628. https://doi.org/10.1134/S0869593806060025.

Laakso, T. A., and D. P. Schrag. 2019. "A Small Marine Biosphere in the Proterozoic." *Geobiology* 17, no. 2: 161–171. https://doi.org/10.1111/gbi.12323.

Lahr, D. J. G., A. Kosakyan, E. Lara, et al. 2019. "Phylogenomics and Morphological Reconstruction of Arcellinida Testate Amoebae Highlight Diversity of Microbial Eukaryotes in the Neoproterozoic." *Current Biology* 29, no. 6: 991–1001. https://doi.org/10.1016/j.cub.2019.01.078.

Lee, A. K., J. H. Wei, and P. V. Welander. 2023. "De Novo Cholesterol Biosynthesis in Bacteria." *Nature Communications* 14: 1. https://doi.org/10.1038/s41467-023-38638-8.

Lee, C., G. D. Love, M. J. Hopkins, B. Kröger, F. Franeck, and S. Finnegan. 2019. "Lipid Biomarker and Stable Isotopic Profiles Through Early-Middle Ordovician Carbonates From Spitsbergen, Norway." *Organic Geochemistry* 131: 5–18. https://doi.org/10.1016/j.orggeochem.2019.02.008.

Lee, C., G. D. Love, L. L. Jahnke, M. D. Kubo, and D. J. Des Marais. 2019. "Early Diagenetic Sequestration of Microbial Mat Lipid Biomarkers Through Covalent Binding Into Insoluable Macromolecular Organic Matter (IMOM) as Revealed by Sequential Chemolysis and Catalytic Hydropyrolysis." *Organic Geochemistry* 132: 11–22. https://doi.org/10.1016/j.orggeochem.2019.04.002.

Lee, C., G. D. Love, L. L. Jahnke, M. D. Kubo, and D. J. Des Marais. 2021. "Diagenetic Transformations and Preservation of Free and Bound Lipids in a Hypersaline Microbial Mat From Guerrero Negro, Baja California Sur, Mexico." *Organic Geochemistry* 153: 104196. https://doi.org/10.1016/j.orggeochem.2021.104196.

Lenton, T. M., R. A. Boyle, S. W. Poulton, G. A. Shields-Zhou, and N. J. Butterfield. 2014. "Co-Evolution of Eukaryotes and Ocean Oxygenation in the Neoproterozoic Era." *Nature Geoscience* 7, no. 4: 257–265. https://doi.org/10.1038/ngeo2108.

Li, S., P. B. Wignall, Y. Xiong, and S. W. Poulton. 2023. "Calibration of Redox Thresholds in Black Shale: Insight From a Stratified Mississippian Basin With Warm Saline Bottom Waters." *GSA Bulletin* 136: 1266–1286. https://doi.org/10.1130/B36915.1.

Li, Z.-X., D. A. D. Evans, and G. P. Halverson. 2013. "Neoproterozoic Glaciations in a Revised Global Palaeogeography From the Breakup of Rodinia to the Assembly of Gondwanaland." *Sedimentary Geology* 294: 219–232. https://doi.org/10.1016/j.sedgeo.2013.05.016.

Liu, K., Q. Feng, J. Shen, M. Khan, and N. J. Planavsky. 2018. "Increased Productivity as a Primary Driver of Marine Anoxia in the Lower Cambrian." *Palaeogeography, Palaeoclimatology, Palaeoecology* 491: 1–9. https://doi.org/10.1016/j.palaeo.2017.11.007.

Loron, C. C., C. François, R. H. Rainbird, E. C. Turner, S. Borensztajn, and E. J. Javaux. 2019. "Early Fungi From the Proterozoic Era in Arctic Canada." *Nature* 570: 232–235. https://doi.org/10.1038/s41586-019-1217-0.

Love, G. D., S. A. Bowden, L. L. Jahnke, et al. 2005. "A Catalytic Hydropyrolysis Method for the Rapid Screening of Microbial Cultures for Lipid Biomarkers." *Organic Geochemistry* 36, no. 1: 63–82. https://doi.org/10.1016/j.orggeochem.2004.07.010.

Love, G. D., E. Grosjean, C. Stalvies, et al. 2009. "Fossil Steroids Record the Appearance of Demospongiae During the Cryogenian Period." *Nature* 457, no. 7230: 718–721. https://doi.org/10.1038/nature07673.

Love, G. D., C. E. Snape, A. D. Carr, and R. C. Houghton. 1995. "Release of Covalently-Bound Alkane Biomarkers in High Yields From Kerogen via Catalytic Hydropyrolysis." *Organic Geochemistry* 23, no. 10: 981–986. https://doi.org/10.1016/0146-6380(95)00075-5.

Love, G. D., and J. A. Zumberge. 2021. *Emerging Patterns in Proterozoic Lipid Biomarker Records*. Cambridge University Press. https://www.cambridge.org/core/elements/emerging-patterns-in-proterozoic-lipid-biomarker-records/4C69E9BDDB7F39E7995C7F01EC012E0B.

Luo, G., C. Hallmann, S. Xie, X. Ruan, and R. E. Summons. 2015. "Comparative Microbial Diversity and Redox Environments of Black Shale and Stromatolite Facies in the Mesoproterozoic Xiamaling Formation." *Geochimica et Cosmochimica Acta* 151: 150–167. https://doi.org/10.1016/j.gca.2014.12.022.

Luo, Q., S. C. George, Y. Xu, and N. Zhong. 2016. "Organic Geochemical Characteristics of the Mesoproterozoic Hongshuizhuang Formation From Northern China: Implications for Thermal Maturity and Biological Sources." *Organic Geochemistry* 99: 23–37. https://doi.org/10.1016/j.orggeochem.2016.05.004.

Lyons, T. W., C. W. Diamond, N. J. Planavsky, C. T. Reinhard, and C. Li. 2021. "Oxygenation, Life, and the Planetary System During Earth's Middle History: An Overview." *Astrobiology* 21, no. 8: 906–923. https://doi.org/10.1089/ast.2020.2418.

14724669, 2026, 5, Downloaded from https://onlinelibrary.wiley.com/doi/10.1111/gbi.70061 by NICE, National Institute for Health and Care Excellence, Wiley Online Library on [07/10/2026]. See the Terms and Conditions (https://onlinelibrary.wiley.com/terms-and-conditions) on Wiley Online Library for rules of use; OA articles are governed by the applicable Creative Commons License

Macdonald, F. A., and N. L. Swanson-Hysell. 2023. "The Franklin Large Igneous Province and Snowball Earth Initiation." *Elements* 19, no. 5: 296–301. https://doi.org/10.2138/gselements.19.5.296.

Mackenzie, A. S., and D. McKenzie. 1983. "Isomerization and Aromatization of Hydrocarbons in Sedimentary Basins Formed by Extension." *Geological Magazine* 120, no. 5: 417–470. https://doi.org/10.1017/S0016756800027461.

Maloof, A. C., S. M. Porter, J. L. Moore, et al. 2010. "The Earliest Cambrian Record of Animals and Ocean Geochemical Change." *GSA Bulletin* 122, no. 11–12: 1731–1774. https://doi.org/10.1130/B30346.1.

Marañón, E. 2015. "Cell Size as a Key Determinant of Phytoplankton Metabolism and Community Structure." *Annual Review of Marine Science* 7: 241–264. https://doi.org/10.1146/annurev-marine-010814-015955.

Marshall, N. L., G. D. Love, V. Grytsenko, and A. Bekker. 2023. "Assessing Marine Communities and Carbon Cycling That Sustained Shallow-Marine Ecosystems on Silurian, Reef-Rimmed Carbonate Platforms." *Organic Geochemistry* 175: 104528. https://doi.org/10.1016/j.orggeochem.2022.104528.

Martinez, A. M., D. L. Boyer, M. L. Droser, C. Barrie, and G. D. Love. 2019. "A Stable and Productive Marine Microbial Community Was Sustained Through the End-Devonian Hangenberg Crisis Within the Cleveland Shale of the Appalachian Basin, United States." *Geobiology* 17, no. 1: 27–42. https://doi.org/10.1111/gbi.12314.

McKirdy, D. M., L. J. Webster, K. R. Arouri, K. Grey, and V. A. Gostin. 2006. "Contrasting Sterane Signatures in Neoproterozoic Marine Rocks of Australia Before and After the Acraman Asteroid Impact." *Organic Geochemistry* 37, no. 2: 189–207. https://doi.org/10.1016/j.orggeochem.2005.09.005.

McLennan, S. M. 2001. "Relationships Between the Trace Element Composition of Sedimentary Rocks and Upper Continental Crust." *Geochemistry, Geophysics, Geosystems* 2, no. 4. https://doi.org/10.1029/2000GC000109.

Melnik, D., T. Parfenova, V. Rogov, J.-P. Duda, and D. Grazhdankin. 2024. "Organic Geochemistry, Sedimentology and Palaeontology of the Khatyspyt Formation, Arctic Siberia: Towards an Integrated View of Ediacaran Biofacies." *Precambrian Research* 410: 107460. https://doi.org/10.1016/j.precamres.2024.107460.

Mel'nikov, N. V. 2009. "Vendian-Cambrian Salt-Bearing Basin of the Siberian Platform." In *Stratigraphy and History of Development*, 148. Izd. SO RAN.

Merdith, A. S., A. S. Collins, S. E. Williams, et al. 2017. "A Full-Plate Global Reconstruction of the Neoproterozoic." *Gondwana Research* 50: 84–134. https://doi.org/10.1016/j.gr.2017.04.001.

Merdith, A. S., S. E. Williams, A. S. Collins, et al. 2021. "Extending Full-Plate Tectonic Models Into Deep Time: Linking the Neoproterozoic and the Phanerozoic." *Earth-Science Reviews* 214: 103477. https://doi.org/10.1016/j.earscirev.2020.103477.

Meyer, K. M., and L. R. Kump. 2008. "Oceanic Euxinia in Earth History: Causes and Consequences." *Annual Review of Earth and Planetary Sciences* 36: 251–288. https://doi.org/10.1146/annurev.earth.36.031207.124256.

Meyer, K. M., A. Ridgwell, and J. L. Payne. 2016. "The Influence of the Biological Pump on Ocean Chemistry: Implications for Long-Term Trends in Marine Redox Chemistry, the Global Carbon Cycle, and Marine Animal Ecosystems." *Geobiology* 14, no. 3: 207–219. https://doi.org/10.1111/gbi.12176.

Meyers, P. A. 1997. "Organic Geochemical Proxies of Paleoceanographic, Paleolimnologic, and Paleoclimatic Processes." *Organic Geochemistry* 27, no. 5: 213–250. https://doi.org/10.1016/S0146-6380(97)00049-1.

Moldowan, J. M., W. K. Seifert, and E. J. Gallegos. 1985. "Relationship Between Petroleum Composition and Depositional Environment of Petroleum Source Rocks." *AAPG Bulletin* 69, no. 8: 1255–1268. https://doi.org/10.1306/AD462BC8-16F7-11D7-8645000102C1865D.

Montañez, I. P., J. L. Banner, D. A. Osleger, L. E. Borg, and P. J. Bosserman. 1996. "Integrated Sr Isotope Variations and Sea-Level History of Middle to Upper Cambrian Platform Carbonates: Implications for the Evolution of Cambrian Seawater 87Sr/86Sr." *Geology* 24, no. 10: 917–920. https://doi.org/10.1130/0091-7613(1996)024%3C0917:ISIVAS%3E2.3.CO;2.

Morais, L., T. R. Fairchild, D. J. G. Lahr, et al. 2017. "Carbonaceous and Siliceous Neoproterozoic Vase-Shaped Microfossils (Urucum Formation, Brazil) and the Question of Early Protistan Biomineralization." *Journal of Paleontology* 91, no. 3: 393–406. https://doi.org/10.1017/jpa.2017.16.

Nagovitsin, K. E., V. I. Rogov, V. V. Marusin, et al. 2015. "Revised Neoproterozoic and Terreneuvian Stratigraphy of the Lena-Anabar Basin and North-Western Slope of the Olenek Uplift, Siberian Platform." *Precambrian Research* 270: 226–245. https://doi.org/10.1016/j.precamres.2015.09.012.

Nguyen, K., G. D. Love, J. A. Zumberge, et al. 2019. "Absence of Biomarker Evidence for Early Eukaryotic Life From the Mesoproterozoic Roper Group: Searching Across a Marine Redox Gradient in Mid-Proterozoic Habitability." *Geobiology* 17, no. 3: 247–260. https://doi.org/10.1111/gbi.12329.

Parfenova, T. M. 2011. "Lanostanes in Cambrian Organic Matter (Southeastern Part of the Siberian Platform)." *Doklady Earth Sciences* 436, no. 1: 143–147. https://doi.org/10.1134/S1028334X10901180.

Patterson, G. W. 1971. "The Distribution of Sterols in Algae." *Lipids* 6, no. 2: 120–127. https://doi.org/10.1007/BF02531327.

Pawlowska, M. M., N. J. Butterfield, and J. J. Brocks. 2013. "Lipid Taphonomy in the Proterozoic and the Effect of Microbial Mats on Biomarker Preservation." *Geology* 41, no. 2: 103–106. https://doi.org/10.1130/G33525.1.

Peakman, T. M., and J. R. Maxwell. 1988. "Early Diagenetic Pathways of Steroid Alkenes." *Organic Geochemistry, Proceedings of the 13th International Meeting on Organic Geochemistry* 13, no. 4: 583–592. https://doi.org/10.1016/0146-6380(88)90078-2.

Peckmann, J., V. Thiel, J. Reitner, M. Taviani, P. Aharon, and W. Michaelis. 2004. "A Microbial Mat of a Large Sulfur Bacterium Preserved in a Miocene Methane-Seep Limestone." *Geomicrobiology Journal* 21, no. 4: 247–255. https://doi.org/10.1080/01490450490438757.

Pehr, K., A. A. Baczynski, A. Bekker, et al. 2023. "Compound-Specific Carbon Isotope Measurements of Individual Lipid Biomarkers From Immature Ediacaran Rocks of Baltica." *Organic Geochemistry* 182: 104641. https://doi.org/10.1016/j.orggeochem.2023.104641.

Pehr, K., G. D. Love, A. Kuznetsov, et al. 2018. "Ediacara Biota Flourished in Oligotrophic and Bacterially Dominated Marine Environments Across Baltica." *Nature Communications* 9, no. 1807: 1–10. https://doi.org/10.1038/s41467-018-04195-8.

Peters, K. E. 1986. "Guidelines for Evaluating Petroleum Source Rock Using Programmed Pyrolysis." *AAPG Bulletin* 70, no. 3: 318–329. https://doi.org/10.1306/94885688-1704-11D7-8645000102C1865D.

Peters, K. E., and M. R. Cassa. 1994. "Applied Source Rock Geochemistry." In *The Petroleum System—From Source to Trap*, vol. 60, 93–120. American Association of Petroleum Geologists.

Peters, K. E., C. C. Walters, and J. M. Moldowan. 2005. *The Biomarker Guide*. Vol. 2. 2nd ed. Cambridge University Press.

Planavsky, N. J., D. Asael, A. D. Rooney, et al. 2023. "A Sedimentary Record of the Evolution of the Global Marine Phosphorus Cycle." *Geobiology* 21, no. 2: 168–174. https://doi.org/10.1111/gbi.12536.

Planavsky, N. J., L. G. Tarhan, E. J. Bellefroid, et al. 2015. "Late Proterozoic Transitions in Climate, Oxygen, and Tectonics, and the Rise of Complex Life." *Paleontological Society Papers* 21: 47–82. https://doi.org/10.1017/S1089332600002965.

14724669, 2026, 5, Downloaded from https://onlinelibrary.wiley.com/doi/10.1111/gbi.70061 by NICE, National Institute for Health and Care Excellence, Wiley Online Library on [07/10/2026]. See the Terms and Conditions (https://onlinelibrary.wiley.com/terms-and-conditions) on Wiley Online Library for rules of use; OA articles are governed by the applicable Creative Commons License

Porter, S. M. 2016. "Tiny Vampires in Ancient Seas: Evidence for Predation via Perforation in Fossils From the 780–740 Million-Year-Old Chuar Group, Grand Canyon, USA." *Proceedings of the Royal Society B: Biological Sciences* 283, no. 1831: 20160221. https://doi.org/10.1098/rspb.2016.0221.

Porter, S. M., and A. H. Knoll. 2000. "Testate Amoebae in the Neoproterozoic Era: Evidence From Vase-Shaped Microfossils in the Chuar Group, Grand Canyon." *Paleobiology* 26, no. 3: 360–385. https://doi.org/10.1666/0094-8373(2000)026%3C0360:TAITNE%3E2.0.CO;2.

Porter, S. M., L. A. Riedman, C. R. Woltz, D. A. Gold, and J. B. Kellogg. 2025. "Early Eukaryote Diversity: A Review and a Reinterpretation." *Paleobiology* 51, no. 1: 132–149. https://doi.org/10.1017/pab.2024.33.

Poulton, S. W. 2021. "The Iron Speciation Paleoredox Proxy." In *Elements in Geochemical Tracers in Earth System Science*. Cambridge University Press. https://doi.org/10.1017/9781108847148.

Poulton, S. W., and D. E. Canfield. 2005. "Development of a Sequential Extraction Procedure for Iron: Implications for Iron Partitioning in Continentally Derived Particulates." *Chemical Geology* 214, no. 3–4: 209–221. https://doi.org/10.1016/j.chemgeo.2004.09.003.

Poulton, S. W., and D. E. Canfield. 2011. "Ferruginous Conditions: A Dominant Feature of the Ocean Through Earth's History." *Elements* 7, no. 2: 107–112. https://doi.org/10.2113/gselements.7.2.107.

Poulton, S. W., P. W. Fralick, and D. E. Canfield. 2010. "Spatial Variability in Oceanic Redox Structure 1.8 Billion Years Ago." *Nature Geoscience* 3, no. 7: 486–490. https://doi.org/10.1038/ngeo889.

Poulton, S. W., and R. Raiswell. 2002. "The low-Temperature Geochemical Cycle of Iron: From Continental Fluxes to Marine Sediment Deposition." *American Journal of Science* 302, no. 9: 774–805. https://doi.org/10.2475/ajs.302.9.774.

Raiswell, R., and D. E. Canfield. 1996. "Rates of Reaction Between Silicate Iron and Dissolved Sulfide in Peru Margin Sediments." *Geochimica et Cosmochimica Acta* 60, no. 15: 2777–2787. https://doi.org/10.1016/0016-7037(96)00141-X.

Raiswell, R., and D. E. Canfield. 1998. "Sources of Iron for Pyrite Formation in Marine Sediments." *American Journal of Science* 298, no. 3: 219–245. https://doi.org/10.2475/ajs.298.3.219.

Reinhard, C. T., N. J. Planavsky, B. C. Gill, et al. 2017. "Evolution of the Global Phosphorus Cycle." *Nature* 541: 386–389. https://doi.org/10.1038/nature20772.

Reinhard, C. T., N. J. Planavsky, B. A. Ward, G. D. Love, G. L. Hir, and A. Ridgwell. 2020. "The Impact of Marine Nutrient Abundance on Early Eukaryotic Ecosystems." *Geobiology* 18, no. 2: 139–151. https://doi.org/10.1111/gbi.12384.

Riedman, L. A., S. M. Porter, and C. R. Calver. 2018. "Vase-Shaped Microfossil Biostratigraphy With New Data From Tasmania, Svalbard, Greenland, Sweden and the Yukon." *Precambrian Research, Descent Into the Cryogenian* 319: 19–36. https://doi.org/10.1016/j.precamres.2017.09.019.

Riedman, L. A., and P. M. Sadler. 2018. "Global Species Richness Record and Biostratigraphic Potential of Early to Middle Neoproterozoic Eukaryote Fossils." *Precambrian Research, Descent Into the Cryogenian* 319: 6–18. https://doi.org/10.1016/j.precamres.2017.10.008.

Rogov, V. I., G. A. Karlova, V. V. Marusin, B. B. Kochnev, K. E. Nagovitsin, and D. V. Grazhdankin. 2015. "Duration of the First Biozone in the Siberian Hypostratotype of the Vendian." *Russian Geology and Geophysics, Special Issue: Topical Problems of Stratigraphy and Evolution of the Biosphere* 56, no. 4: 573–583. https://doi.org/10.1016/j.rgg.2015.03.016.

Rohrssen, M., G. D. Love, W. Fischer, S. Finnegan, and D. A. Fike. 2013. "Lipid Biomarkers Record Fundamental Changes in the Microbial Community Structure of Tropical Seas During the Late Ordovician Hirnantian Glaciation." *Geology* 41, no. 2: 127–130.

Rooney, A. D., J. Austermann, E. F. Smith, et al. 2017. "Coupled re-Os and U-Pb Geochronology of the Tonian Chuar Group, Grand Canyon." *GSA Bulletin* 130, no. 7–8: 1085–1098. https://doi.org/10.1130/B31768.1.

Rullkötter, J., and R. Marzi. 1988. "Natural and Artificial Maturation of Biological Markers in a Toarcian Shale From Northern Germany." *Organic Geochemistry, Proceedings of the 13th International Meeting on Organic Geochemistry* 13, no. 4: 639–645. https://doi.org/10.1016/0146-6380(88)90084-8.

Ruttenberg, K. C., and R. A. Berner. 1993. "Authigenic Apatite Formation and Burial in Sediments From Non-Upwelling, Continental Margin Environments." *Geochimica et Cosmochimica Acta* 57, no. 5: 991–1007. https://doi.org/10.1016/0016-7037(93)90035-U.

Schwark, L., and P. Empt. 2006. "Sterane Biomarkers as Indicators of Palaeozoic Algal Evolution and Extinction Events." *Palaeogeography, Palaeoclimatology, Palaeoecology* 240: 236–255. https://doi.org/10.1016/j.palaeo.2006.03.050.

Shen, Y., V. Thiel, J.-P. Duda, and J. Reitner. 2018. "Tracing the Fate of Steroids Through a Hypersaline Microbial Mat (Kiritimati, Kiribati/Central Pacific)." *Geobiology* 16, no. 3: 307–318. https://doi.org/10.1111/gbi.12279.

Sinninghe Damsté, J. S., F. Kenig, M. P. Koopmans, et al. 1995. "Evidence for Gammacerane as an Indicator of Water Column Stratification." *Geochimica et Cosmochimica Acta* 59, no. 9: 1895–1900. https://doi.org/10.1016/0016-7037(95)00073-9.

Slomp, C. P., J. Thomson, and G. J. de Lange. 2004. "Controls on Phosphorus Regeneration and Burial During Formation of Eastern Mediterranean Sapropels." *Marine Geology* 203, no. 1: 141–159. https://doi.org/10.1016/S0025-3227(03)00335-9.

Song, Y., F. T. Bowyer, B. J. W. Mills, et al. 2023. "Dynamic Redox and Nutrient Cycling Response to Climate Forcing in the Mesoproterozoic Ocean." *Nature Communications* 14, no. 1: 6640. https://doi.org/10.1038/s41467-023-41901-7.

Stolper, D. A., G. D. Love, S. Bates, et al. 2017. "Paleocology and Paleoceanography of the Althel Silicilyte, Ediacaran-Cambrian Boundary, Sultanate of Oman." *Geobiology* 15: 401–426. https://doi.org/10.1111/gbi.12236.

Summons, R. E., S. C. Brassell, G. Eglinton, et al. 1988. "Distinctive Hydrocarbon Biomarkers From Fossiliferous Sediment of the Late Proterozoic Walcott Member, Chuar Group, Grand Canyon, Arizona." *Geochimica et Cosmochimica Acta* 52, no. 11: 2625–2637. https://doi.org/10.1016/0016-7037(88)90031-2.

Summons, R. E., and M. R. Walter. 1990. "Molecular Fossils and Microfossils of Prokaryotes and Protists From Proterozoic Sediments." *American Journal of Science* 290-A: 212–244.

Suslova, E. A., T. M. Parfenova, S. V. Saraev, and K. E. Nagovitsin. 2017. "Organic Geochemistry of Rocks of the Mesoproterozoic Malgin Formation and Their Depositional Environments (Southeastern Siberian Platform)." *Russian Geology and Geophysics* 58: 516–528.

Takishita, K., Y. Chikaraishi, G. Tanifuji, et al. 2017. "Microbial Eukaryotes That Lack Sterols." *Journal of Eukaryotic Microbiology* 64: 897–900. https://doi.org/10.1111/jeu.12426.

Tang, Q., K. Pang, X. Yuan, and S. Xiao. 2020. "A One-Billion-Year-Old Multicellular Chlorophyte." *Nature Ecology & Evolution* 4: 543–549. https://doi.org/10.1038/s41559-020-1122-9.

Tarhan, L. G., M. L. Droser, N. J. Planavsky, and D. T. Johnston. 2015. "Protracted Development of Bioturbation Through the Early Palaeozoic Era." *Nature Geoscience* 8, no. 11: 865–869. https://doi.org/10.1038/ngeo2537.

ten Haven, H. L., J. W. De Leeuw, J. S. Sinninghe Damsté, P. A. Schenck, S. E. Palmer, and J. E. Zumberge. 1988. "Application of Biological Markers in the Recognition of Palaeohypersaline Environments." *Geological Society, London, Special Publications* 40: 123–130. https://doi.org/10.1144/GSL.SP.1988.040.01.11.

14724669, 2026, 5, Downloaded from https://onlinelibrary.wiley.com/doi/10.1111/gbi.70061 by NICE, National Institute for Health and Care Excellence, Wiley Online Library on [07/10/2026]. See the Terms and Conditions (https://onlinelibrary.wiley.com/terms-and-conditions) on Wiley Online Library for rules of use; OA articles are governed by the applicable Creative Commons License

ten Haven, H. L., M. Rohmer, J. Rullkötter, and P. Bisseret. 1989. "Tetrahymanol, the Most Likely Precursor of Gammacerane, Occurs Ubiquitously in Marine Sediments." *Geochimica et Cosmochimica Acta* 53, no. 11: 3073–3079. https://doi.org/10.1016/0016-7037(89)90186-5.

Thompson, J., S. W. Poulton, R. Guilbaud, K. A. Doyle, S. Reid, and M. D. Krom. 2019. "Development of a Modified SEDEX Phosphorus Speciation Method for Ancient Rocks and Modern Iron-Rich Sediments." *Chemical Geology* 524: 383–393. https://doi.org/10.1016/j.chemgeo.2019.07.003.

Thomson, D., R. H. Rainbird, N. Planavsky, T. W. Lyons, and A. Bekker. 2015. "Chemostratigraphy of the Shaler Supergroup, Victoria Island, NW Canada: A Record of Ocean Composition Prior to the Cryogenian Glaciations." *Precambrian Research* 263: 232–245. https://doi.org/10.1016/j.precamres.2015.02.007.

Tulipani, S., K. Grice, P. F. Greenwood, et al. 2015. "Molecular Proxies as Indicators of Freshwater Incursion-Driven Salinity Stratification." *Chemical Geology* 409: 61–68. https://doi.org/10.1016/j.chemgeo.2015.05.009.

Turner, E. C., and A. Bekker. 2016. "Thick Sulfate Evaporite Accumulations Marking a Mid-Neoproterozoic Oxygenation Event (Ten Stone Formation, Northwest Territories, Canada)." *GSA Bulletin* 128, no. 1–2: 203–222. https://doi.org/10.1130/B31268.1.

Tziperman, E., I. Halevy, D. T. Johnston, A. H. Knoll, and D. P. Schrag. 2011. "Biologically Induced Initiation of Neoproterozoic Snowball-Earth Events." *PNAS* 108, no. 37: 15091–15096.

Van Cappellen, P., and E. D. Ingall. 1994. "Benthic Phosphorus Regeneration, Net Primary Production, and Ocean Anoxia: A Model of the Coupled Marine Biogeochemical Cycles of Carbon and Phosphorus." *Paleoceanography* 9, no. 5: 677–692. https://doi.org/10.1029/94PA01455.

Van Cappellen, P., and E. D. Ingall. 1996. "Redox Stabilization of the Atmosphere and Oceans by Phosphorus-Limited Marine Productivity." *Science* 271, no. 5248: 493–496. https://doi.org/10.1126/science.271.5248.493.

van Kaam-Peters, H. M. E., J. Köster, S. J. van der Gaast, M. Dekker, J. W. de Leeuw, and J. S. Sinninghe Damsté. 1998. "The Effect of Clay Minerals on Diasterane/Sterane Ratios." *Geochimica et Cosmochimica Acta* 62, no. 17: 2923–2929. https://doi.org/10.1016/S0016-7037(98)00191-4.

Vinnichenko, G., A. J. M. Jarrett, J. M. Hope, and J. J. Brocks. 2020. "Discovery of the Oldest Known Biomarkers Provides Evidence for Phototrophic Bacteria in the 1.73 ga Wollogorang Formation, Australia." *Geobiology* 18, no. 5: 544–559. https://doi.org/10.1111/gbi.12390.

Vogel, M. B., J. M. Moldowan, and D. Zinniker. 2005. "Biomarkers From Units in the Uinta Mountain and Chuar Groups." *Unita Mountain Geology* 33: 75–96.

Volkman, J. K. 2005. "Sterols and Other Triterpenoids: Source Specificity and Evolution of Biosynthetic Pathways." *Organic Geochemistry* 36: 139–159. https://doi.org/10.1016/j.orggeochem.2004.06.013.

Volkman, J. K., S. M. Barrett, S. I. Blackburn, M. P. Mansour, E. L. Sikes, and F. Gelin. 1998. "Microalgal Biomarkers: A Review of Recent Research Developments." *Organic Geochemistry* 29, no. 5: 1163–1179. https://doi.org/10.1016/S0146-6380(98)00062-X.

Volkman, J. K., P. Kearney, and S. W. Jeffrey. 1990. "A new Source of 4-Methyl Sterols and 5α(H)-Stanols in Sediments: Prymnesiophyte Microalgae of the Genus Pavlova." *Organic Geochemistry* 15, no. 5: 489–497. https://doi.org/10.1016/0146-6380(90)90094-G.

Wang, F., Y. Liao, and C. S. Hsu. 2025. "On-Line Hydropyrolysis Gas Chromatography-Mass Spectrometry (HyPy-GC–MS) for Kerogen-Bound Biomarkers." *Organic Geochemistry* 200: 104927. https://doi.org/10.1016/j.orggeochem.2024.104927.

Wei, G.-Y., T. Chen, S. W. Poulton, et al. 2021. "A Chemical Weathering Control on the Delivery of Particulate Iron to the Continental Shelf." *Geochimica et Cosmochimica Acta* 308: 204–216. https://doi.org/10.1016/j.gca.2021.05.058.

Wei, J. H., X. Yin, and P. V. Welander. 2016. "Sterol Synthesis in Diverse Bacteria." *Frontiers in Microbiology* 7, no. 990: 990. https://doi.org/10.3389/fmicb.2016.00990.

Wiley, B. H., C. M. Dehler, S. A. Ghazi, L.-C. Kuo, and S. L. Rauzi. 2002. "Geologic Description, Sampling, and Petroleum Source Rock Potential of the Awatubi and Walcott Members, Kwagunt Formation, Chuar Group of the Sixtymile Canyong Section, Grand Canyon, Arizona (Open File Report Nos. 02–01; p. 84)." Arizona Geological Survey.

Xia, L., J. Cao, C. Lee, E. E. Stüeken, D. Zhi, and G. D. Love. 2021. "A New Constraint on the Antiquity of Ancient Haloalkaliphilic Green Algae That Flourished in a Ca. 300 ma Paleozoic Lake." *Geobiology* 19, no. 2: 147–161. https://doi.org/10.1111/gbi.12423.

Xiao, S., and Q. Tang. 2018. "After the Boring Billion and Before the Freezing Millions: Evolutionary Patterns and Innovations in the Tonian Period." *Emerging Topics in Life Sciences* 2, no. 2: 161–171. https://doi.org/10.1042/ETLS20170165.

Xiong, J., Z. Liu, Y. Yan, et al. 2022. "Role of Clay Minerals in Controlling Phosphorus Availability in a Subtropical Alfisol." *Geoderma* 409: 115592. https://doi.org/10.1016/j.geoderma.2021.115592.

Xiong, Y., R. Guilbaud, C. L. Peacock, et al. 2019. "Phosphorus Cycling in Lake Cadagno, Switzerland: A Low Sulfate Euxinic Ocean Analogue." *Geochimica et Cosmochimica Acta* 251: 116–135. https://doi.org/10.1016/j.gca.2019.02.011.

Yang, C., A. D. Rooney, D. J. Condon, et al. 2021. "The Tempo of Ediacaran Evolution." *Science Advances* 7: eabi9643. https://doi.org/10.1126/sciadv.abi9643.

Zimmerman, A. R., and E. A. Canuel. 2000. "A Geochemical Record of Eutrophication and Anoxia in Chesapeake Bay Sediments: Anthropogenic Influence on Organic Matter Composition." *Marine Chemistry* 69, no. 1: 117–137. https://doi.org/10.1016/S0304-4203(99)00100-0.

Zumberge, J. A., G. D. Love, P. Cárdenas, et al. 2018. "Demosponge Steroid Biomarker 26-Methylstigmastane Provides Evidence for Neoproterozoic Animals." *Nature Ecology & Evolution* 2, no. 11: 1709–1714. https://doi.org/10.1038/s41559-018-0676-2.

Zumberge, J. A., D. Rocher, and G. D. Love. 2020. "Free and Kerogen-Bound Biomarkers From Late Tonian Sedimentary Rocks Record Abundant Eukaryotes in Mid-Neoproterozoic Marine Communities." *Geobiology* 18: 326–347. https://doi.org/10.1111/gbi.12378.

Zumberge, J. E. 1987. "Prediction of Source Rock Characteristics Based on Terpane Biomarkers in Crude Oils: A Multivariate Statistical Approach." *Geochimica et Cosmochimica Acta* 51, no. 6: 1625–1637. https://doi.org/10.1016/0016-7037(87)90343-7.

Supporting Information

Additional supporting information can be found online in the Supporting Information section. **Table S1:** Organic and inorganic carbon isotopes and carbonate oxygen isotopes for Lena-Anabar Basin samples. All isotope values are relative to the Vienna Pee Dee Belemnite (VPDB) isotope standard. **Table S2:** Strontium isotope data and related parameters for the Burskaya-3410 drill-core, Lena-Anabar Basin. **Table S3:** Iron, phosphorus, and major and minor element abundance data for Lena-Anabar Basin and Visingsö Group samples. **Table S4:** Lipid biomarker ratio parameters for sedimentary rocks from the Upper Walcott Member, Chuar Group. **Table S5:** Absolute abundances of selected polycyclic biomarker alkane compounds for Chuar Group and Lena-Anabar Basin rocks analyzed in this investigation. **Table S6:** Selected triaromatic steroid data (m/z 231) from Lena-Anabar Basin and the Chuar Group. **Figure S1:** gbi70061-sup-0007-Supinfo.docx. $^{87}Sr/^{86}Sr$ as a function of Fe/Sr. (left) and Mn/Sr. right for selected carbonates from the Burskaya-3410 core. Shaded ranges indicate late Tonian (post-Bitter Springs excursion)

14724669, 2026, 5, Downloaded from https://onlinelibrary.wiley.com/doi/10.1111/gbi.70061 by NICE, National Institute for Health and Care Excellence, Wiley Online Library on [07/10/2026]. See the Terms and Conditions (https://onlinelibrary.wiley.com/terms-and-conditions) on Wiley Online Library for rules of use; OA articles are governed by the applicable Creative Commons License

and late Ediacaran (post-Gaskiers)-earliest Cambrian $^{87}Sr/^{86}Sr$ ranges (Kuznetsov et al. 2017). In the Taimylyr Formation samples, Fe/Sr. (-6×10^{-6}, $R^2=0.07$) and Mn/Sr. ($m=-2\times10^{-6}$, $R^2=0.0$) are uncorrelated with $^{87}Sr/^{86}Sr$. All but one sample has Mn/Sr. <3, a threshold suggested by Kaufman et al. (1993) to increase chances of robust strontium isotopes, and excluding the outlier does not change the inferred age of the Taimylyr Formation. **Figure S2:** Total Ion Current (TIC) chromatograms for the extractable saturated hydrocarbon fractions for: (top) Bur-40, a representative Tonian sample, and (bottom) Bur-67, an Ediacaran sample. The *n*-alkane peaks are labeled by their carbon number signifying the overall linear chain length; Pr = pristane (acyclic C_{19} isoprenoid), Ph = phytane (acyclic C_{20} isoprenoid). **Figure S3:** MRM chromatograms for C_{27} steranes ($372\rightarrow217$ transition) analyzed with a 2°C/min oven heating rate to demonstrate separation between βαα R and ααα S steranes. Top: HyPy pyrolysate of *Ciocalypta carballoi*, a demosponge (Zumberge et al. 2018). This is biomass that has not undergone diagenesis or catagenesis and as such contains only the immature βαα and ααα R isomers. Under these chromatographic conditions, βαα R elutes 0.1 min after ααα S. The Bur-56 and Bur-40 samples contain predominantly ααα S, not βαα R. **Figure S4:** GC-MRM-MS chromatogram of the *m/z* 414 > 259 transition for saturated fractions. The Tonian Bur-40 (Top), from the Khastakh formation of the Burskaya core in the Lena-Anabar basin, the Tonian V19 from the Visingsö Group (second from top, Zumberge et al. 2020), FN 4065, extracted from Permian sedimentary rock deposited in a saline alkaline lake (Xia et al. 2021), and a synthetic lanostane standard (Chiron). TPP = tetracyclic polyprenoids (Holba et al. 2000), a doublet peak that is common in many geological samples. Lan = lanostane. **Figure S5:** Additional trace metal redox parameters for (a) Khastakhskaya-930 and (b) Burskaya-3410 cores. See Figure 3 for stratigraphic abbreviations. (i) wt. % TOC (ii) U (ppm), with the upper crustal average of 2.8 ppm (McLennan 2001) shown as a vertical line. (iii) U_{EF}, defined as $(U/Al)_{sample}/(U/Al)_{UCA}$, where UCA is upper crustal average. Vertical line is at $U_{EF}=1.37$, identified as a threshold for anoxia by Li et al. (2023) in their calibration. (iv) U/Mo, with U/Mo = 2 shown as a vertical line. U/Mo < 2 may indicate euxinic conditions if consistent with other factors (Li et al. 2023). (v) Mo (ppm), with upper crustal average Mo = 1.5 ppm (McLennan 2001) shown as a vertical line. (vi) Mo_{EF}, defined as per U_{EF}, with the 4.8 threshold for euxinia calibrated by Li et al. (2023) shown as a vertical line. **Figure S6:** (a) U_{EF} vs. Fe_{HR}/Fe_T (Song et al. 2023) differentiated by aluminum content, for samples with < 50% carbonate from all sampled formations from both cores in the Lena-Anabar Basin. For a given element X, $X_{EF}=(X/Al)_{sample}/(X/Al)_{UCC}$, where UCC = average upper continental crust value (McLennan 2001). **Figure S7:** Molar ratios of C_{org} vs. P_{org} (filled symbols) and P_{reac} (open symbols) for Tonian and Ediacaran samples from the Lena-Anabar Basin, coded by redox. Triangles are samples where redox could not be assigned due to $Fe_T < 0.5$ wt%, oxic squares are samples with $Fe_{HR}/Fe_T < 0.38$, anoxic circles are samples with $Fe_{HR}/Fe_T \geq 0.38$. Plots show the canonical Redfield ratio of C/P = 106:1, as well as the proposed Precambrian P-limited biological ratio of C/P = 300:1 (Reinhard et al. 2017). **Figure S8:** Partial Ion Chromatogram of *m/z* 231 for aromatic hydrocarbon fractions showing triaromatic steroids in two samples from the Burskaya-3410 core. C_{26} triaromatic steroids are derived from C_{27} sterols (e.g., cholesterol), C_{27} triaromatic steroids are derived from C_{28} sterols, and C_{28} triaromatic steroids are derived from C_{29} sterols (e.g., stigmasterol). Note the C_{26} triaromatic sterane dominance in the late Tonian rocks which matches and confirms the C_{27} (cholestane) dominance for steranes. Data are tabulated in Table S6. **Figure S9:** Plot of P_{det2}, the recalcitrant, residual P fraction, versus Al (weight %) from all sampled formations from both cores in Lena-Anabar Basin. Linear fit trendline shows a strong relationship between P_{det2} and sedimentary aluminum content ($R^2=0.87$, $p<2e\text{-}16$). **Figure S10:** C_{29}/C_{27} sterane ratios vs. Fe_{HR}/Fe_T, indicating water column redox, for Neoproterozoic samples with available iron speciation data. Dotted lines indicate the 0.22 cutoff for oxic conditions and the 0.38 threshold cutoff for anoxic samples. All Tonian samples have a value of 0 for C_{29}/C_{27}. Visingsö Group sterane data from Zumberge et al. (2020), Baltica data from Pehr et al. (2023). Same-sample iron speciation data were not measured for the Chuar Group so they are not plotted, but they are presumed to be anoxic based on Johnston et al. (2010).

14724669, 2026, 5, Downloaded from https://onlinelibrary.wiley.com/doi/10.1111/gbi.70061 by NICE, National Institute for Health and Care Excellence, Wiley Online Library on [07/10/2026]. See the Terms and Conditions (https://onlinelibrary.wiley.com/terms-and-conditions) on Wiley Online Library for rules of use; OA articles are governed by the applicable Creative Commons License